Modelling Mineral Liberation of Ore Breakage to Improve the Overall Efficiency of Mining Operations

Jeremy Gottheil

A thesis submitted in partial fulfillment of the requirements for the master's degree in Applied Sciences in Chemical Engineering

Department of Chemical and Biological Engineering

University of Ottawa

August 18th, 2021

ABSTRACT

As the demand for a low-carbon and environmentally friendly future increases, so does the importance of mineral and metal commodities. The production of solar panels, wind turbines, energy storage systems and other green technologies require large quantities of minerals and rare earth metals. Natural Resources Canada noted that in 2019, Canada was a global leading producer in minerals required for green technology including graphite, nickel, cobalt, and others [1]. While mineral production continues to rise year over year, the ore grade, i.e., the concentration of a desired material, of multiple common minerals continues to decline.

To liberate valuable minerals from low ore grade deposits size reduction processes such as crushing and grinding are required; however, these processes account for over half of all energy consumption on the average mine. As mines are typically remote, fossil fuels are normally used as the main energy source, producing large amounts greenhouse gases, necessitating the need for more efficient size reduction processes. This could be accomplished by predicting how a particular orebody would break. With the surge in image sensing and computing technologies at mining sites many researchers are exploring ore texture and processability characteristics of the ore body. If distinct processability characteristics change based on ore textural feature from a 2D image, then general trends for optimal size reduction of orebodies of similar texture can developed.

This work builds on previous work by simulating ore breakage through the superimposition of a predetermined fragmentation pattern, called a mask, onto multiple ore textures. Synthetic, periodic black and white 2D ore textures were created to find a link between simple textural features such as different mineral grain shape, size, and orientation and processability characteristics. A Monte Carlo simulation was performed to generate a large quantity of realistic product particles using the Voronoi tessellations masking technique. To assess the processability of different textures, the percentage area distribution of valuable minerals of each ore texture was compared across the complete range of particle sizes. The valuable mineral percentage area distributions were analyzed for rate and shape of the distribution as particle size decreases, with noticeable differences between textures. The distributions were also parameterized using a two-beta mixture distribution model, expanding on the traditional one beta model developed by King [2,3,4]. These distributions can eventually help the mining industry make informed decisions on how much grinding and crushing will be required to liberate desired minerals from waste rock.

SOMMAIRE

Au fur et à mesure que la demande pour un avenir faible en carbone et respectueux de l'environnement augmente, il en va de même pour l'importance des matières premières minérales et métalliques. La production de panneaux solaires, d'éoliennes, de systèmes de stockage d'énergie et d'autres technologies vertes nécessite de grandes quantités de minéraux et de métaux terres rares. Ressources naturelles Canada a indiqué qu'en 2019 le Canada était l'un des principaux producteurs mondiaux de ces minéraux, notamment le graphite, le nickel, le cobalt et d'autres [1]. Alors que la production minérale continue d'augmenter d'année en année, la teneur du minerai, c'est-à-dire la concentration d'un matériau désiré, de plusieurs minéraux communs continue de baisser.

Pour extraire les minéraux de grande valeur des gisements à faible teneur en minerai, des procédés de réduction de la taille tels que le concassage et le broyage sont nécessaires; cependant, ces procédés représentent plus de la moitié de toute la consommation d'énergie pour une mine moyenne. Les mines étant généralement éloignées des grands centres, les combustibles fossiles sont normalement utilisés comme principale source d'énergie, produisant de grandes quantités de gaz à effet de serre, nécessitant des procédés de réduction de taille plus efficaces. Cela pourrait être accompli en prédisant comment un gisement en particulier se briserait. Avec la progression notable des technologies de reconnaissance d'image et de calcul sur les sites miniers, de nombreux chercheurs explorent la texture du minerai et les caractéristiques de transformabilité des gisements. Si les caractéristiques de traitement changent en fonction de la caractéristique de texture du minerai à partir d'une image 2D, alors des tendances générales pour une réduction optimale de la taille des gisements de textures similaires peuvent être développer.

Ce travail s'appuie sur des travaux antérieurs en simulant la rupture du minerai par la superposition d'un motif de fragmentation prédéterminé, appelé masque, sur plusieurs textures de minerai. Des textures de minerai 2D synthétiques et périodiques en noir et blanc ont été créées pour trouver un lien entre des caractéristiques texturales simples telles que la forme, la taille, l'orientation et les caractéristiques de transformation des grains minéraux. Une simulation de Monte Carlo a été réalisée pour générer une grande quantité de particules de produit réalistes en utilisant la technique de masquage des pavages de Voronoi. Pour évaluer l'applicabilité au traitement de différentes textures, la distribution en pourcentage de noir de chaque texture de minerai a été comparée

sur l’ensemble de la gamme de tailles de particules. Les distributions en pourcentage de noir ont été analysées pour le taux et la forme de la distribution lorsque la taille des particules diminue, avec des différences notables entre les textures. Les distributions ont également été paramétrées en utilisant un mélange de deux distributions bêta, montrant une meilleure correspondance que le modèle à un facteur bêta traditionnel développé par King [2,3,4]. Ces distributions peuvent éventuellement aider l'industrie minière à prendre des décisions éclairées sur la quantité de broyage et de concassage qui sera nécessaire pour libérer les minéraux désirés des déchets rocheux.

STATEMENT OF CONTRIBUTIONS OF COLLABORATORS

The completion of this thesis, along with the development of two computer programs, mineral liberation data collection and data analysis were supervised by Dr. Andrew Sowinski of the University of Ottawa. I hereby swear that I am the sole author of this thesis. All chapters and appendices were solely written by me with editorial suggestions and comments given by Dr. Andrew Sowinski and Dr. Andriy Plugatyr from the National Research Council (NRC) High Efficiency Mining (HEM) team.

Both computer programs were written by me, to generate, collect, analyze, and parametrize mineral liberation data. Dr. Andrew Sowinski, Dr. Andriy Plugatyr and Mr. Christopher Baxter from the NRC HEC team provided background knowledge on the coding language Wolfram Mathematica as well as coding suggestions to improve the computational efficiency of developed programs.

TABLE OF CONTENTS

LIST OF FIGURES

LIST OF TABLES

NOMENCLATURE

Abbreviation	Description
A	pre-exponential exponent, exponential decay function
A_p	particle area (#pixels)
$A_{p,s}$	scaled particle area
A_T	total texture area (#pixels)
α	alpha shape parameter
α_1	alpha shape parameter for beta distribution 1
α_2	alpha shape parameter for beta distribution 2
β	beta shape parameter
β_1	beta shape parameter for beta distribution 1
β_2	beta shape parameter for beta distribution 2
$Beta_1$	beta distribution 1
$Beta_2$	beta distribution 2
$B(\alpha,\beta)$	beta function
CH	constitutional heterogeneity
FS	area of the free surface
$f(x;\alpha,\beta)$	probability density function of a single beta distribution
$g(x;\alpha_1, \alpha_2, \beta_1, \beta_2)$	probability density function of a two-beta mixture distribution
IA	interfacial area
k	exponential exponent, exponential decay function
m	distribution mean
m_1	beta distribution 1 mean
m_2	beta distribution 2 mean
SA	surface area
SF	particle area scaling factor for changes in texture size
u	beta function integrand
w	mixture distribution weight
v	distribution variance
v_1	beta distribution 1 variance
v_2	beta distribution 2 variance
x	random variable
X	2D image dimensions

ACKNOWLEDGEMENTS

I would like to thank Dr. Andrew Sowinski for connecting me with the NRC HEM team to develop this thesis project. Furthermore, I would like to thank Dr. Andrew Sowinski for his constant support, and guidance over that past two and a half years.

I would like to thank Dr. Andriy Plugatyr and Mr. Christopher Baxter from the NRC HEM team for providing me with a great introduction to the mining industry and high efficiency mining research. I would also like to thank Dr. Plugatyr and Mr. Baxter for their constant support and guidance.

I would like the NRC and the University of Ottawa for funding this research, which gave me an opportunity to dive into a complete new and interesting research area. As a chemical engineer, it was important to get out of my comfort zone and apply the knowledge I have learnt in my undergraduate degree to applications beyond traditional chemical engineering operations.

CHAPTER 1
INTRODUCTION

The need for valuable materials from the Earth's crust for today's modern technology is an unavoidable reality. Extracted minerals are used in a very wide range of industries that effect every part of modern society. Today large mining processes involve the collaboration of multiple scientists, engineers, statisticians, and geologists to solve complex problems. The mining industry is a very important part of Canada's economy accounting for a Gross domestic product (GDP) of $71 billion or 3.3% of Canada's total GDP in 2019 [1]. As seen in Figure 1, in 2019, 19% of Canada's domestic exports were minerals and metals [1].

Figure 1.1: Canada's domestic mineral exports, 2019 (adapted from [1]).

The mining and minerals sector directly employs 392,000 while indirectly employing 327,000 with high quality jobs at an average annual salary of $126,000 [1]. Furthermore, mining sector jobs are often in remote, rural, and northern locations increasing the opportunity of high paying jobs across

Canada. In 2019, Gold (21%), coal (12%), potash (fertilizer production, 12%), iron ore (12%), and copper (9%) accounted for 66% of all mineral production in Canada, by value [1].

As the demand for a low-carbon and environmentally friendly future increases, the importance of mining commodities increases as well. Often not discussed, is the large quantity of minerals and metals required to produce multiple technologies used for renewable energy, high energy storage and other green technologies. Canada is a global leading producer in minerals such as graphite, nickel, cobalt, and rare earth metals which are required for the production of green and clean energy technologies from wind turbines and solar panels to hydrogen fuel cells, advanced batteries and more [1]. While the mining industry is vital for the production of green technologies, the mining industry itself has a distinct impact on greenhouse gas (GHG) emissions. In 2018, the Canadian mining industry (including iron/steel production and petroleum refining) accounted for 122.7 Mt of CO_2 or 23.8% of Canada's total GHG emissions [5]. It is clear that Canada's mining industry is a vital part of the future of Canada's economy as well as the future of clean, green and energy efficient technologies. Therefore, it is important that the mining industry continues to become more efficient as the demand for many minerals and metals increases.

1.1 Current Status of Ores Worldwide

As mineral production increases, ore grades across many mineral types continue to decline, which has led to a need to develop technology that can more efficiently extract these valuable minerals [6]. Ore grade is an economic term and refers to the relative amount of commercially valuable mineral to commercially worthless material (gangue) in an orebody [7]. The decline of ore grades can be attributed to multiple factors such as the technological improvement of low grade and bulk mining techniques as well as the depletion of high ore grade deposits over time. For example, from Figure 1.2, the average ore grade of gold in Australia in the early 1900s was approximately 1600 g gold/ton of rock, which has declined to approximately 50 g gold/ton of rock in the 2000s, showing an 97% decline in ore grades [6]. An overview of the general steps in mineral resource extraction, from mineral deposit to commercially valuable metals, is given by Table 1-1 [7].

Table 1-1: Mineral extraction overview: from mineral deposits to pure metals [7].

Step:	Overview:
1.) Mineral Exploration	is used to find valuable mineral deposits which can be extracted profitably. Mineral exploration includes obtaining the relevant government licenses/permits, reviewing literature, the collection and analysis of geophysical data as well as the evaluation of ore samples from core drilling and other sampling methods.
2.) Mining	extracts valuable minerals from the earths crust with as little gangue as possible. Large rocks are drilled and/or blasted and child rocks are collected for downstream mineral processes. Mining can either be done at the surface of the earths crust (open-pit mining) or underground depending on the location of mineral deposits. Seventy percent (70%) of worldwide mineral production uses surface mining techniques. The more expensive option, underground mining, may be employed when ore deposits are deep underground or when it is uneconomical to perform surface mining due to the high gangue to mineral ratio.
3.) Mineral Processing	separates valuable materials from commercially worthless gangue materials. In the mining industry, mineral processing is also often referred to as “ore dressing”, “mineral dressing”, or “mineral beneficiation”. Haldar et. al. (2018) categorized four distinct activities which encompass mineral processing: 1.) size reduction and liberation of minerals through crushing and grinding, 2.) ore sorting/screening by particle size, 3.) mineral concentration through physical and chemical separation techniques, 4.) dewatering to reduce potential hazards and shipment costs.
4.) Mineral Concentration	separates concentrated valuable minerals (concentrate) from gangues (tailings). Depending on separation efficiency as will as physical and chemical properties of the feed slurry, different

	mineral concentration techniques may be used such as further ore sorting, leaching, gravity concentration, flotation, and more.
5.) Metal Smelting/Refining	The goal of metal smelting is to recover metals from ores and mineral concentrates. Gangue materials separate from metals in a furnace at high temperature due to difference in density. The goal of metal refining is to purify feed metals to its highest purity (99.9%). For example, electrolytic refining can purify metals through electrolysis. After application of an electrical current, impure metals dissolve from the anode while pure metal ions deposit onto the cathode. Impurities either dissolve in the electrolytic solution or precipitate out.

Size reduction processes are required to separate valuable minerals in an orebody from gangue. Valuable materials which are physically separated from gangue are said to be completely liberated. Therefore, completely liberated particles have 100% ore grade. Size reduction processes can be used to create small particle sizes that contains the liberated minerals which must still be separated from the gangue using downstream separation systems.

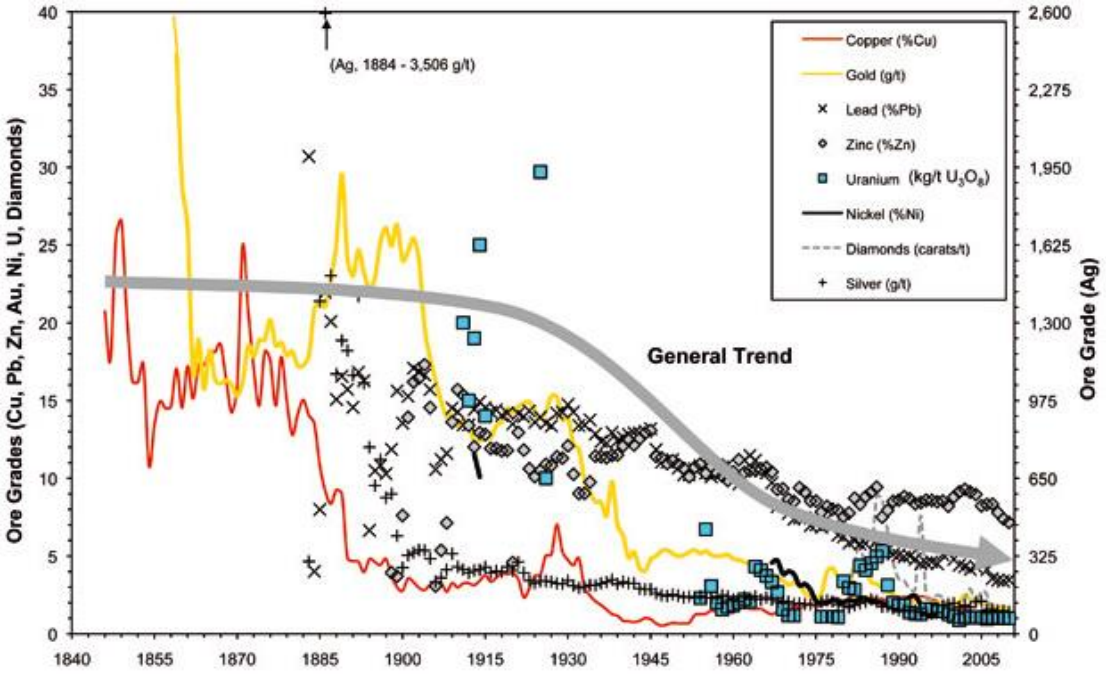

Figure 1.2: Combined average ore grades over time for Australian base and precious metals (adapted from [7]).

With declining ore grades, more size reduction processes may be required to extract the same quantity of valuable minerals. For example, as seen in Figure 1.3, the energy intensity of copper mineral extraction exponentially increases as copper ore grade decreases, with a sharp increase in energy intensive below a copper ore grade of 0.5%, for multiple extraction methods [8]. Size reduction is easily the most energy intensive process in the minerals and mining sector, with estimates that size reduction uses 3% of all electric power generated worldwide and at least 50% of the average mine site energy consumption [9,10]. Depending on the relative contribution of renewable and non-renewable energy to the grid, size reduction processes will also indirectly increase GHG emissions through energy consumption of non-renewable sources. Many mining sites are off main grid infrastructure, therefore natural gas generators are commonly used as on-site electricity production instead [10]. Though, as renewable energy technology becomes more affordable, remote mining sites have started to add renewable sources to their energy production [10].

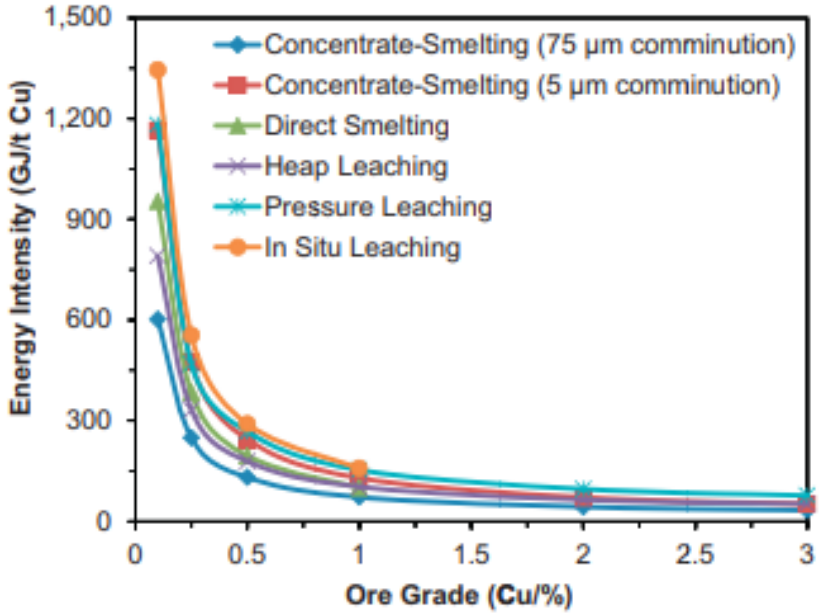

Figure 1.3: Energy intensity of different process pathways of copper production (adapted from [8]).

1.1.1 Mineral Liberation and Extraction Techniques

The degree of mineral liberation is directly related to the amount of crushing and grinding required and is therefore inherently connected to the energy costs of the process. Some minerals do not need to be ground to the smallest particle size to be liberated and separated from the gangue. Therefore, a balance between adequate liberation of valuable minerals and energy consumption should be made. Finding this optimal point, between high mineral liberation of valuable materials and reduced energy consumption is a key interest in high efficiency mining research area.

Size reduction processes such as blasting, grinding, and crushing are one of the main contributors to the energy costs of mineral extraction [6]. At the largest scale, dynamite is used to break up the orebody into large chunks by blasting. Different types of crushers are used to crush the chunks into smaller particles. Grinding may also be used to reduce particle size even further. Once the orebody is crushed or ground into smaller particle sizes, separation methods such as froth flotation, gravity separation, leaching and other methods can be utilized to their optimal potential to separate liberated valuable minerals from gangue.

The degree of liberation and the way in which particles liberate has a major effect on downstream separation efficiency [11]. Particles may have a very high volumetric ore grade with no surface exposure of valuable minerals, particles may have high surface exposure, but low volumetric ore grade, or somewhere in between. Depending on particle characteristics such as particle size, ore grade, and valuable mineral surface exposure, different separation methods may be more efficient. For example, the optimal characteristics of feed particles for three common separation techniques were compared: gravity separation, flotation, and leaching.

In gravity separation, particles are separated based on their on specific gravity. An example of a gravity separation process is illustrated in Figure 1.4, where a feed slurry enters a rotating drum. The centrifugal forces contribute to the gravity separation of particles into "lights" and "heavies" [12]. A higher ore grade difference between valuable particles and gangue particles results in a larger difference in specific gravity and a better separation. Therefore, the degree of liberation for gravity separation directly depends on the volumetric grade of particles. The efficiency of gravity separation drops when average particle size is small and if the specific gravity difference between the valuable mineral and gangue is minor [12,13].

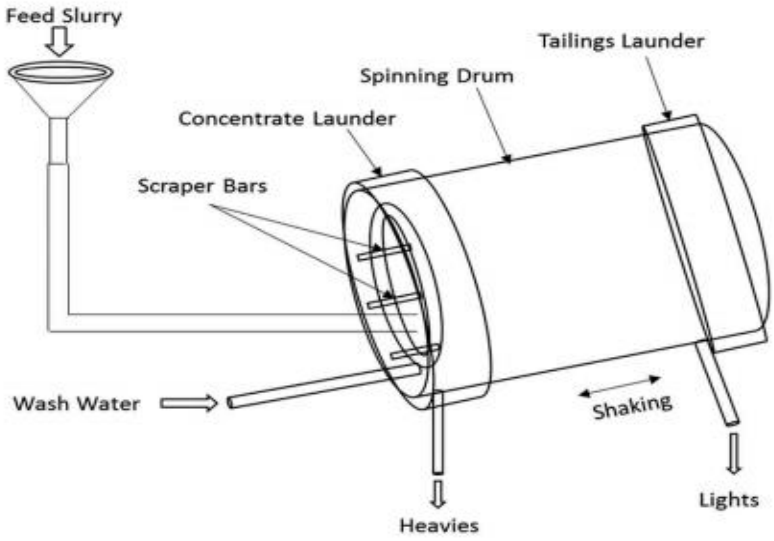

Figure 1.4: Example of a gravity separation process (adapted from [12]).

Flotation is a separation process in which air bubbles carry valuable minerals through a colloidal suspension by physiochemical differences in the interfaces and can be used in cases where gravity separation is less efficient [13]. For flotation to proceed, the surface of the valuable mineral must

be hydrophobic while the surface of the gangue is hydrophilic [13]. The valuable minerals are selectively attached to air bubbles through surface interactions which are then concentrated into a froth and separated as seen in Figure 1.5 [13]. Due to surface interactions between air bubbles and particles, it is most important that valuable material is exposed at the surface. Therefore, for flotation processes, the degree of liberation depends on the degree of surface exposure of valuable material.

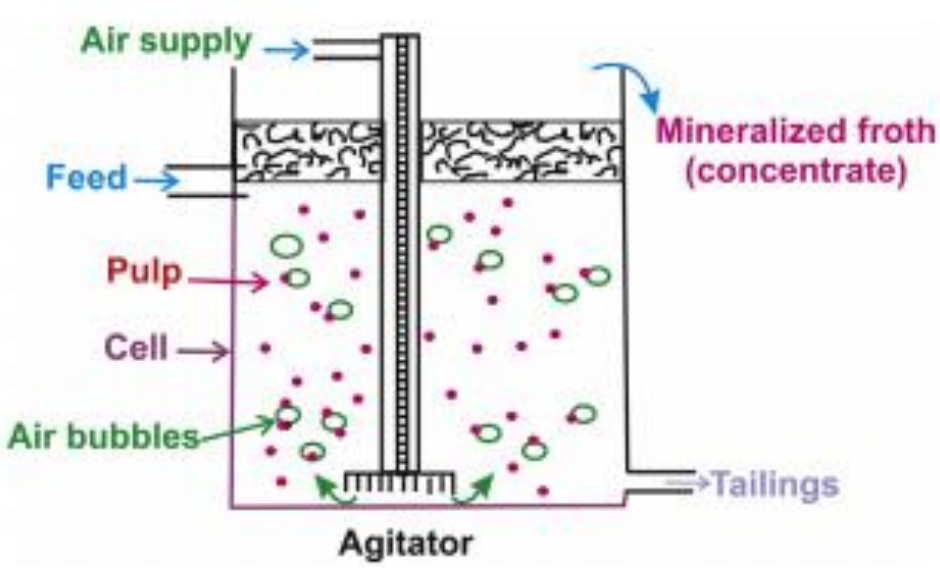

Figure 1.5: An example of a froth flotation apparatus (adapted from [13]).

Chemical leaching is a hydrometallurgy extraction technique which uses acidic solutions as a solvent to selectively dissolve solid valuable minerals and recover them from the gangue [7]. A continuous leaching process is illustrated in Figure 1.6. First, a leaching solvent such as sulfuric acid is exposed to a crushed ore heap to dissolved valuable minerals. Valuable metal ions are concentrated through After the leaching solution dissolves the valuable minerals from the broken ore heap, metal ions can be concentrated by multiple methods such as selective precipitation, solvent extraction, and liquid/liquid extraction [7,14].

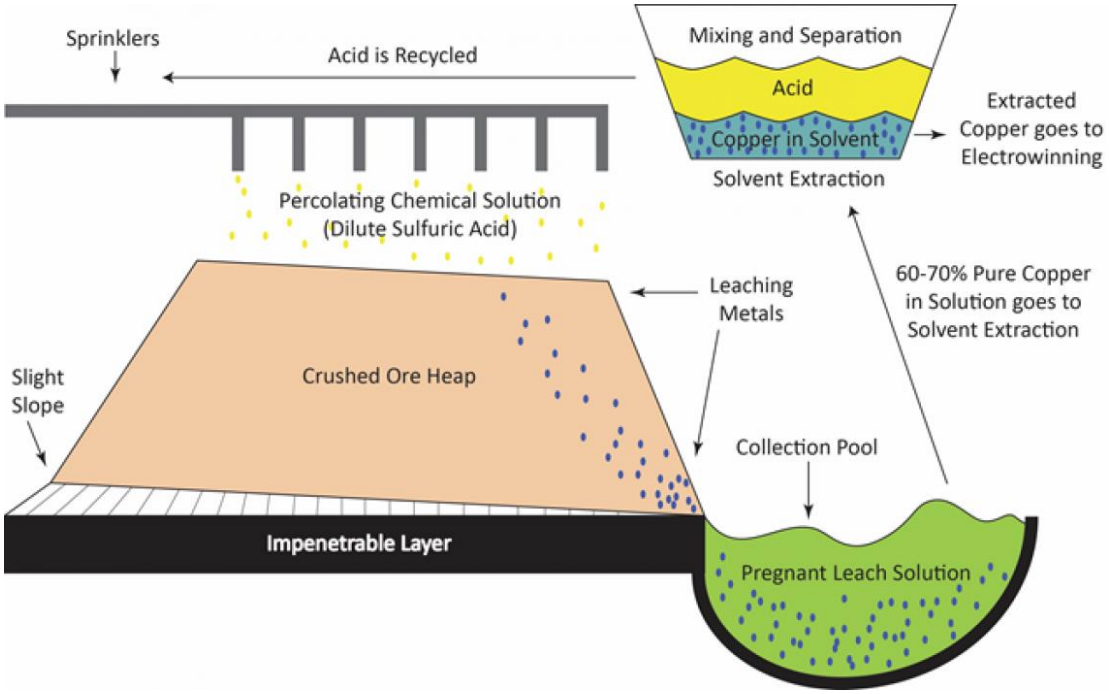

Figure 1.6: Heap Leaching Process Diagram (adapted from [14]).

In the chemical leaching process, the liquid solvent requires as much exposure to the valuable material as possible to dissolve the solute. It is easier for the solvent to dissolve valuable material which is closer to the surface of a particle then material which is deeper as the solvent will incur mass transfer limitations. Therefore, the degree of liberation for leaching depends on surface exposure of valuable material, as well as the distance from the entrapped valuable material to the surface of the particle. There may be particles of high ore grade which separate easily in gravity separation, but have no surface exposure, meaning the leaching solution will have to diffuse into the particle a certain distance before the valuable mineral can be dissolved.

1.1.2 Exploiting Image Analysis for More Efficient Size Reduction Processes

Since grinding all orebodies to minute particle sizes is not a viable option and different separation techniques require different liberation criteria, predicting how an orebody would break would be invaluable knowledge. Prior to downstream separation processes, data analysis can be employed to predict the liberation of the valuable material more efficiently in size reduction processes and ore sorting. Due to the sheer scale of mining operations, small core (cylindrical orebody) samples may not be representative of the entire mine and multiple point core sampling across the mine site is arguably too expensive to be economically viable [15]. Therefore, there is a need to develop new testing methods that can help guide decision-making for mineral liberation and allow for

inferential analysis. Using historical data, some key geometallurgical attributes can be modelled and help determine how mineral liberation will proceed. If one knows how a typical orebody will break during size reduction processes, crushing can be tuned appropriately to provide child particles with optimal size for valuable mineral liberation. A major geometallurgical attribute of liberating particles is the distribution of ore grades of child particles at different particle sizes [16]. If one can predict the ore grade distribution of a given orebody at any particle size, an optimal particle size can be chosen with particles of sufficiently high ore grade for downstream sorting and separation processes.

Data collection and digitalization can be viewed as the main driver in the transformation of the mining sector. National Research Council (NRC) have noted that geo sensors and sensors-based sorting is a key research and development area for investment in high efficiency mining operations. Sensor based technologies already have many applications in the mining industry including core scans and core logging, sensor-based sorting, mineral liberation analysis and more. Multiple two-dimension (2D) sensors such as scanning electron microscopy (SEM), visual, RGB, x-ray fluorescence (XRF), and three-dimension (3D) sensors such as x-ray micro topography (XMT) and light detecting and ranging (LiDAR) can be used to develop analytical tools for the assessment of orebodies and their subsequent mineral liberation during size reduction processes [7]. Ore texture has been studied in literature to examine and explore the link between textural features and the processability characteristics of a given orebody such as the ore grade by size distribution of child particles.

The effect of ore texture on mineral liberation has been explored extensively in the high efficiency mining research area. An example of a 2D ore texture is given by Figure 1.7. Ore textures in 2D and 3D are made up of multiple textural features including mineralogical composition, mineral grain size and size distribution, mineral grain shape and mineral grain orientation in 2D or 3D space. Mineral grains are defined as an all-encompassing mineral within an orebody or as a particle [7]. An example of a molybdenite mineral grain in a 2D ore texture is circled in yellow, middle right, in Figure 1.7. Key textural features of ore textures are summarized in Table 1-1.

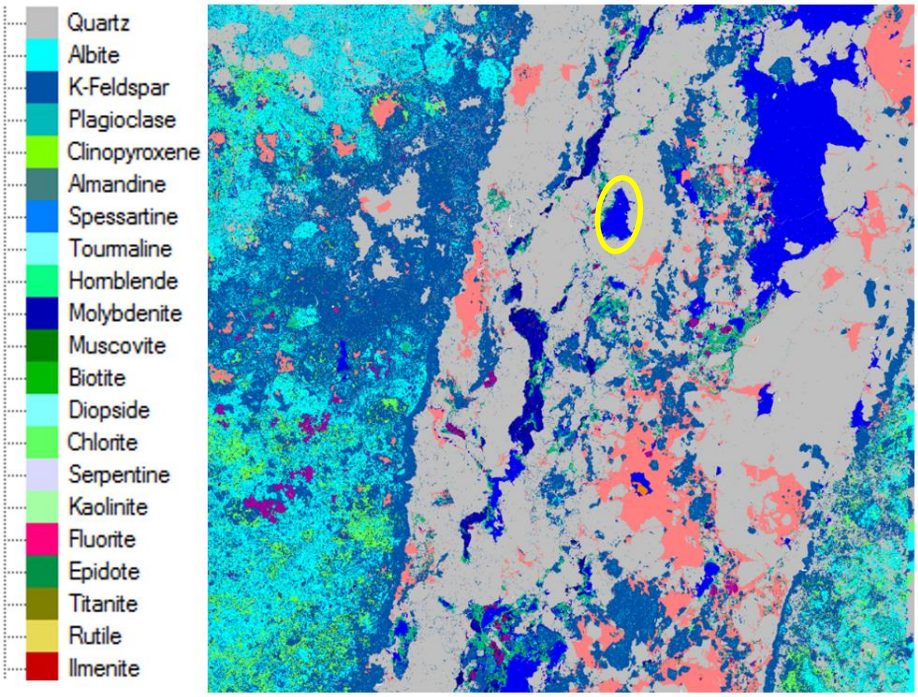

Figure 1.7: False colour image of polished rock section. Each colour is associated to a mineral. Provided by NRC High Efficiency Mining (HEM) Team (2021).

It one knows how a certain ore texture will break, then inferential analysis can be applied to ore textures with similar textural features to predict mineral liberation in different portions in the mine. In other words, ore texture analysis can be performed to better understand data collected on the mine site and extend the applicability of collected data across the mine site [15]. Texture analysis has been leveraged multiple times in high efficiency mining literature to develop predictive mineral liberation models.

Table 1-2: Ore texture features.

Textural Feature	Illustration
Mineralogical Composition (colour)	
Mineral Grain Size	
Mineral Grain Size Distribution	
Mineral Grain Shape	
Mineral Grain Orientation	

1.2 Predictive Liberation Models

Mariano et al. (2016), noted that due to orebodies being heterogeneous, mineral liberation can be split into two simple categories, random or non-random breakage [17]. In reality, hardness as well as other mechanical properties of minerals present effect how mineral liberation will proceed. For example, a softer material may liberate faster with less energy required for size reduction. Mariano et al. (2016) found that the common themes between authors who defined random breakage, also referred to as non-preferential breakage, were that random breakage is independent of texture, mineral composition, mineral mechanical properties, as well as breakage which is non-preferential along grain boundaries [17]. Therefore, non-random breakage, can be assumed to be breakage which depends on preferential breakage along grain boundaries, as well as breakage depending on mineral mechanical properties, ore grade, and texture [17]. Many authors in literature have leveraged the random breakage assumption to simplify mineral liberation simulations. If one assumes random breakage, random Monte Carlo simulations can be performed to simulate breakage and create a very large dataset of particles without the requirement of specific rules dictating non-random breakage.

Many different techniques have been developed in literature to predict ore breakage using texture analysis. With increasing complexity in mineral characterization and image processing, the

methods can have limitations including processing power (large image sizes), and scaling issues. Most ore textures images are small polished rock samples on the micrometer to centimeter scale which may not be a representative ore texture if you zoom out to the meter or larger scale. Multiple predictive mineral liberation models which leverage texture analysis are summarized in Table 1-2.

Table 1-3: Literature review of mineral liberation models in the high efficiency mining research area.

Authors:	Mineral Liberation Model Summary:
Van der Wielen (2017) [18]	Developed a Voronoi tessellation masking model to predict mineral liberation. A mask can be viewed as a pre-determined fragmentation pattern for an ore texture. Random Voronoi tessellation patterns were superimposed onto ore textures to simulate breakage. The overall particle size distribution was calibrated to a real sulfide ore mill product.
Hilden and Powel (2017) [19]	Proposed a random breakage model to reconstruct a 3D ore texture and the mineral liberation characteristics of the texture's breakage products after size reduction. Often ore textures exhibit relative degrees of mineral clustering in which there are some areas with major mineral veining and some areas which are almost completely gangue. Therefore, the degree of mineral clustering was also modeled by applying a distribution function for each mineral phase present in the texture.
King (2000) [2]	Proposed a mineral liberation model for binary ore textures using the beta distribution as the distribution function of choice. The model assumes that the ore grade distribution of child particles at all sizes can be described by a single Beta distribution. King noted that crushing and grinding can be viewed as the superimposition of a fragmentation pattern onto a heterogeneous texture. Similar to Gay (1998), a

	collection of particles from a real size reduction product were mounted in resin in order to develop the fragmentation masks and simulate ore texture breakage. King also defined five distinct types of non-random breakage: 1.) differential breakage, 2.) preferential breakage, 3.) phase boundary fracture, 4.) liberation by detachment, and 5.) boundary region fracture.
Gay (1998) [20]	Presented a non-random breakage model which estimates the mineral liberation distribution of child particles from size reduction processes using data collected from previously crushed real ore samples. Real particles from the crushed samples were mounted in resin in order to develop a partially non-random breakage mask. This mask was applied as a fragmentation pattern to 2D ore textures to simulate the size reduction process. Using the proposed model, the mineral liberation profile of size reduction products of similar size can be predicted.
Barbery and Ledoux (1988) [21]	A model was developed to predict particle distribution composition after size reduction processes. Breakage was assumed to be independent of textural features or mineral phase, following the random breakage assumption.

1.2.1 Geostatistical models

With a large dataset, it would be useful to apply statistical techniques to predict processability characteristics of orebodies in unsampled locations in the mine. Statistical models can be used to develop a mathematical relationship between key parameters by fitting mathematical equations to experimental data [16]. Geostatistics, an extension of tradition statistics, was developed for the mining and petroleum industry in the 1950-1960s by the collective contributions of Danie Krige and Georges Matheron [16]. Geostatistics are used to estimate quantities which vary is space. With

reference to the mining industry, the goal would be to estimates properties of unsampled locations on the mine by efficiently analyzing property values at sampled locations [16]. By having a good estimate for key parameters such as ore grade and ore composition at different particle sizes, the size reduction process can be specifically tailored to generate the desired degree of liberation at specific particle sizes. Overall geostatistics is useful for large scale operations such as mining sites as multi point core sampling is expensive and often considered economically unfeasible.

1.2.2 Beta Distribution

Population distributions can be used to fit mathematical equations for development of geostatistical models [2,15,16]. One such distribution commonly used to model mineral liberation in literature is the beta distribution [2,15]. The beta distribution is a continuous probability distribution defined by two shape parameters, α and β greater then 0, with a range of: $0 < x < 1$ [2,15]. The probability density function for the beta distribution is given by the equations 1.1 and 1.2 below [22].

$$f(x;\alpha,\beta) = \frac{1}{B(\alpha,\beta)} x^{\alpha-1}(1-x)^{\beta-1} \quad [1.1]$$

$$B(\alpha,\beta) = \int_0^1 u^{\alpha-1}(1-u)^{\beta-1} du \quad [1.2]$$

Where α and β are beta distribution shape parameters, B(α,β) is the Beta function, u is the Beta function integrand, x is the random variable, and f(x;α,β) is the mathematical function.

The beta distribution probability density function form can be interpreted as a measure of the probability of success for a given set of data [2,15]. As α increases, the probability of success increases leading to the distribution to skew to the right as seen in Figure 1.8 for $\alpha = 5$, $\beta = 1.5$. As β increases, the probability of success decreases leading to the distribution to skew to the left, for example, $\alpha = 1.5$, $\beta = 5$ in Figure 1.8. With reference to mining operations, an important geometallurgical attribute, ore grade, varies from 0 to 100% (0 to 1) analogous to the range of the beta distribution. Therefore, the beta distribution can be a useful tool in modelling the ore grade distribution of populations of particles as size reduction proceeds.

When both shape parameters are equal and below one, U-shaped curves are formed. When both shape parameters are equal and above one, a single positive parabola is formed. This behavior mirrors the general change in shape of the ore grade by size distribution of child particles. At large particle sizes, child particles form a narrow peak around the overall mean ore grade of the parent orebody [2]. At small particles sizes, particles form a binomial distribution of either completely liberated or completely gangue particles [2]. Particle size has major effect on the shape and speed of the changing ore grade distribution of particles as size reduction proceeds. Due to the beta distributions flexibility, it can model the many modes of the changing mineral liberation profile as particle size changes from large too small [2,16]. As seen in Figure 1.8, the probability density function form of the Beta distribution has multiple modes depending on the values of the two shape parameters α and β.

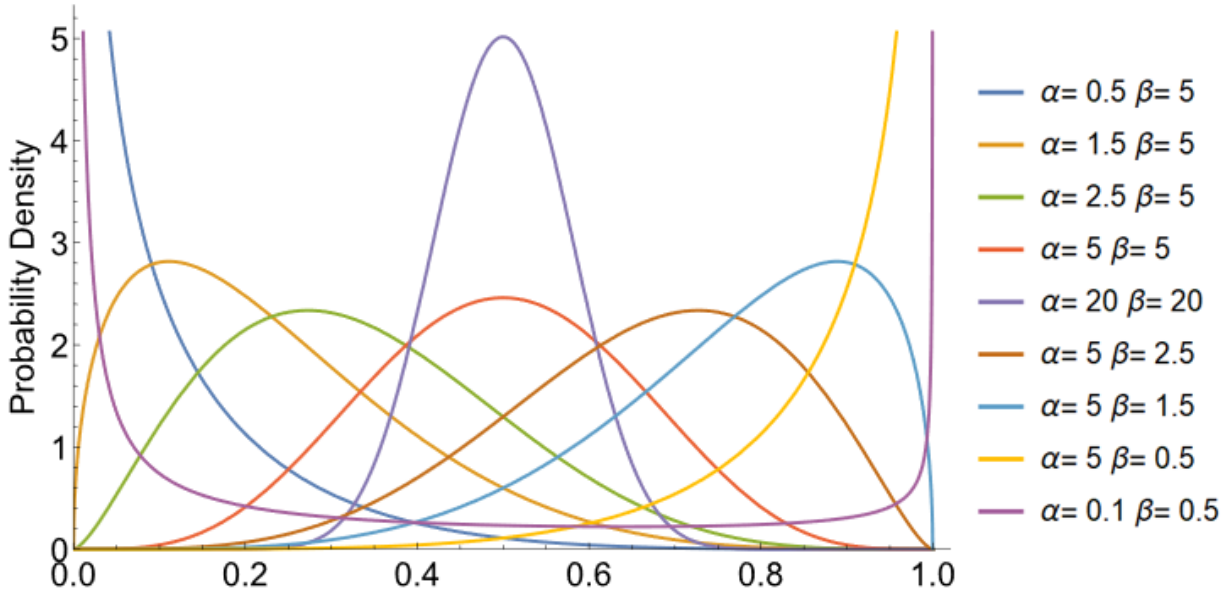

Figure 1.8: Beta Distribution at multiple shape parameter values.

Often ore textures generate complex ore grade by size distributions which are difficult to model with the contribution of a single distribution. To model the effects of mineral liberation profiles more accurately, a weighted mixture distribution of two Beta distributions can be created. The probability density function for the two-beta mixture distribution is given by equation 1.3.

$$g(w, \alpha_1, \alpha_2, \beta_1, \beta_2,) = w[f(x; \alpha_1, \beta_1)] + (1 - w)[f(x; \alpha_2 \beta_2)] \quad [1.3]$$

Where g(w,α_1,α_2 β_1 , β_2) is the probability density function of the mixture distribution and w is the distribution weight.

Mixture distributions have the weighted contribution of two or more distributions of choice as seen in Figure 1.9. As an example, the mixture distribution with form g(0.926,0.73 ,50.6 ,0.73 ,50.6) was generated from the relative contribution of f(0.73,0.73) and f(50.6,50.6). 92.6% of the mixture distribution contribution came from the U-shaped blue curve f(0.73,0.73). The small peak seen at 0.5 for the green curve comes from the small contribution of f(50.6,50.6) to the overall mixture distribution. Therefore, multiple forms of a single beta distribution can be combined to model more complex ore grade distributions.

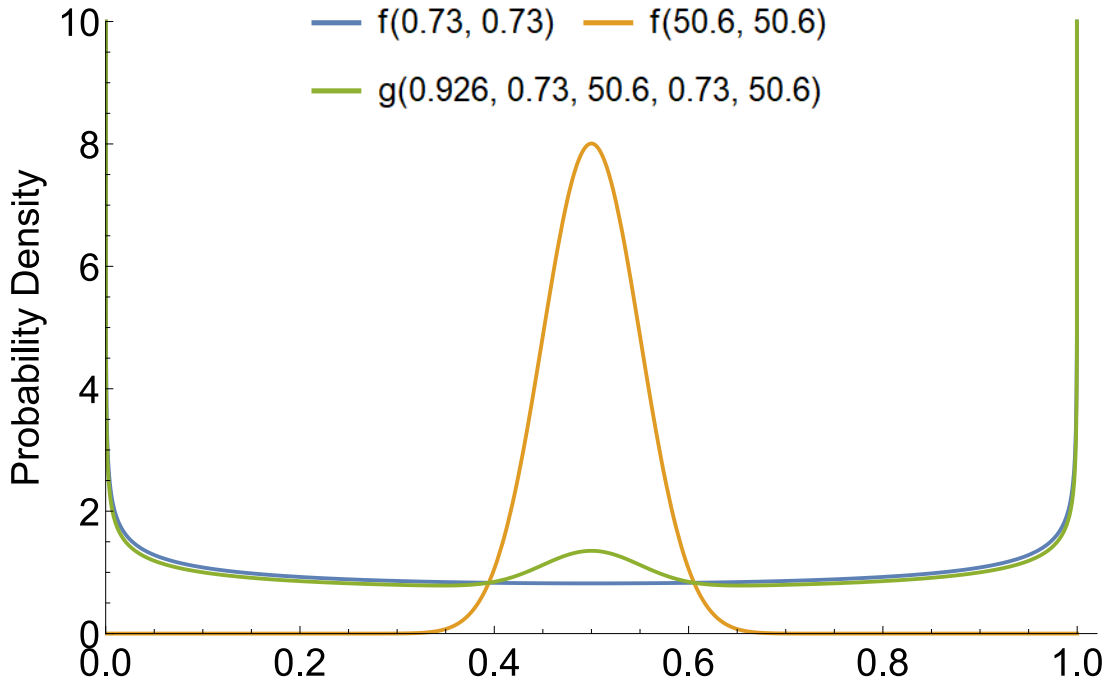

Figure 1.9: Two beta mixture distribution and the relative single beta contributions.

1.2.3 Masking techniques

Masking techniques are a useful tool in developing a geostatistical model for estimation of key parameters. To liberate valuable minerals more efficiently from gangue, it would be useful to be able to predict the required degree of liberation prior to the size reduction process. By leveraging image analysis of ore textures, analytical tools can be developed to make educated predictions on

the geometallurgical attributes of the mine. Masking techniques are one of said tools. As the name suggests, masking techniques start by creating a mask. This mask is a pre-determined fragmentation pattern for 2D ore textures. By superimposing the mask onto a 2D ore texture, size reduction can be simulated, and geostatistical data such as the ore grade distribution of particles by size can be collected. In two dimensions, the ore grade of particles changes from a volumetric value to the percent area of valuable mineral in a given particle. An example of a mask is illustrated in Figure 1.10.

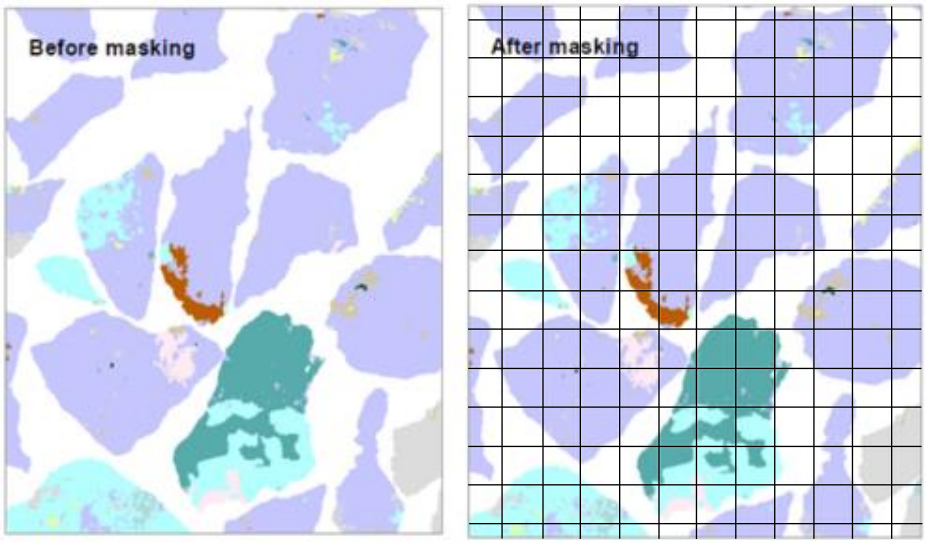

Figure 1.10: Application of a random breakage square pattern mask on coarse particulate material (adapted from [23]).

These masks are developed according to many methodologies in literature and can be superimposed on 2D ore textures to simulate breakage, providing data on the degree of liberation of valuable minerals and size distribution of progeny particles. Most masking techniques created in literature are independent of texture and mineral composition meaning the ore texture chosen has no influence on the fragmentation pattern; therefore, they follow the random breakage assumption. One such masking methodology used in high efficiency mining literature is the Voronoi tessellation pattern masking technique.

1.2.4 Voronoi Tessellations and their Applicability to Mineral Liberation Modelling

Voronoi tessellations in 2D and 3D space have become an increasingly popular computational geometry tool used for modelling in multiple research fields including biotechnology, high efficiency mining and many more [17,18,24,25,26].

In particular, Voronoi tessellations are a useful tool to study the heterogeneity in ore textures. The irregularly shaped Voronoi cells that Voronoi tessellations can create particles which are visually resemble typical ore breakage products [18]. Although a good estimate, Voronoi tessellations do not completely model all possible comminution products. Voronoi tessellations provide convex polygons/polyhedra while it is possible that size reduction products can be concave [18].

Many masking techniques do not create a realistic size distribution of child particles. As seen in Figure 1.10, it is clear that that a square masking pattern will generate a narrow size distribution of particles centered around an individual squares area. More complex masking techniques such as Voronoi tessellations have been used in literature to create particle size distributions which are realistic [18]. For example, Van der Wielen et. al. (2017), successfully calibrated a generated Voronoi tessellation size distribution to the particle size distribution of a real mill product [18].

A Voronoi tessellation is the partition of a 2D or 3D space into smaller regions called Voronoi cells, with each cell each containing one generating seed. Voronoi tessellations follow the nearest-neighbour rule, meaning each Voronoi cell is the region closest to the associated seed. Therefore, the line segments (2D) or planes (3D) can be viewed as the boundaries between the nearest generated seeds. It is analogous to looking for the nearest gas station on a map. The map is a 2D representation of a region and depending on where one is geographically on the map, the closest gas station (seed) may change. An example of a 2D Voronoi diagrams is illustrated below (Figure 1.11). 25 generating seeds were randomly placed in a 2D bounded box to create the Voronoi tessellation pattern. Increasing the number of seeds in a given bounding box area will reduce the average area of Voronoi cells while increasing the number of Voronoi cells present. These generating seeds can either be specified (x,y coordinates) or randomly placed. Therefore, depend on the ruleset guiding the placement on Voronoi seeds in 2D space, the Voronoi mask can either be randomly generated or non-randomly generated. This means that Voronoi tessellations are flexible in the sense that they can generate random as well as non-random breakage patterns.

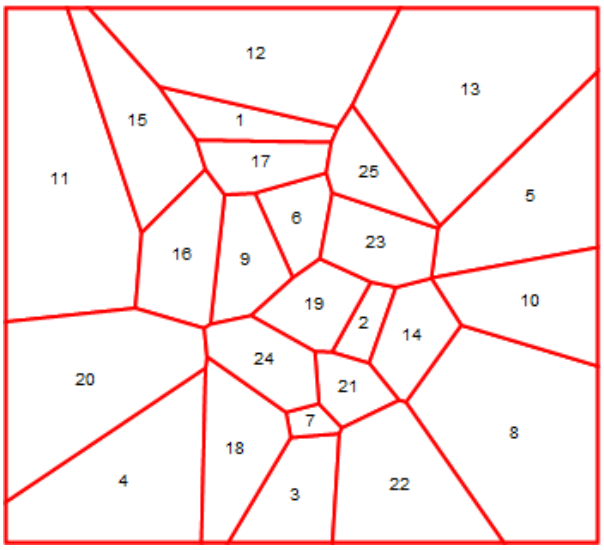

Figure 1.11: An example of a 2D Voronoi diagram generated in Mathematica. Each number represents a generating seed.

Multiple authors have used 2D Voronoi Tessellations as a random breakage masking technique for the simulation of ore texture breakage. [18,24,25]. An example of a Voronoi tessellation mask is shown in Figure 1.12.

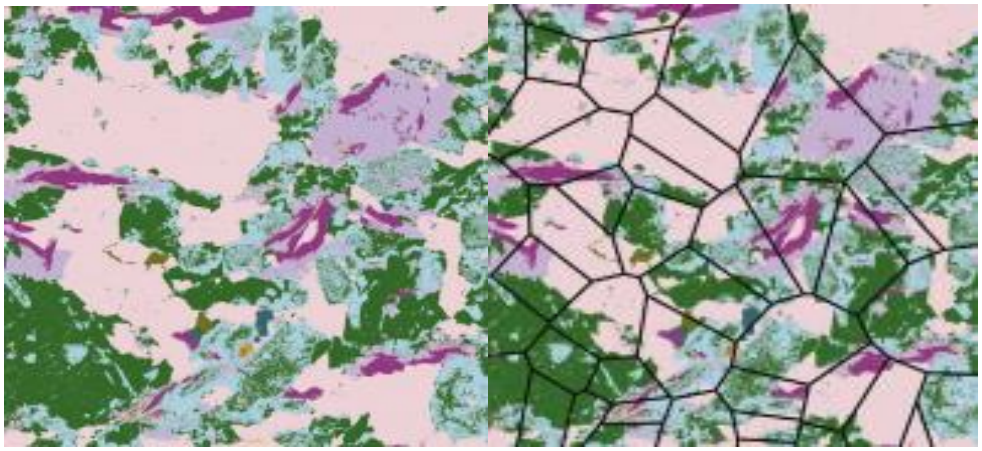

Figure 1.12: False colour image of an ore texture with and without a superimposed Voronoi mesh (adapted from Van der Wielen et al. 2017).

Van der Wielen et. al. (2017) developed a Voronoi tessellation-based model which was used to predict the liberation behaviour of ore textures through image analysis [18]. Voronoi tessellations were used as mask to simulate the fragmentation pattern of size reduction. The size distribution of child Voronoi cells was calibrated to a real size reduction product to provide a realistic size

distribution of child particles. Modeled mineral liberation behaviour using Voronoi tessellations aligned well against a real mill product sulfide ore sample which it was tested against [18].

Voronoi tessellation have also been used in the gold grain liberation simulations. In gold extraction processes, it is important to have high gold surface exposure to allow the leaching solution to reach the gold. As previously mentioned in Section 0, the degree of liberation for leaching processes depends on the surface exposure of valuable minerals [18]. Khalesi et al. (2009) developed a liberation model which was created to study ore with vary low mineral content such as gold [25]. Random child particles were created using Voronoi tessellations which were simulated around a gold grain as shown below (Figure 1.13).

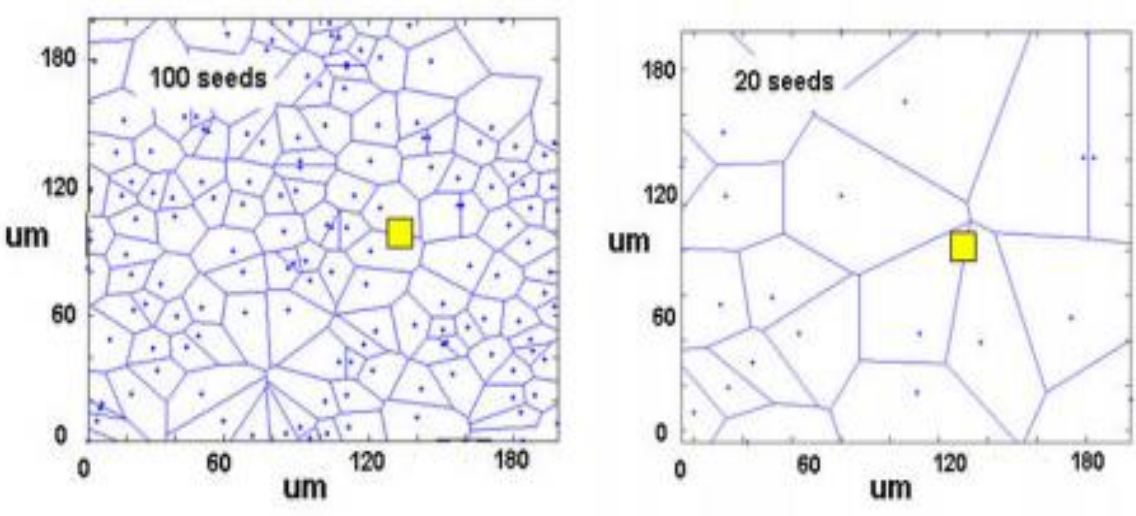

Figure 1.13: Progeny particles created by Voronoi tessellations (100 seeds and 20 seeds) around a square gold grain (adapted from [25]).

The small gold grains were simulated as liberated, exposed at the surface, or locked inside the gangue. The minimum distance to edge was calculated for all gold grains locked inside the gangue which correlates to the distance the leaching solution must travel to reach the grain [18].

Cellular automata have also been used as a 2D masking technique analogous to Voronoi tessellations. Cellular automata create realistic progeny particles during size reduction simulation similarly to Voronoi tessellations. Cellular automata are units of a mathematical model that have simple rules governing their replication or destruction [27]. A cellular automata model is useful to simulate systems that evolve in space at time such as the size reduction process in mineral processing. Cellular automata constitute a dynamic system composed of cells that evolve in time

according to defined rules [27]. Guimarães et al. (2006) developed an algorithm to simulate the size reduction process by superimposing a fragmentation pattern over 2D ore textures analogous to other masking techniques (Figure 1.14). Each of the child particles created by the fragmentation pattern grew according to rules related to the probability of agglomeration between different seeds (analogous to Voronoi seeds) [27]. The rules associate with the particle growing process considers mineral chemical attributes and properties, therefore, the fragmentation pattern created is partly non-random [27].

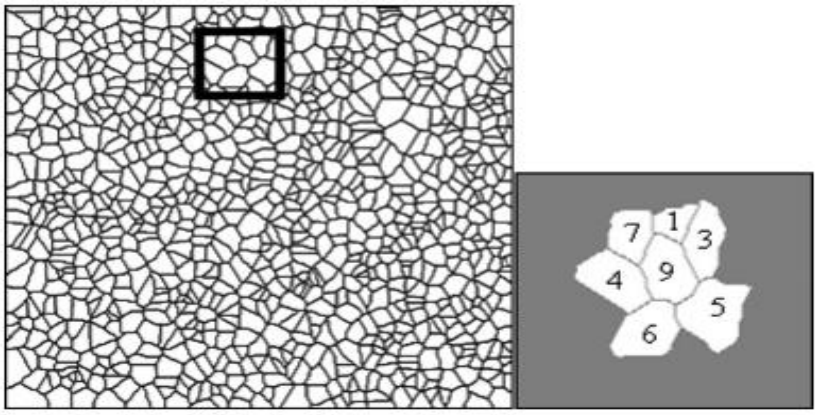

Figure 1.14: Generated 2D fragmentation pattern by cellular automata (adapted from [27]).

1.2.5 Random Breakage Assumption and Non-random Breakage

A random breakage assumption is commonly used in liberation modelling due to the simplicity and efficiency of randomized simulations. The random breakage assumption is useful in simulation experiments as Voronoi tessellations can be created randomly, without specific rules guiding breakage. Therefore, multiple tessellation patterns can be randomly generated using less computational power then if there were constraints or rules. In reality, minerals can have varying hardness and other mechanical properties which can affect the preferential breakage of certain minerals versus others. Therefore, there have been multiple researchers in literature who have developed breakage models which do consider non-random breakage.

Mirzaei and Khalesi (2019) developed a 2D Voronoi based liberation model using Leibner's method for determining the contributions of random and non-random breakage [24]. Leibner et al. (2016) introduced a method to determine the relative contributions of trans-granular and intergranular fracture based on 2D analysis. The basic principle being that the surface area (*SA*) of

a mineral in a 2D image is composed of an interfacial area (*IA*) and the area of the free surface (*FS*) as illustrated by equation 1.4 [24,28].

$$SA = IA + FS \quad [1.4]$$

The simulated ore before breakage was simulated as an empty space (gangue) with distributed square grains throughout. The generated Voronoi polygons were simulated as the fragmentation pattern as seen in Figure 1.15 [24].

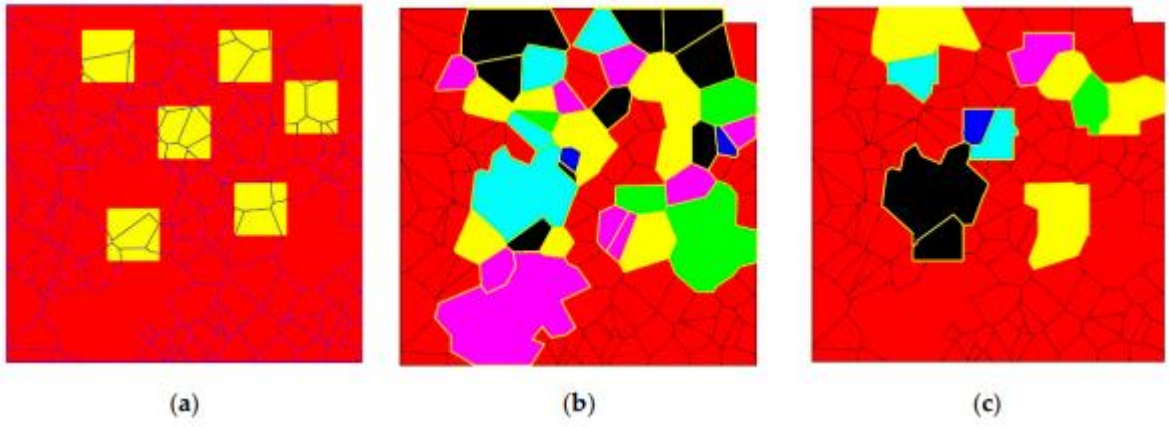

Figure 1.15: a) Voronoi diagram with red as the gangue matrix and yellow as mineral grains, b) random-breakage c) non-random breakage (adapted from [24]).

Voronoi tessellation of different sizes were used to generate fragmentation patterns at different grinding energy levels. Validation on artificial two-phase stones was performed to show the accuracy of the model algorithm to determine relative contribution of random and non-random breakage [26].

Gay (1998) presented a non-random breakage model which estimates the liberation distribution of child particles from size reduction processes. Particles from a typical size reduction product were mounted in resin to develop a mask [20]. This mask can then be applied to a binary or multiphase ore texture to generate a new set of progeny particles as shown in Figure 1.16 below. By simulating typical size reduction products of similar size, the liberation distribution of valuable minerals can be estimated using the proposed model. Gay uses previous size reduction information to predict have future ore textures will break [20].

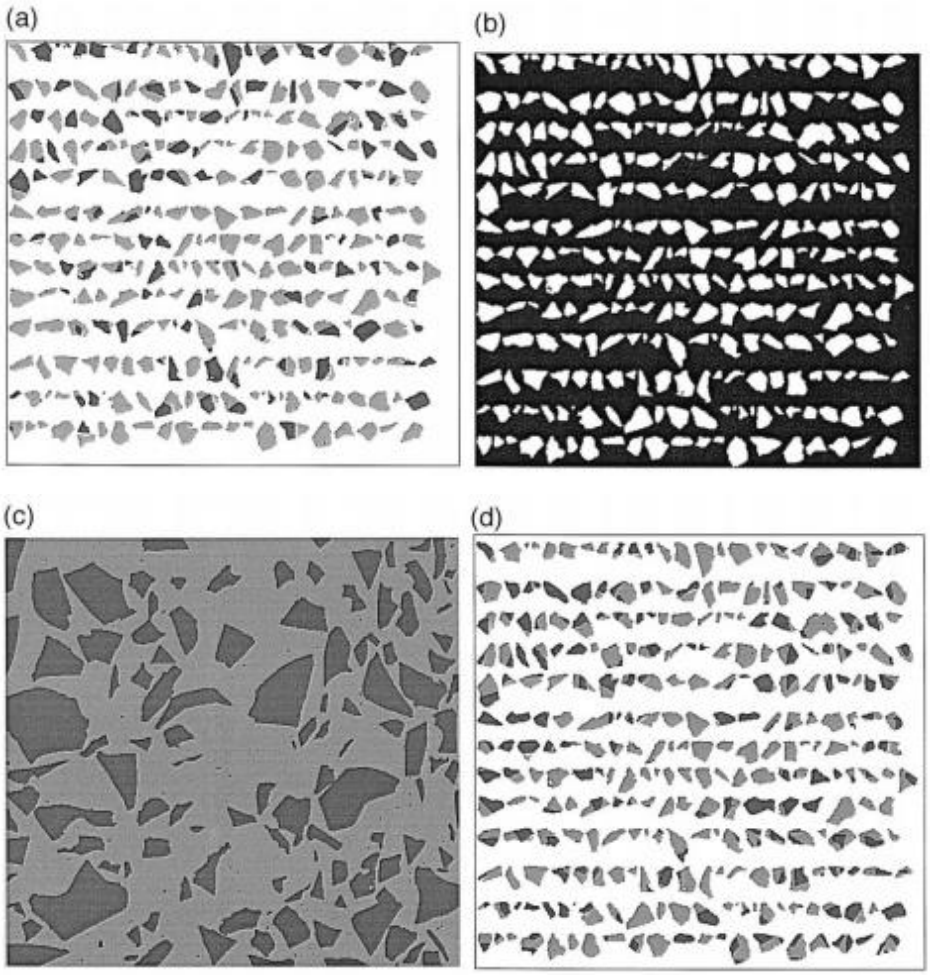

Figure 1.16: a) Particles mounted in resin, b) Generated mask c) Simulated ore texture, d) Progeny particles created after applying the mask, (adapted from [20]).

1.2.6 Stereology

In reality orebodies, particles, and grinded fines are 3D objects. While the majority of ore texture analysis is performed in 2D, there are 3D imaging techniques available to analyze mineral content of orebodies. 3D imaging techniques such as X-ray tomography (XMT) can be used to generate 3D ore textures from mineral samples, but it can be a long, expensive and data intensive process [7]. The 3D interpretation of 2D data is particularly important in the field of ore analysis as it is much easier to collect and interpret 2D images.

Most mineralogical data collected are still 2D textures; however, some error is associated with it, namely stereological bias. Stereology can be derived from its Greek roots. The prefix stereo- refers to the associated Greek word which means “solid”. Therefore, stereology is the study of solids, more specifically the study of 3D structures and the measurement of key geometrical parameters

based on 2D image analysis. Basically, the inference of 3D structure using 2D information. Ueda et. al. illustrated, as seen in Figure 1.17, the associated error with the inference of 3D structure from 2D data [30,31]. The error associated with this interpretation is called stereological bias 30,31].

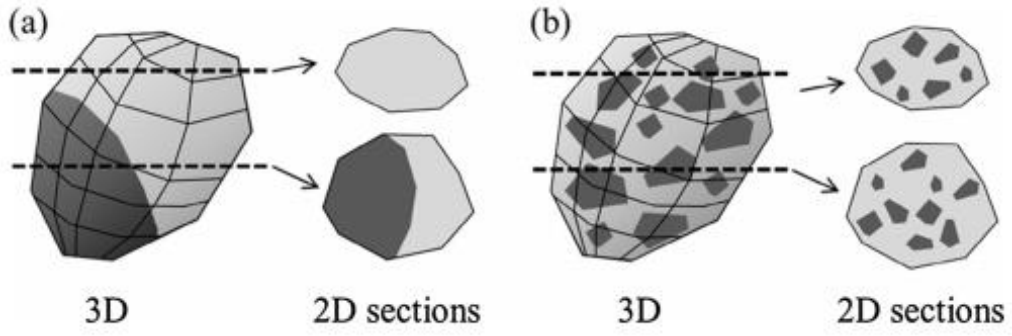

Figure 1.17: Stereological bias in 2D ore textures a) simple texture b) complex texture (adapted from [30,31]).

Depending on the depth of the slice taken in Figure 1.17a) and b), the associated 2D image changes. Therefore, these 2D slices will not recreate the same 3D ore texture and both will not recreate the parent 3D ore texture due to stereological bias. As the ore texture heterogeneity increases from Figure 1.17a) to b), the difference between 2D cuts is less apparent [30,31]. Therefore, for more complex and heterogeneous textures, the effect of stereological bias is lower [30,31]. Minimizing stereological error using stereological correction factors has been a major area of research in the area of mineral liberation.

As mentioned previously, stereological bias varies depending on the complexity of the ore texture [31]. Figure 1.18 illustrates how particles with complex texture have minimal bias while simple textures have a large bias. When most particles are unliberated, they have their highest heterogeneity and therefore a minimal stereological bias [31]. As particles liberate and they become more homogenous stereological bias has a major impact. Once particles are completely liberated, there is no bias related to the degree of liberation as it is 100% [31].

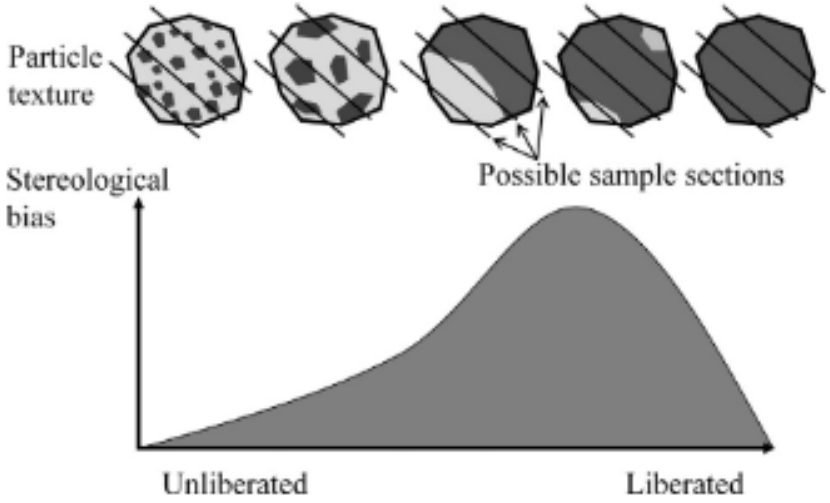

Figure 1.18: How liberation varies with particle complexity and degree of liberation (adapted [31]).

While the degree of stereological bias may be minimal for complex textures, the complexity of texture has not been quantitatively defined in literature. Therefore, Ueda (2016) proposed a model to quantitatively determine the complexity of textures to access the degree of stereological bias [32]. The model is composed of a binary particle numerical simulation of spherical particles. Discrete element method (DEM) was used to model randomly settled spherical particles in a processed sample. An example of a randomized particle bed in shown in Figure 1.19 [32].

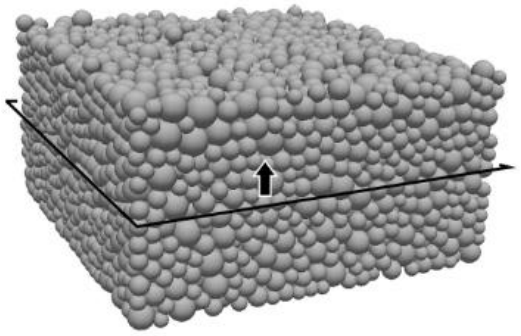

Figure 1.19: Simulated spherical bed of particles (adapted from [32].

The degree of liberation for 2D and 3D measurements were compared to determine the stereological error associated with the simulated texture. A correlation between the overestimate of the degree of liberation and the fractal dimension was obtained for 2D measurements of the simulated texture. The fractal dimension can be interpreted as a measure of complexity for self-similar figures such as particles. The fractal dimension and area fraction can be found through

cross-sectional 2D measurements; therefore, the developed stereological correction factor only depends on 2D information [32].

1.2.7 3D Voronoi Tessellations and Assessing Stereological Bias

Voronoi tessellations have been used to model many 3D structures when multiple separate cells are needed. Examples range across research fields including examining the stereology of 3D ore textures, froth in flotation processes and others [29,30,31].

3D Voronoi tessellation can be used to assess the stereological bias between 2D cross section measurements versus complete 3D data. For example, Ueda et al. (2018) developed a 3D Voronoi model to simulate the internal mineral grain structure of a binary mineral ore texture in 3D [31]. The degree of liberation from random particle cross sections in 2D was compared with the degree of liberation in 3D [31]. From this comparison a quantitative stereological bias was found in terms of volume fraction and size of mineral phase.

X-ray micro-tomography (XMT) has also been used to assess stereological bias. XMT has been used extensively in the medical field for many years. XMT is a tool that can analyze the liberation, fracture network, porosity, and grain size distribution of orebody samples [33]. Scanning electron microscopy (SEM) is also widely used for mineral liberation analysis. Reyes et al. (2017) proposed a methodology for collecting mineralogical information by combining information from 2D SEM images and 3D XMT images [33]. The XMT 3D information was also used to assess the stereological bias associated with 2D SEM images. Crack propagation was observed in ore samples using SEM, XMT systems [33]. Through the analysis of the material properties of the mineral phases present, the occurrence of non-random breakage in the size reduction process can also be identified.

1.3 Objectives and Thesis Outline

Although the global ore grades continue to decline over the years, the surge in computational power and characterization techniques gives hope that a more efficient mineral extraction process can be designed. Mining: however, has complex problems due to the heterogeneity of the ore, where sampling in one area does not necessarily give a complete picture of the entire mine due to the scale of operations. Similarly, small test work results based on core samples are often difficult to interpret and multiple point sampling is, arguably, too expensive to be economically feasible.

Therefore, there is a need to develop new testing and modeling methods that can help overcome these shortcomings and exploit the intrinsic heterogeneity of orebodies to improve mineral liberation and ore sorting. This can be potentially achieved by analyzing textures from core images. The analysis and predictive models can be used to infer a link between texture and processability of certain ore by predicting how the orebody would break under different grinding and crushing conditions. Naturally, a model would need to be computational efficient, and operate at numerous scales throughout the mine to be effective in a real-life setting.

For this work, 2D Voronoi tessellations will be used to simulate ore breakage on textures. Due to the complexity, stereological bias will not be investigated. Therefore, the objectives for this work are:

1. Simulate ore breakage and generate ore grade distributions for different textures using the Voronoi tessellation masking technique.
2. Analyze the different ore grade distributions using different parameterized approaches to model the ore breakage for different textures. Expand on the one beta distribution model provided by King [2,3,4].

This thesis is divided into four main chapters. Chapter 1 provided the background and objectives of this work. Chapter 2 will focus on Objective 1, namely discuss the techniques used to generate the ore grade distributions for different textures. Chapter 3 will focus on Objective 2, that is the analysis and parameterization of the different ore grade distributions. Finally, Chapter 4 draws in the conclusions of this work and suggests other paths for future work.

CHAPTER 2
SYNTHETIC ROCK TEXTURES DISTRIBUTIONS

Simulation of the breakage of binary black/white 2D synthetic ore textures using Voronoi masks was developed into a computer program using Wolfram Mathematica. This program involved the creation of synthetic ore textures, simulation of ore texture breakage, and the collection of mineral liberation data. Table 2.1 provides the summary of the steps involved in the generation and collection of mineral liberation data. Note that ore grade is in terms of percentage area of the valuable mineral as all textures tested are in 2D. For the experiments performed in this work, black pixels were determined to be the desired mineral to be extracted. Therefore, the percentage black of a given ore texture or particle is equivalent to its ore grade.

Table 2-1: Mineral liberation data generation summary.

Data Generation
1.) Generated binary 2D synthetic ore textures
2.) Simulated ore texture breakage using the Voronoi masking technique
3.) Collected the ore grade by size distribution for all textures tested

2.1 Data Generation and Coding Software

Data generation and subsequent data analysis was developed into a computer program, using Wolfram Mathematica (Version 12.1). Mathematica is a technical computing software which covers many fields of interest including data science, image processing, neural networks, and more. Mathematica has extensive options for image creation, manipulation, and processing which

were used to simulate ore texture breakage as well as data analysis options to examine the generated mineral liberation profiles.

2.1.1 Difficulties in Simulating Breakage of Real Ore Textures

Real rock textures commonly have many different textural features as well as a large number of minerals present. Figure 2.1 provides an illustration of how many textural characteristics are present in a small area of a polished rock sample. These complexities can be split into two major textural characteristics: mineralogical composition, and the wide distribution of grain attributes outlined in Table 1-1 (size and size distribution, shape, orientation).

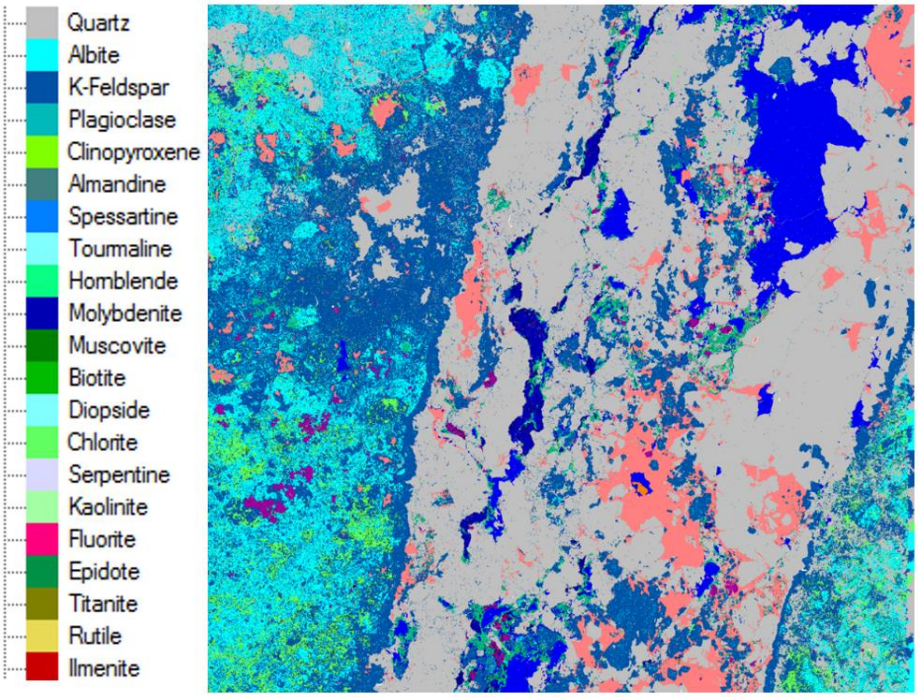

Figure 2.1: False colour MLA image of a polished rock sample. Each colour represents a mineral. Provided by NRC HEM team (2021).

From an economic sense, the minerals in Figure 2.1 can be split up into two groups: commercially valuable minerals and commercially worthless material. If random breakage is assumed, then textural features will have no effect on the fragmentation pattern of the rock texture. Therefore, the rock texture can be simplified to a binary colour scheme, with black being desirable minerals and white being undesirable minerals. In Figure 2.2, different image filters of Figure 2.1 can be created depending on the desirable mineral (blue, pink, grey, cyan). Not only does binarizing the

rock texture simplify modeling, but there is also a reduction in computational time for breakage simulations as less colour data has to be stored for each simulated particle.

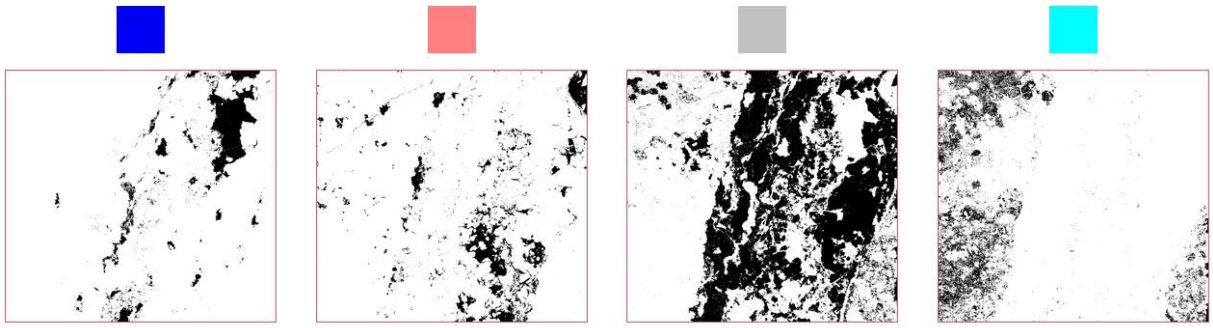

Figure 2.2: Examples of binary filtering of MLA image based on a desirable mineral. The black represents the desired mineral with the original colour shown above from Figure 2.1.

While binarizing simplifies the mineralogical composition of rock texture, there is still a wide range of grain attributes which adds complexity to modeling such as grain size and size distribution, grain shape and grain orientation. Instead of starting with complex textures with multiple textural features, simple textures were synthetically generated, each extracting one or a few textural features. By generating multiple simple textures, distinct textural features can be compared by examining their grade by size distribution after ore breakage simulation. Depending on textural features present, the speed and shape of the changing mineral liberation profile will vary. Therefore, simple, and distinct textural features can be linked to the processability of a given ore texture to be able to predict how similar ore textures will break during size reduction processes. As seen in Figure 2.3 these simple textures can then be used as a baseline for more complex textures, such as the checkerboard and stripes composite, which has multiple textural features. By analyzing and modeling how simple textural patterns will break, combinations of them can be used to explain more complex textures.

Synthetic textures were separated into two groups: 1.) 50/50 black/white textures and 2.) uneven black/white ratio textures. All synthetic textures have two minerals present: valuable minerals represented as black pixels and gangue represented as white pixels. For 50/50 black/white textures, two limiting cases were generated: checkerboard and stripes. The checkerboard texture is alternating in black and white in both the horizontal and vertical directions in 2D as seen in Figure 2.3. The checkerboard texture can be approximated as the simple dissemination of a valuable material in a gangue matrix. The stripes texture is only alternating in one direction and completely

homogenous in the other. The stripes texture can be approximated as a layered structure or alternating rectangular mineral veins. These two limiting cases act as the boundaries from a very heterogenous texture (checkerboard) to an alternating but homogeneous texture (stripes). A composite of 50% checkerboard and 50% stripes was also made to represent more complex rock texture that have more than one textural feature. Two 60/40 black/white textures were created: 1.) staircase, and 2.) staircase + checkerboard. Both of the 60/40 black/white textures were generated to combine checkerboard and stripes textural characteristics. The staircase texture can be viewed as a stripes texture which has been strained or skewed due to mechanical stress. The staircase + checkerboard texture can be viewed as a combination of skewed/strained mineral veins alongside disseminated minerals in a gangue matrix. Finally, a low percentage black stripes texture was generated to compare the percentage black by size distribution of textures with different percentage black but similar texture features.

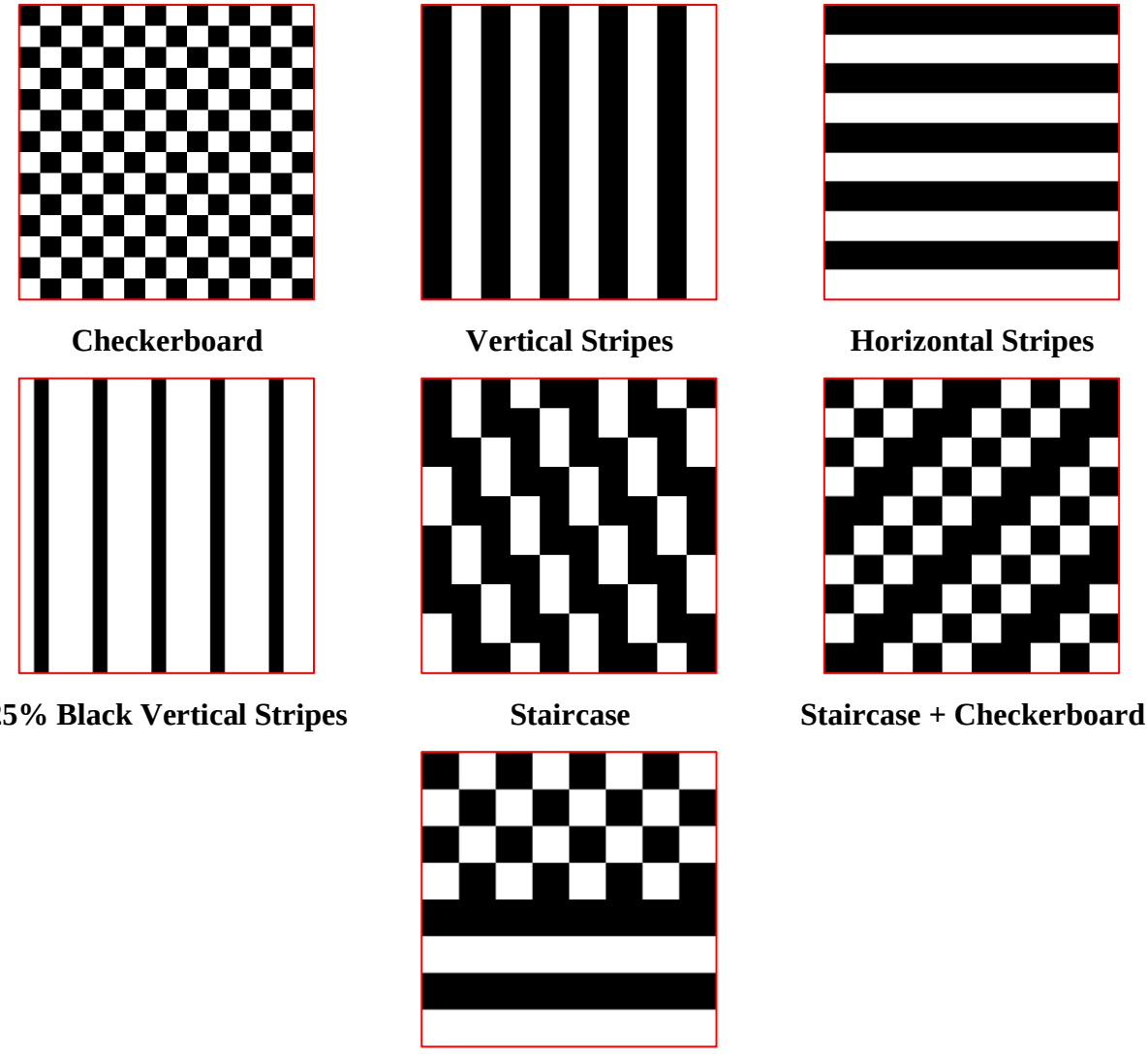

Figure 2.3: Synthetic binary 2D rock textures.

2.1.2 Generating 2D Synthetic Ore Textures

All textures in Figure 2.3 can be mathematically generated using Mathematica. The synthetic ore textures were generated using binary 2D arrays of 1s and 0s with 0s being white pixels and 1s being black pixels. The texture generation process is illustrated in Figure 2.4. Each element of the 2D array represents a pixel of an image. Therefore, different 2D binary textures can be created by modifying the placement of 1s and 0s in the 2D array. The ore grade of the texture can be varied by changing the ratio of 1s to 0s. As mentioned previously, for 2D textures, ore grade can be assumed to be percentage area valuable mineral (in this case percentage black) instead of a volumetric parameter. This will introduce stereological bias in the interpretation of 3D particle

characteristics such as ore grade from 2D texture analysis data. An image is then created by using the location of 1s and 0s in the array as the associated pixel location in the image, and the value (0 or 1) as the pixel colour. All textures created were periodic texture meaning they are infinitely repeating patterns. The base pattern for each periodic texture is given by Table 2-2. The base pattern was defined as the smallest possible permutation of the periodic texture. Each base pattern is made up of smaller base parts, called primitive cells, also illustrated in Table 2-2. The dimensions of each base pattern are equivalent to the number of primitive cells required to make up the base pattern. For example, for the checkerboard texture, 2 black primitive cells and 2 white primitive cells make up the checkerboard base pattern for a total of 4 primitive cells.

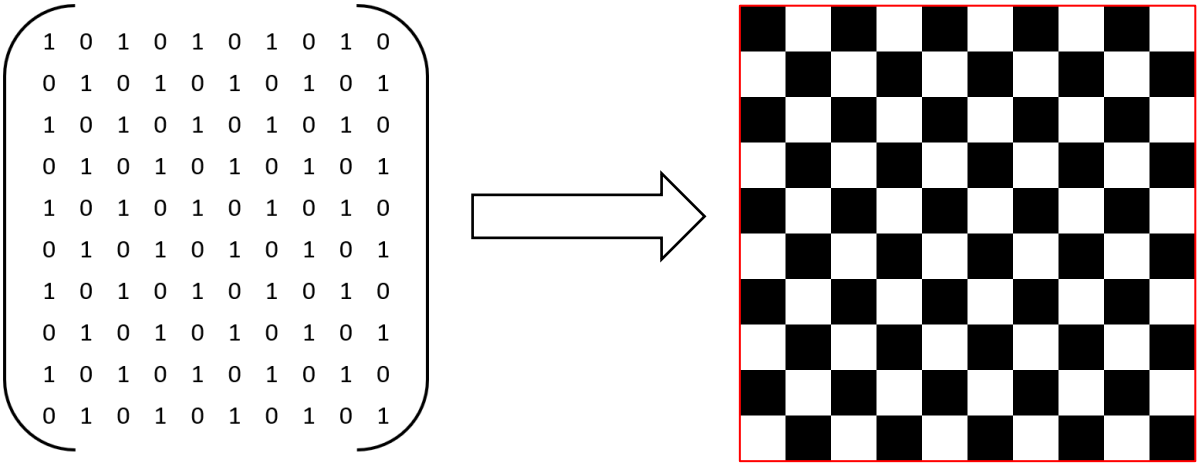

Figure 2.4: Synthetic texture generation from binary array to black and white image.

Table 2-2: Base patterns for all synthetic textures generated.

Texture Name:	Periodic Texture	Base Pattern	Primitive Cell (Green)
Checkerboard	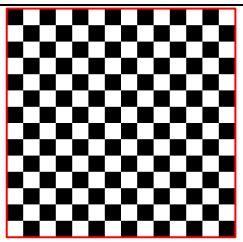	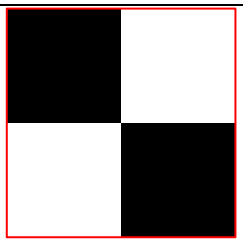	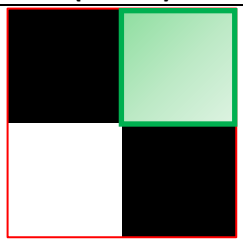
Vertical Stripes	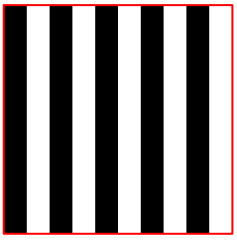		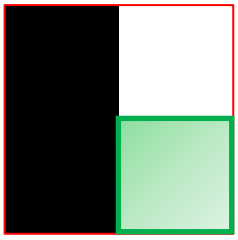
Horizontal Stripes	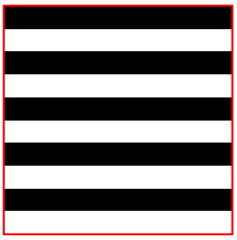		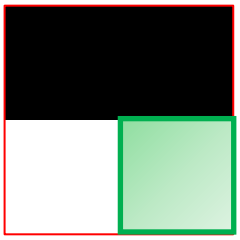
Staircase	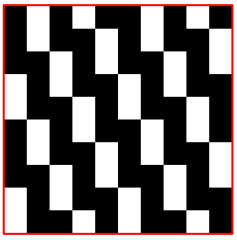	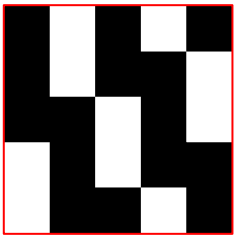	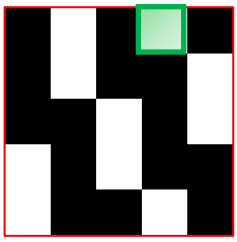
Staircase + Checkerboard	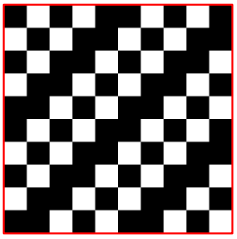	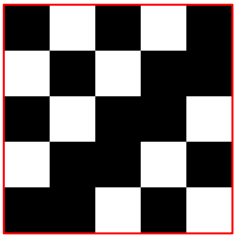	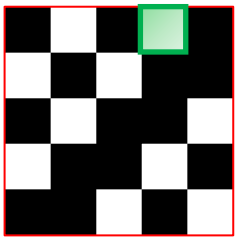
25% Black Vertical Stripes	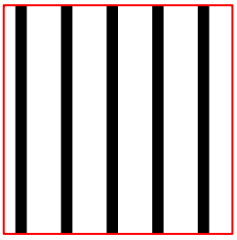		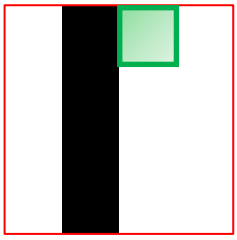

2.1.3 Voronoi Mask Algorithm and Ore Grade by Size Data Collection

Voronoi tessellations was the masking technique chosen for size reduction simulations as Voronoi tessellation patterns form realistic and varied product child particles [18]. Voronoi tessellation masks were created using a built-in Mathematica function with a few key inputs. The first input were the random generating seeds used to create the Voronoi cells. These seeds were generated as (x,y) coordinates in a 1000 x 1000-pixel bounded box using Mathematica's random number generator. A bounding box was created to insure the Voronoi mask had the same dimensions as the ore texture to broken up. This will introduce slight inherent border bias associated with border Voronoi cells. The bounding box may cut off portions of border cells which introduces bias in the ore grade distribution of border cells. If Voronoi cell size is too large, bias associated with border cells becomes larger as there is a larger ratio of border to inside cells If Voronoi cell size is too small, unrealistic pixelated particles are formed. Therefore, a balance was made between realistic particles and border bias.

Voronoi seeds were then slightly modified by using a process called relaxation. By creating a Voronoi mask at the mean vertex positions of the previously generated Voronoi cells, the generating seeds start to move towards the center providing higher circularity to generated particles. Figure 2.5 shows the progressive increase in circularity of Voronoi cells as relaxation is applied.

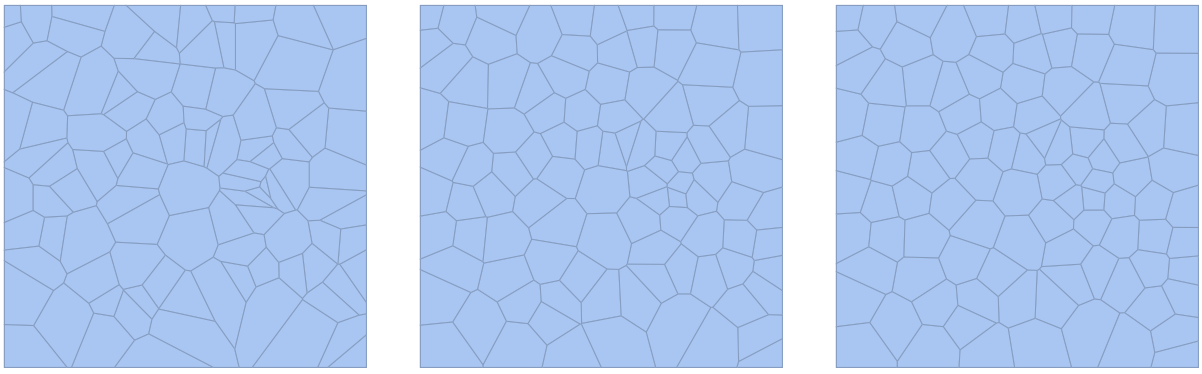

Figure 2.5: Relaxation of a Voronoi mesh with a) no relaxations, b) one relaxation, and c) two relaxations.

To create a sufficient number of particles to analyze and model, a total of 1000 equally sized Voronoi masks were randomly generated with each Voronoi mask containing a fragmentation

pattern for 1000 particles. In other words, one million Voronoi cells were generated to create sufficient mineral liberation data for statistical analysis. A large quantity of particles over a wide range of particle sizes is important to reduce noise in the collected ore grade by size distribution.

These Voronoi masks were then superimposed onto synthetic textures to simulate ore breakage. The pixel values in the synthetic ore texture must be assigned to the associated Voronoi cells to simulate ore breakage and create child particles of varying sizes and percentage black. As seen in Figure 2.6, a problem arises when superimposing a Voronoi mask defined by a real number (i.e., decimals) over a pixel image based on integer locations. Each texture is created using an integer number of pixels, in this case, one million. At the pixel level, Voronoi mask edges may cut across the center of a pixel leaving a portion of one pixel in two or more particles. This can lead to double counting or more of pixels where the same pixel is assigned to multiple Voronoi cells which can be seen in Figure 2.6b between the boundary of cells 1 and 5.

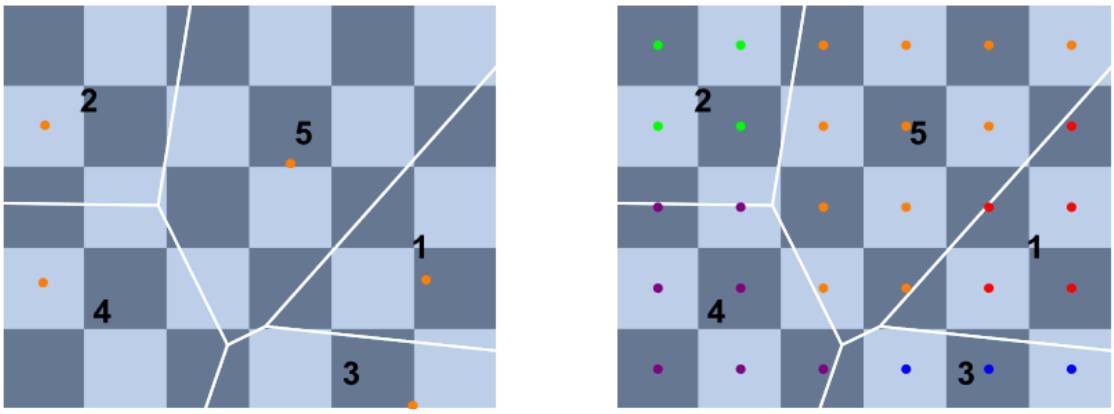

a) b)

Figure 2.6: Superimposing a Voronoi mesh onto a pixel texture. Each square represents one pixel, with a) the location of the seeds (orange dots) of the mesh, and b) the assigned pixels to each Voronoi cell.

Although the case presented in Figure 2.6 is an extreme example due to the small image size (30 pixels), double counting was still observed with 1000x1000 pixel images. Double counting of pixels leads to the addition of artificial data into the overall particle ore grade data set. To avoid double or more, two pieces of logic were added to the program for particle border pixels. Firstly, if most of a pixel area is in a certain cell, that cell will be assign that pixel and secondly, if the pixel area is split evenly between relevant cells, then randomly assign the pixel to one of the cells.

2.1.4 Widening the Size Distribution of Synthetic Progeny Particles by Scaling

It is easier and computationally faster to generate differently size particles by scaling texture size instead of changing the size of Voronoi masks. For the same pixel area, larger particles required exponentially more simulations for the same number of particles as they take up more pixel space in the texture. Due to the periodic nature of the synthetic ore textures created, image size can be scaled to generate a wide range of particle sizes after particle area scaling. Instead of varying the Voronoi mask size, the same group of Voronoi masks were applied to multiple sizes of the same texture. As seen in Figure 2.7, moving from a) to c), the squares in the checkerboard texture become smaller, analogous to zooming out from a) to b) to c). If it is presumed that a single checkerboard square in Figure 2.7 has the same area in each image then, the red particle size increases from a) to c). By varying texture size for the same Voronoi mask, particles of varied sizes can be generated quickly. For each texture type, five texture sizes were generated to be able to widen the size distribution of particles.

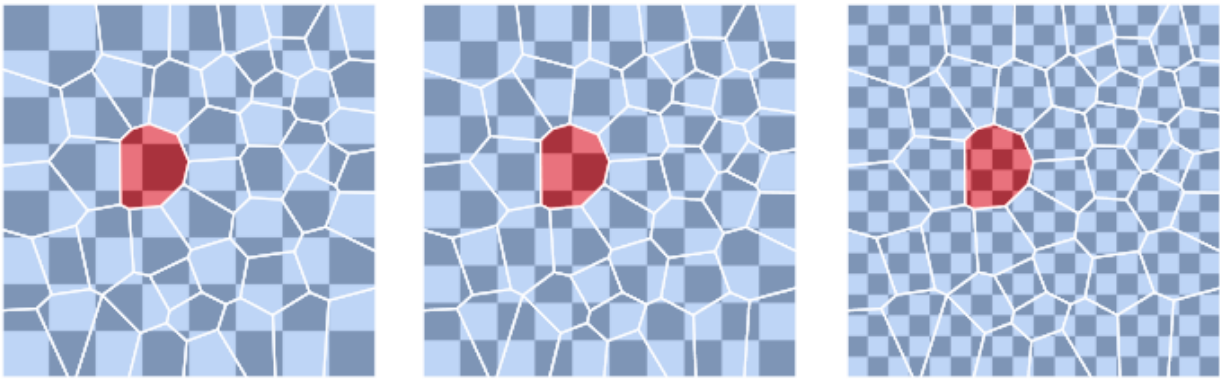

a) 8x8 b) 10x10 c)18x18

Figure 2.7: Scaling particle size by varying image textural feature size, a) 8x8 checkerboard squares, b) 10x10 checkerboard squares, c) 18x18 checkerboard squares.

To combine particle populations of different texture sizes, particles must be brought to the same basis. The size scale of a given texture is dictated by the number of primitive cells present in the image. The primitive cell for all synthetic textures is highlighted in green in Table 2.2. The more primitive cells present in a texture, the larger scaled particles will be after normalization. The scaled area formula is given by equation 2.1 and 2.2. At a scaled particle area of 1, the particle area is equivalent to the primitive cell area. A scaled particle area of 1 is of particular interest as this is the point where particles for all texture types can be completely liberated. By contrast,

particles may completely liberate above a scaled area of 1 due to the organization of primitive cells into different textural features.

$$SF = \frac{A_T}{\#\ of\ Primitive\ Cells} \quad [2.1]$$

$$A_{p,s} = \frac{A_p}{SF} \quad [2.2]$$

Where A_T is total texture area, SF is scaling factor, A_p is particle area, and $A_{p,s}$ is scaled particle area.

After particle area scaling, the area of one primitive cell is assumed to be equal for all texture sizes. By scaling the particle area of all particles, particles from different texture sizes can be grouped and a wide size distribution of particles can be formed.

Simulated particles with assigned black and/or white pixels are then organized into separate particle size classes and mineral liberation data is extracted including percentage black (ore grade) as well as particle area. By separating particles into size classes, the percentage black distribution of particles can be examining across the range of large to small particles to view the shape and speed of the changing mineral liberation profile. As seen in Figure 2.8, depending on particle size, the percentage black distribution can vary greatly. At large particle sizes, almost all particles are likely to be centered around the overall mean percentage black of the ore texture. At medium particle sizes the peak widens as there is a greater variation in particle percentage black. At small particle sizes, a binomial distribution starts to form where most particles are either completely white (0) or completely black (1). The simulation conditions for Monte Carlo Voronoi mask simulations are given by Table 2-3.

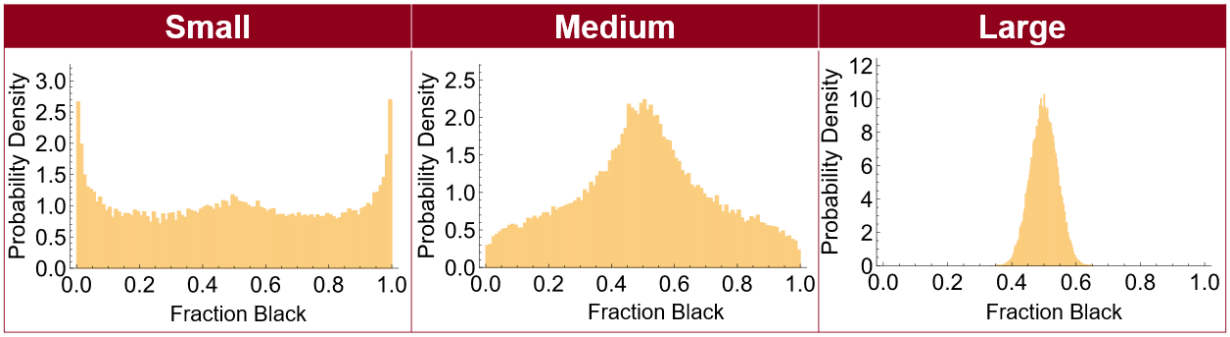

Figure 2.8: Example of an ore grade by size distribution of a binary 50/50 black/white 2D checkerboard texture.

Table 2-3: Voronoi mask simulation conditions repeated for each texture type given in Figure 2.3.

Step	Counts
1.) 1000 x 1000 Pixel synthetic ore texture	1,000,000 pixels/image
2.) 1000 Cell randomly generated Voronoi mesh x 1000	1,000,000 particle/image
3.) 5 Texture sizes per texture type	5,000,000 particles
4.) Particles separated into 100 equal bin sizes	~ 50,000 particles/bin
5.) Mix distribution parameters generated per bin size	100 percentage black distributions

2.2 50/50 Black/White Rock Textures Mineral Liberation Profile

50/50 binary synthetic texture have predictable symmetry in the speed and shape of the changing percentage black distribution as particle size decreases during size reduction simulation. There is an equal number of black and white pixels present in 50/50 textures therefore, it is equally likely that a particle increases in percentage white or in percentage black as particle size decreases. 50/50 synthetic textures tested are given by Figure 2.9. Depending on texture type, the speed and shape of the changing mineral liberation profile varies greatly.

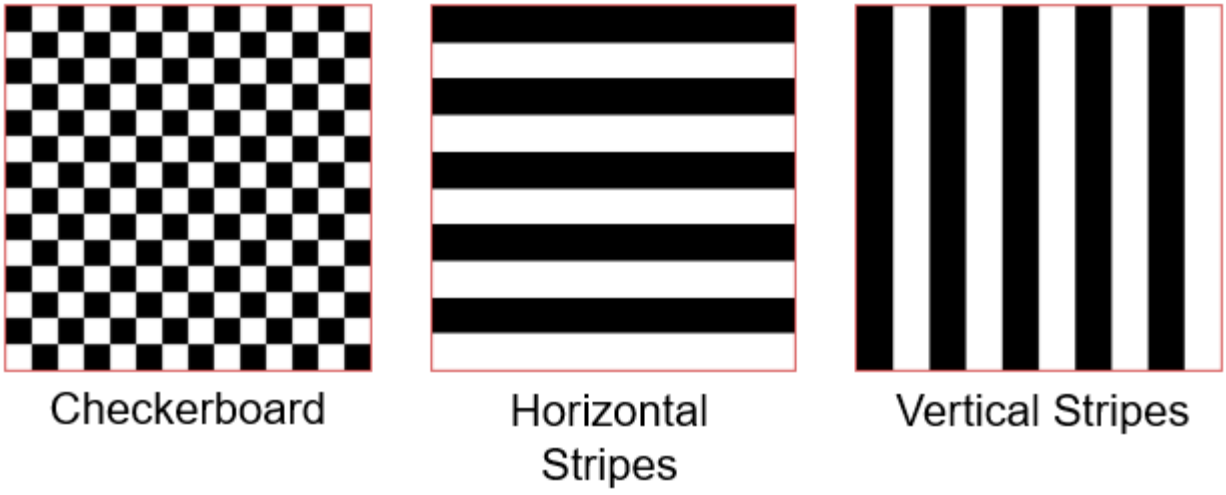

Figure 2.9: 50/50 Synthetic Textures: a) Checkerboard pattern, b) Horizontal stripes pattern, c) Vertical stripes pattern

As noted in Section 2.1.3, a binary texture mineral liberation profile follows the general form of a single peak at large particle sizes centered around the overall texture ore grade. As particle size decreases, the peak widens, moving towards a bimodal distribution where particles are either 100% one mineral or the other at small particle sizes. In this general case, there are three distinct stages populations of particles can be in:

1. unliberated particles centered around the overall texture mean ore grade,
2. liberating particles, and
3. liberated particles.

2.2.1 Stripes Texture Ore Grade by Size Distribution

The stripes texture pattern is analogous to a layered structure, in which minerals grains alternate between layers. Each stripe, white or black, has equivalent area in the case of a 50/50 texture with the overall texture having an even number of stripes. If there is no orientational bias during the creation of the Voronoi mask, the liberation profile of stripes in the x or y axis should be the same. If there is orientational bias, depending on striping orientation in the texture, the shape and speed of the changing mineral liberation profile will vary. For example, in an instance in which Voronoi cells are on average longer along the x-axis then y-axis, liberation of valuable material is more likely when the texture stripes are also orientated in the horizontal direction. Therefore, ore breakage simulations were performed on both horizontal stripes and vertical stripes textures to confirm that no there is no orientational bias in the production of Voronoi masks.

2D probability density histograms across a wide range of scaled particle sizes were used to illustrate the complete percentage black by size distribution. The collection of 2D percentage black by size distribution histograms provides the likelihood of a given particle being a given percentage black across a range of particle sizes as the size reduction process proceeds. The x-axis provides the area fraction of black for a given particle with 0 being completely white particles and 1 being completely black particles. The vertical y-axis provides the probability density, in other words, the likelihood that a particle is a given fraction black. The z-axis is the scaled particle area. As particle area changes, so does the percentage black distribution. As seen in Figure 2.10, the changing stripes texture mineral liberation profile has four identifiable populations of particles over the complete range of particle areas: 1.) Particles which are still unliberated centered around the overall stripes texture percentage black, 2.) particles which are increasing in percentage black, and 3.) particle which are decreasing in percentage black (increasing in percentage white), 4.) liberated particles.

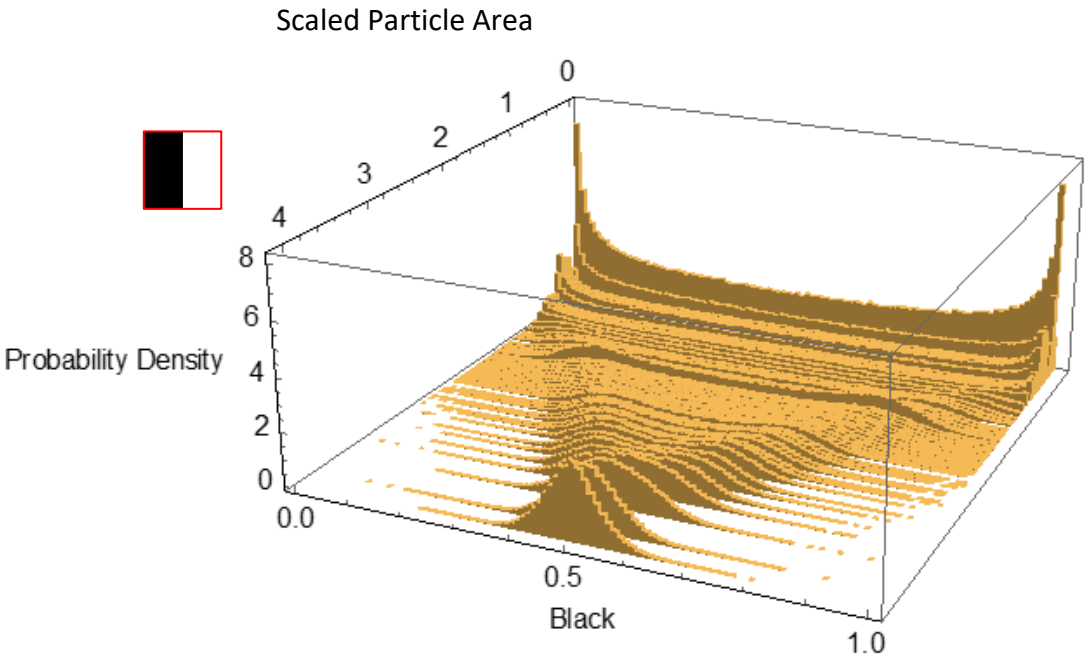

Figure 2.10: Collection of 2D Ore grade histograms for scaled areas 0 – 4, stripes texture.

From Figure 2.10, four snapshots along the size reduction process were taken to illustrate the change in the percentage black distribution as scaled particle area changes, as seen in Figure 2.11. In Figure 2.11c), at a scaled particle area of 1.5, the initial peak of unliberated particles widens into two symmetrical peaks which move towards the extremities of completely white/black

particles as seen in Figure 2.11a). These particle populations are liberating equally in opposite directions. The two peaks of liberating particles are symmetrical as the overall white/black ratio is 50/50, therefore it is equally likely that a particle increases in percentage white or in percentage black. Completely liberated particles (100% white or 100% black) can be seen at smaller scaled particle areas below 1.0 as seen in Figure 2.11a) & b). The population of particles yet to liberate particles is harder to identify as particle area decreases and can be more clearly viewed at large particle areas. As seen in Figure 2.11d), at large scaled particle areas above 3.0, almost all particles are centered around the overall stripes texture percentage black of 50%. Overall, there was no difference in the percentage black by size distribution of vertical and horizontal stripes, therefore only the results for vertical stripes are shown.

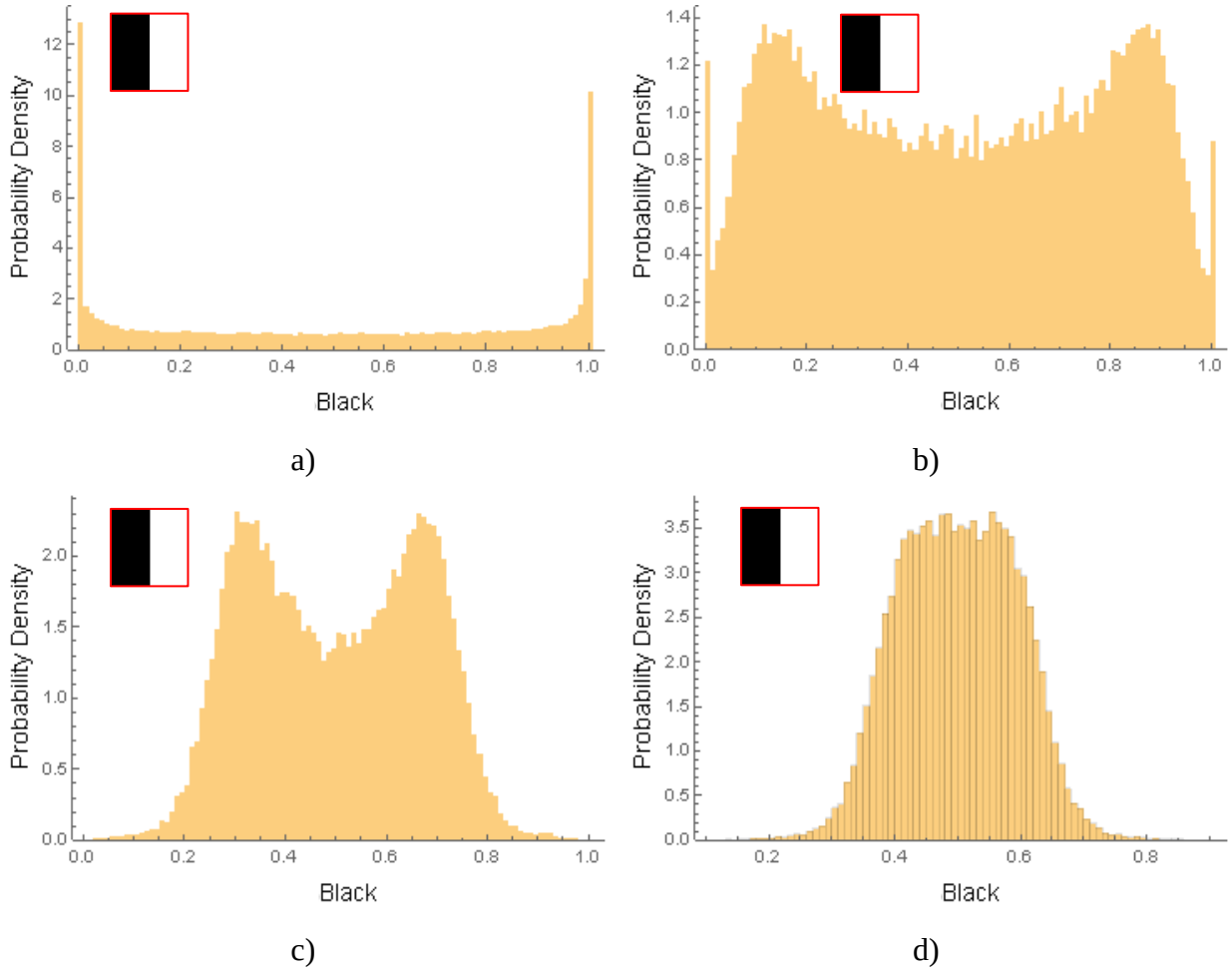

Figure 2.11: 2D Ore grade histogram snapshots, stripes texture at a) 0.5, b) 1.0, c) 2.0, and d) 3.0 scaled particle sizes.

2.2.2 Checkerboard Texture Ore Grade by Size Distribution

The checkerboard pattern can be viewed as a uniform version of disseminated minerals in a gangue matrix. Each mineral grain, black or white, is a square of equivalent area. There is no potential for orientational bias for the checkerboard pattern as there is no change between textural features in the horizontal and vertical direction. Analogous to the striping pattern, the checkerboard texture percentage black by size distribution also has the same four identifiable particle populations as particle size decreases as seen in Figure 2.12:

1. unliberated particles,
2. particles increasing in grade,
3. particles decreasing in grade, and
4. liberated particles.

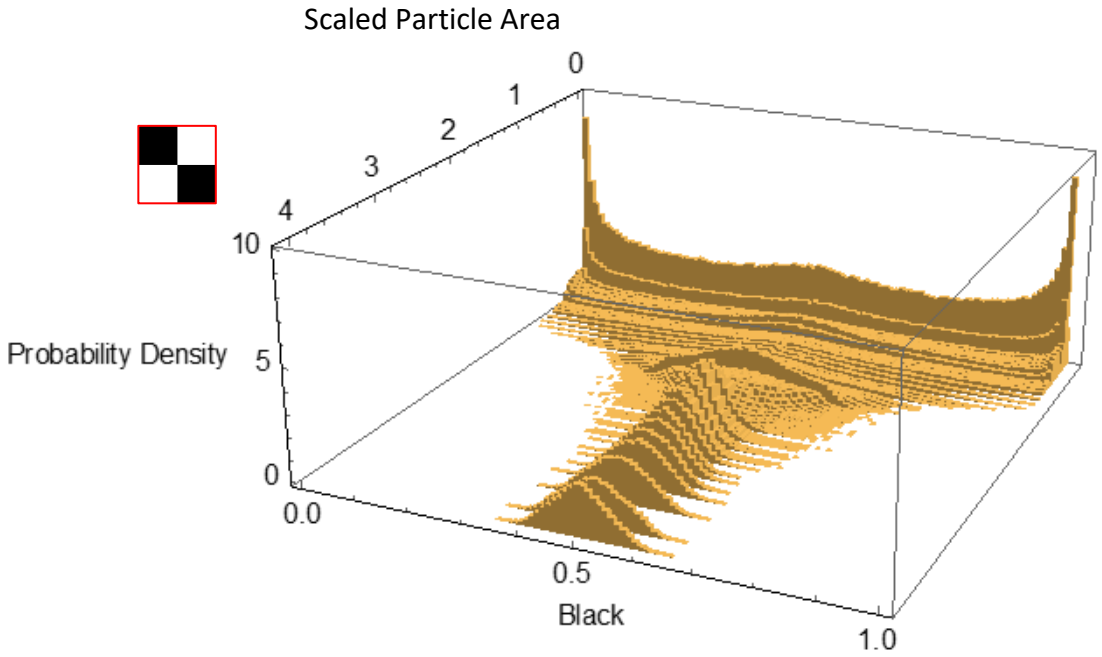

Figure 2.12: Collection of 2D ore grade histograms for scaled areas 0 - 4, checkerboard texture.

In Figure 2.13, four 2D histogram snapshots were taken from Figure 2.12 to show the change in percentage black distribution as scaled particle area decreases. The liberating populations are more clearly seen at scaled areas between 1.0-2.0 as seen in in Figure 2.13b) & c). As the initial peak of particles centered around the stripes texture percentage black of 50% widens, two symmetrical shoulders move towards the extremities (100% white or 100% black). The population of unliberated particles centered around the 50% black is distinct and can be seen even at low particle areas such as in Figure 2.13a). Completely liberated white or black particles only start to appear below scaled particle areas of 1 when the average particle area is equal or smaller than the area of the primitive cell.

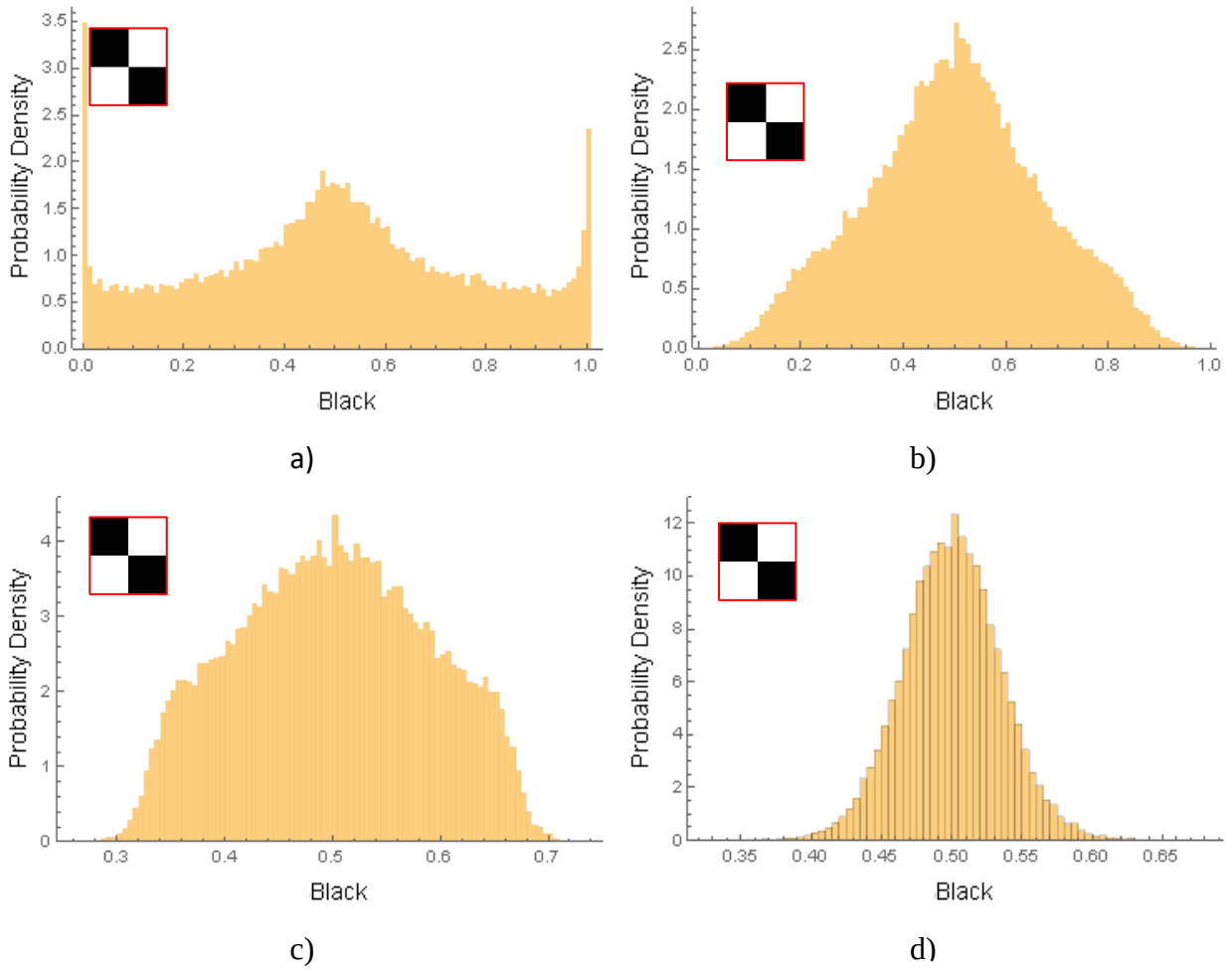

Figure 2.13: 2D Ore grade histogram snapshots, checkerboard texture at a) 0.5, b) 1.0, c) 2.0, and d) 3.0 scaled particle sizes.

There are major differences between the speed of mineral liberation, as well as the shape of the changing mineral liberation profile for the checkerboard and stripes texture. As particle area decreases, a greater proportion of unliberated particles start to symmetrically liberate in the striping texture when compared with the checkerboard texture. For the checkerboard texture, as particle area decreases, a larger portion of particles remain unliberated centered around the overall checkerboard texture percentage black of 50% while a smaller portion of particles start to liberate towards 100% white or black. This makes intuitive sense as the stripes texture is alternating colours in one orientation, but homogenous in the given stripe orientation while the checkerboard texture is alternating in both orientations. Therefore, particles reducing in size are more likely to increase in percentage white or percentage black in a striping pattern due to the homogenous nature of mineral grains present.

2.3 Uneven Black/White Rock Textures

More complex synthetic textures were generated to combine textural effects from simple textures such as checkerboard and striping as well as introduce more textural effects in 2D space. The following textures generated, as seen in Figure 2.14 are not 50/50 black/white, therefore the liberating populations will not be symmetrical.

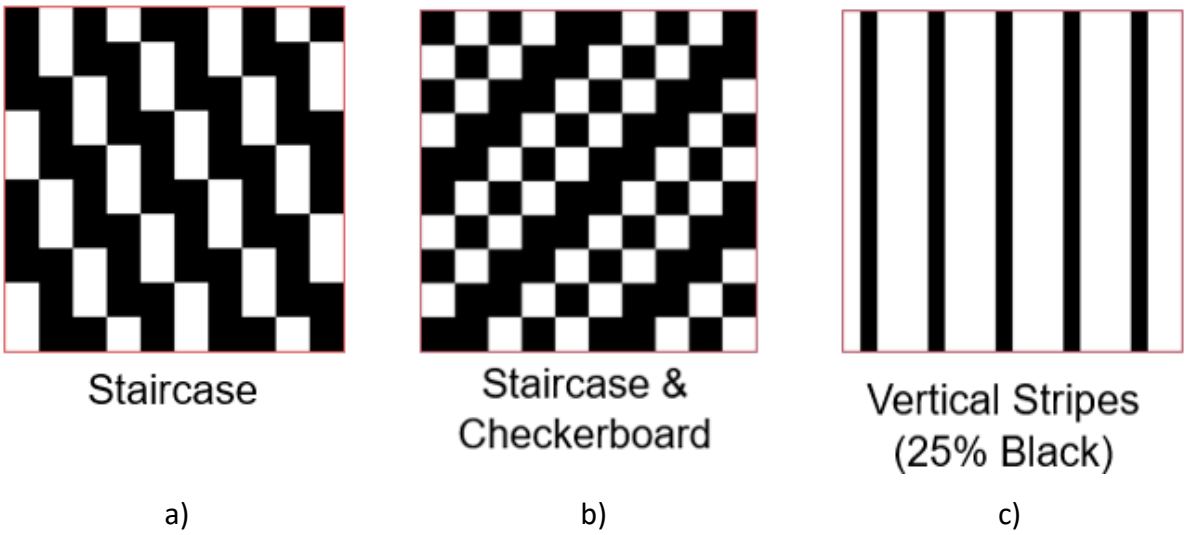

Figure 2.14: Uneven Black/White Ratio Textures: a) 60/40 Staircase pattern, b) 60/40 Staircase & checkerboard pattern, c) 25/75 Vertical Stripes pattern.

2.3.1 Staircase Texture Ore Grade by Size Distribution

The 60% black, 40% white staircase texture can be viewed as a layered structure that has been strained, changing the orientation of mineral grains. As illustrated in Figure 2.15, the staircase pattern also has four distinct particle populations: unliberated, increasing or decreasing percentage black, and liberated particles (100% white or 100% black). As seen in Figure 2.16, four percentage black distributions at multiple scale particle areas along the size reduction process were extracted from Figure 2.15. Liberating particles are most easily seen in Figure 2.16b), where two population of particles move towards the extremities of 100% black or 100% white. The peak of particles moving towards 100% black is larger due to the 3:2 ratio of black to white pixels in the overall texture. Therefore, it is more likely that particles increase in percentage black then percentage white as particle area decreases. Completely liberated particles start to appear as 100% black particles first and can be seen below a scaled particle area of 2.0. An unliberated population of

particles centered around the overall texture percentage black of 60% is seen in Figure 2.16d) at high scaled particle areas above 3.0.

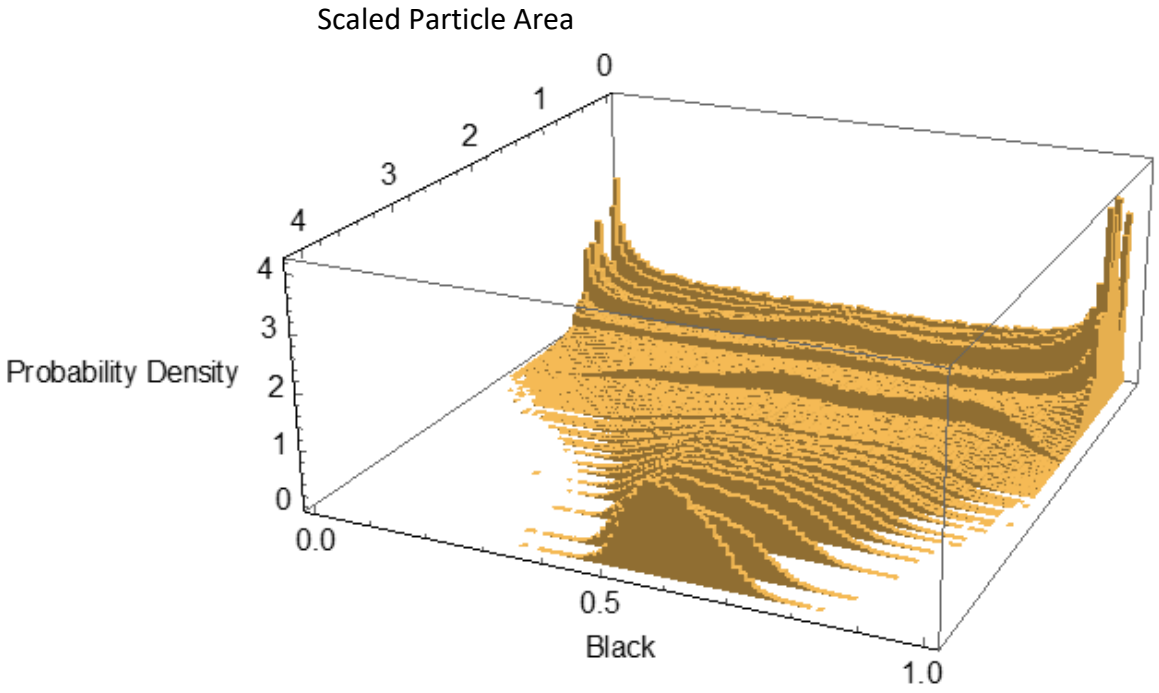

Figure 2.15: Collection of 2D ore grade histograms for scaled areas 0 - 4, staircase texture.

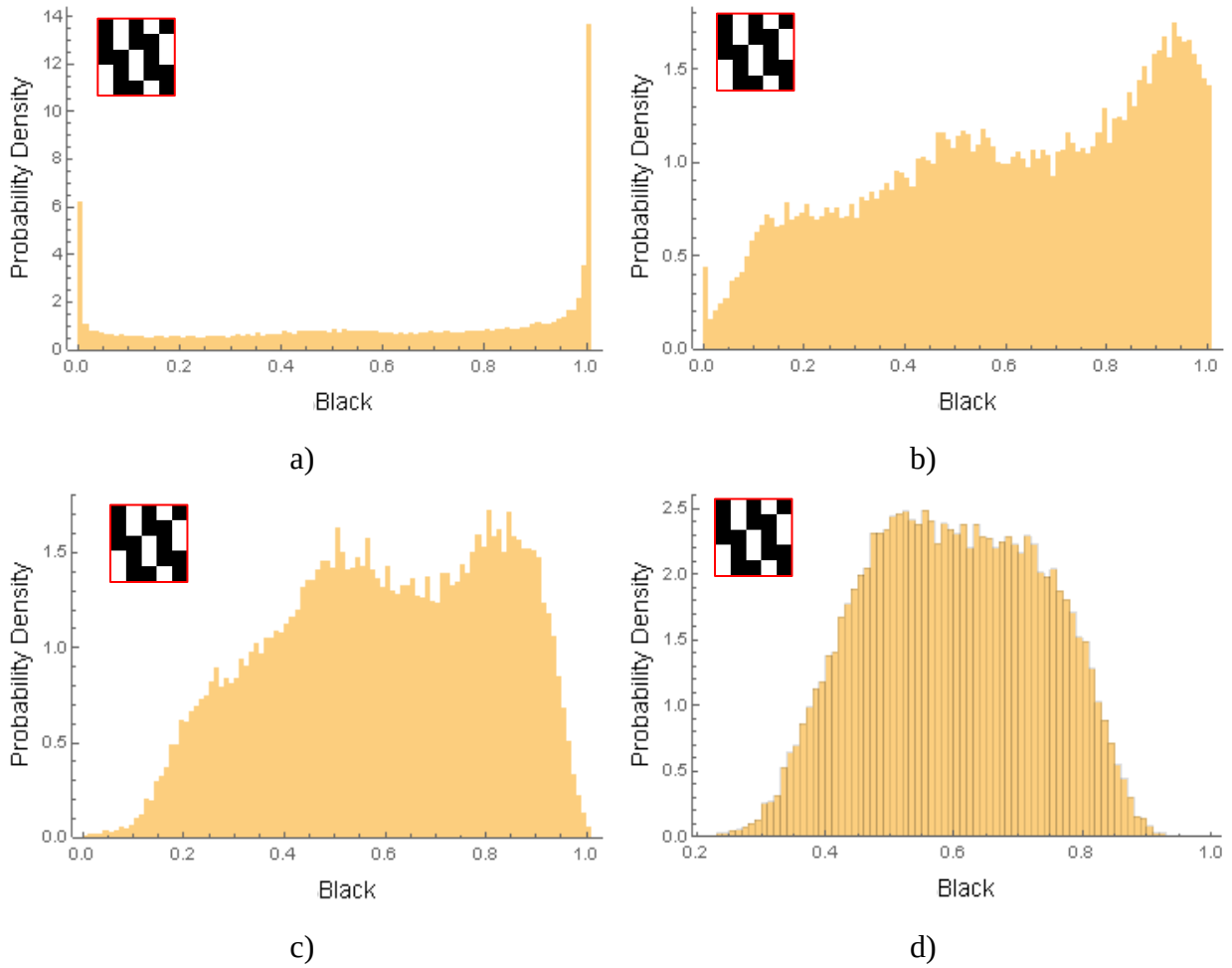

Figure 2.16: 2D Ore grade histogram snapshots, staircase texture at a) 0.5, b) 1.0, c) 2.0, and d) 3.0 scaled particle sizes.

2.3.2 Staircase + Checkerboard Texture Ore Grade by Size Distribution

The 60% black, 40% white checkerboard + staircase texture can be viewed as a mixture of simplified dissemination and a diagonal strained structure. This texture both incorporates long homogenous diagonal mineral grains alongside small disseminated mineral grains to add texture complexity. From Figure 2.17 one can see visually that there are more distinct populations present over the range of scaled particle areas then previous textures. Figure 2.18 provides four snap shots of the percentage black by size distribution as the size reduction process proceeds for the staircase + checkerboard texture.

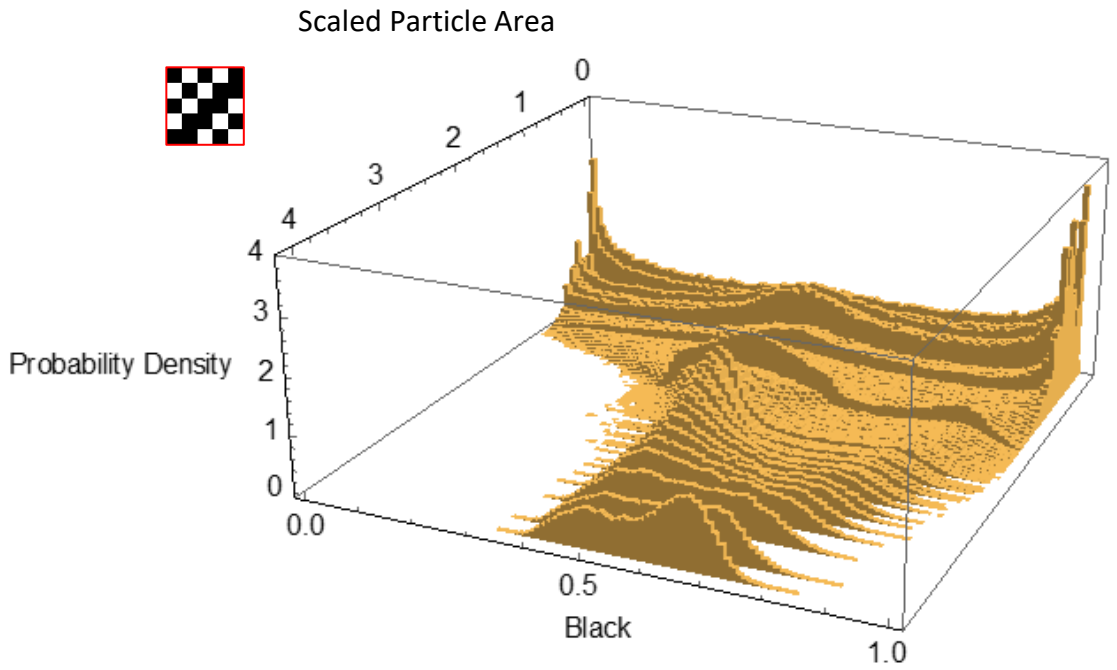

Figure 2.17: Collection of 2D ore grade histograms for scaled areas 0 - 4, staircase + checkerboard texture.

The checkerboard portions of the texture contribute to particles liberating in symmetrical shoulders, mostly clearly seen in Figure 2.18b), centered around 50% black as particle area decreases. As seen in Figure 2.18b) & c), there is a third identifiable liberating population of particles due to the diagonal homogenous black mineral grains in the overall texture leading to a higher likelihood of high percentage black particles. Similar to the staircase texture, completely liberated particles start to appear as 100% black particles first, as scaled particle area decreases below 1.0. The populations of unliberated particles are harder to identify due to the different textural features present.

Even at a large scaled area of 4, there are still two distinct peaks of particles present in the percentage black distribution with the smaller peak at 50% black, and the larger peak slightly above 60% black (Figure 2.17). Table 2.4 illustrates how particles created in different positions across the texture surface contribute to the two peaks. When particles contain the staircase portion of the texture, the percentage black of the particle is high leading to the larger peak above just above 60% black. When the particle contains the checkerboard portion of the texture the percentage black of the particle becomes around 50% leading to the small peak. Due to the distinct difference in textural features between the checkerboard and staircase portion of this texture, much

larger particles of scaled areas equal to the base pattern (25 scaled area) would be required to see a single peak centered around the overall texture percentage black of 60%.

Table 2-4: Change in ore grade based on position of blue particle

Particle Position	Base Pattern with Simple Square Blue Particle: (Scaled Area = 4)	Ore Grade of Blue Particle
Top Left	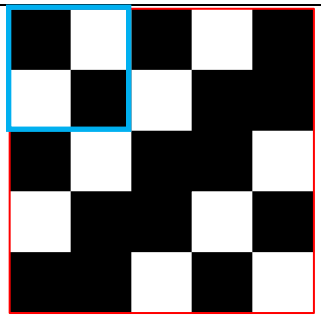	50%
Top Right	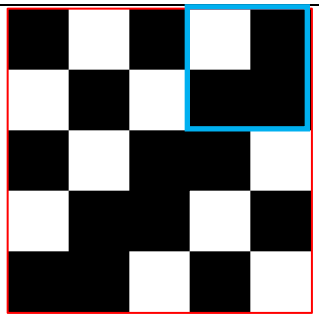	75%
Bottom Left	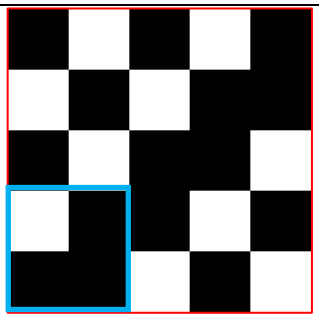	75%
Bottom Right	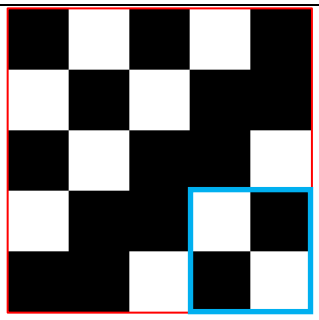	50%

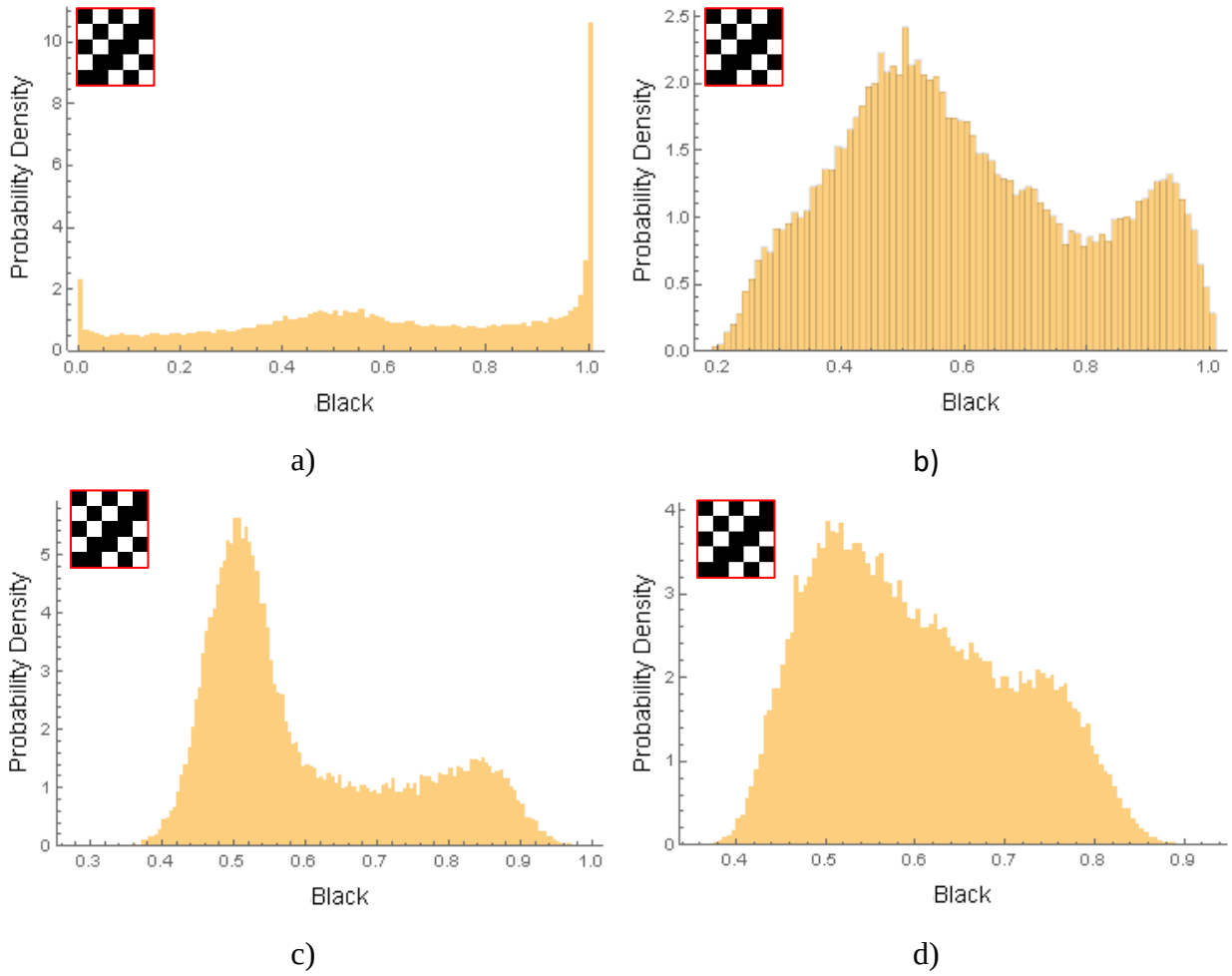

Figure 2.18: 2D Ore grade histogram snapshots, staircase + checkerboard texture, at a) 0.5, b) 1.0, c) 2.0, and d) 3.0 scaled particle areas.

2.3.3 Low Grade Vertical Stripes Ore Grade by Size Distribution

The 25% black, 75% white striping pattern can be viewed as mineral veining in a large gangue matrix. In real ore extraction operations, the average ore grade of common orebodies is typically low and has been declining year over year. Therefore, a low percentage black synthetic texture was generated to simulate the mineral liberation profile of low ore-grade orebodies. Liberation of particles in the low percentage black stripe texture proceeds similarly to 50/50 black/white stripes with four distinct populations, liberated particles, unliberated particles, as well as two peaks of particles moving towards the extremities of either completely white or black, as seen in Figure 2.19. Due to the 3/1 ratio of white to black pixels, particles are much more likely to

increase in percentage white then percentage black as scaled area decreases. Figure 2.20 provides four snapshots of the percentage black by size distribution over a very wide range of scaled particle areas. As seen in Figure 2.20c) , completely white particles start to appear at larger scaled areas below 10. Completely liberated black particles do not start to appear until scaled particle area decreases below 1.0. At very large scaled areas above 20, unliberated particles can be seen centered around the overall texture percentage black of 25%.

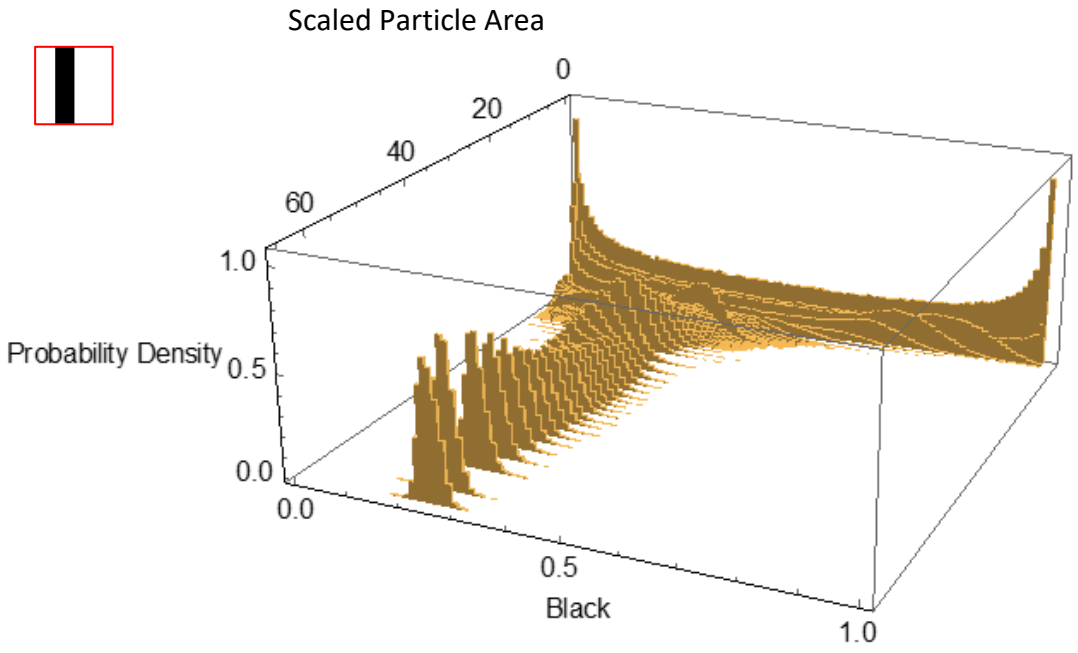

Figure 2.19: Collection of 2D ore grade histograms for scaled areas 0 - 65, low percentage black stripes texture.

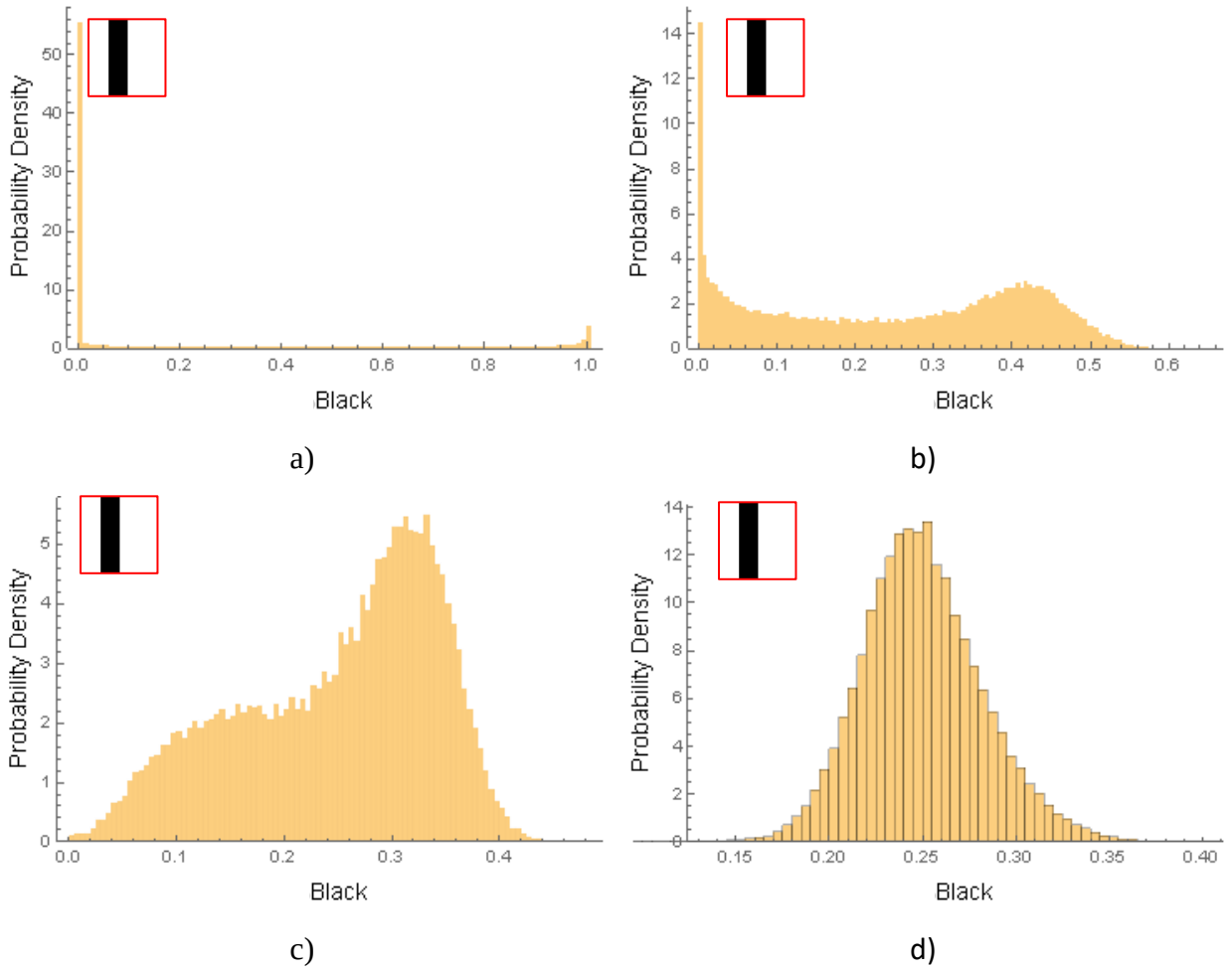

Figure 2.20: 2D Ore grade histogram snapshots, low percentage black stripes texture, at a) 0.5, b) 5, c) 10, and d) 20 scaled particle sizes.

2.4 Composite Rock Textures

As mentioned Section 1.1.2, real rock textures are a combination of many textural features including mineral composition, mineral grain size and size distribution, grain shape, and grain orientation. A composite of striping and checkerboard patterns was generated, as illustrated in Figure 2.21, to examine the effect of combining multiple simple textural features.

Figure 2.21: 50/50 Checkerboard + Horizontal Stripes composite texture.

The expected ore grade by size distribution is seen in Figure 2.22, in which as particle sizes decreases, there are two sets of symmetrical populations of liberating particles that are moving towards the extremities of 100% white or black. The first set of symmetrical populations comes from particles liberating in the striping section of the texture. As seen in Figure 2.23c), these particles liberate quicker due to the homogeneous texture colour of stripes, albeit alternating, in the horizontal direction.

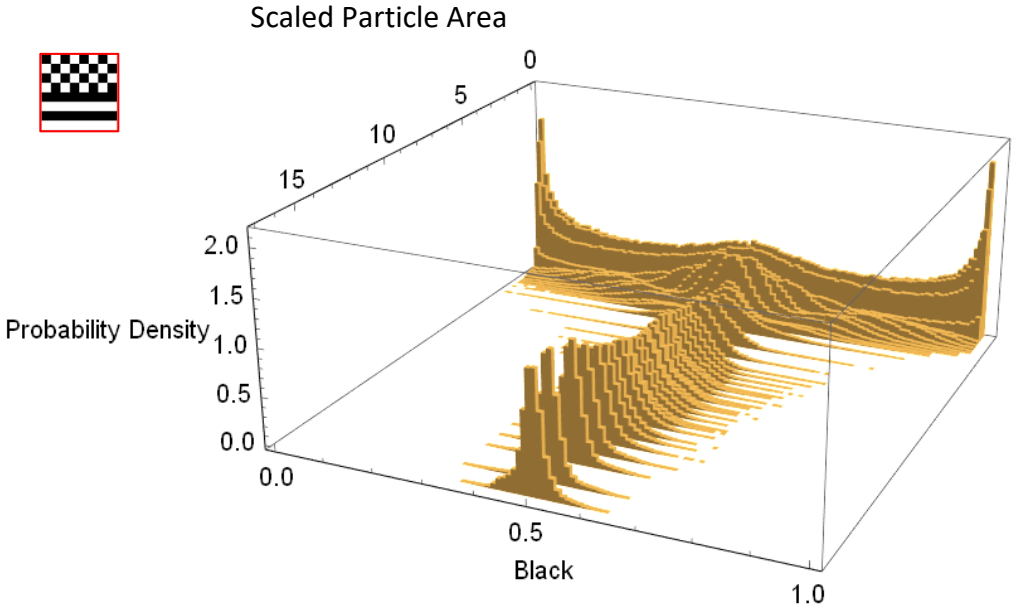

Figure 2.22: Collection of 2D ore grade histograms for scaled areas 0 - 25, composite texture.

The second set of symmetrical populations come from particles which are slowly liberating in the checkerboard section of the texture. Analogous to the simple checkerboard texture liberation profile, two symmetrical shoulders move towards the extremities of 100% black or white slower than particles in the striping section. Both sets of liberating particle populations are most clearly seen in Figure 2.23a) at a moderate scaled area of 2. Completely white or black particles start to

appear at moderate scaled areas of 1.5, as particles liberating in the striping portion of the reach the extremities of completely white or black. Finally, there is a sixth peak present of "remaining" unliberated particles (50/50) which decreases as particle size decreases and can be seen in all scaled area snapshots of Figure 2.23.

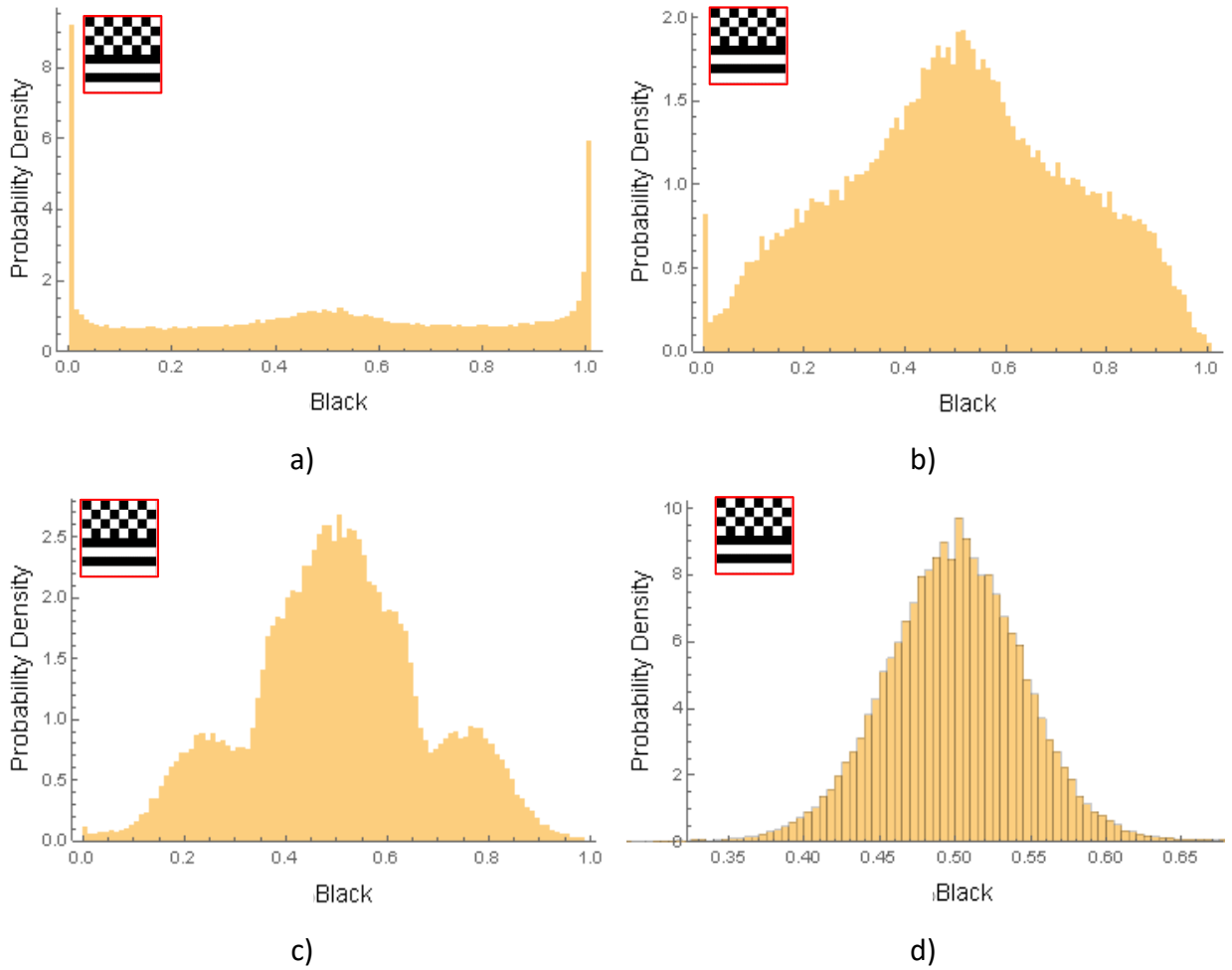

Figure 2.23: 2D Ore grade histogram snapshots, composite texture at a) 0.5, b) 1.5, c) 2.0, d) 4.5 scaled particle areas.

Overall, it is clear that textural features have a distinct effect on the percentage black by size distribution. Depending on texture type, the speed and shape of the mineral liberation profile changes dramatically. Simulated particles from the stripes texture liberated quickly and at higher scaled particle areas when compared with the checkerboard texture. This makes intuitive sense based on the relative heterogeneity of both textures: with stripes being homogeneous in one direction and alternating in the other and checkerboard being alternating in both directions.

For the 60/40 textures, liberating profiles of white and black particles were not symmetrical due to the higher ratio of black to white pixels (3:2). When comparing the staircase and the staircase + checkerboard textures, it was clear that simulated particles from the staircase texture are more likely to liberate at larger scaled particle areas than the staircase + checkerboard texture. Due to the presence of the checkerboard textural feature, many particles from the staircase + checkerboard texture liberated more slowly than others.

A low percentage black stripes texture was examined as many mineral deposits worldwide are low ore grade mineral deposits. Due to the small ratio of black to white pixels (1:3), completely liberated white particles as expected start to appear at very high scaled areas around 10, with completely black particles only starting to appear as scaled particle area drops below 1.

Finally, a checkerboard + stripes composite texture was made to explore the processability characteristic of texture with multiple textural features. As expect, the percentage black by size distribution contained contributions from particles liberating quickly in the stripes portion and particles liberating slowly in the checkerboard portion. While intuitively the percentage black by size distribution of all synthetic ore textures makes sense, the speed and shape of the changing mineral liberation profile has not been quantified. Therefore, in order to quantify how different textural features effect processability, the constitutional heterogeneity of each particle population was examined.

CHAPTER 3
DISTRIBUTION ANALYSIS AND MODEL FITTING

In order to find the link between ore texture and processability characteristics, analysis, and parameterization of collected mineral liberation data was performed. The speed and shape of the changing mineral liberation profile was quantified by examining the distribution variance of particle populations from different texture types. Furthermore, a two-beta mixture distribution model was fitted to model the percentage black by size distribution of simulated particles for the checkerboard and stripes texture respectfully.

Table 3-1: Mineral liberation data analysis summary

Data Analysis
1.) Monitor the change in variance of the ore grade by size distribution for multiple synthetic ore textures
2.) Parametrize the ore grade by size distribution for multiple synthetic ore textures

3.1 Constitutional Heterogeneity

Constitutional heterogeneity (*CH*) was used to examine the speed and shape of generated particle liberation distributions. To defined *CH,* heterogeneity and constitutional properties must first be defined. Gy (2004) noted that a group of objects, such as a group of ore particles, is heterogeneous when not all objects in the group are identical [57,58,59]. Therefore, a group of objects which are all identical are said to be homogenous [57,58,59]. It is the goal of size reduction processes to increase the heterogeneity (reduce the similarity) of a group of particles sufficiently for adequate liberation of valuable minerals.

Gy (2004) defined constitutional properties as the intrinsic properties of a group of objects [57,58,59]. The constitutional properties of groups of solid objects can be modified through size reduction processes as well as agglomeration [57,58,59]. Furthermore, mixing as well as homogenizing well not have an effect on constitutional properties [57,58,59]. In the context of constitutional heterogeneity, mixing objects within the group will not have an effect on the difference in composition between objects. Therefore, a group of objects is constitutionally heterogeneous if the objects within the grouping do not have identical composition [57,58,59]. As the difference in composition increases between objects in the grouping, the constitutional heterogeneity will increase. With reference to size reduction, as particles size decreases the composition difference between particles increases, which increases the constitutional heterogeneity of the group of particles.

CH can be mathematically defined by equation 3.1. The variance of an ore grade distribution can be used as measure of heterogeneity as well. As ore grade variance increases, heterogeneity increases which is the goal of size reduction processes. Therefore, a high variance is an indication of mineral liberation. *CH* can be viewed as a measure of the variance of the ore grade distribution normalized by the mean ore grade. This normalization enables comparison between ore grade distributions of textures with different overall texture ore grades. *CH* can range from zero to infinity and any non-zero *CH* means that the group is made up of different constituent units.

$$CH = \frac{v}{m^2} \qquad [3.1]$$

Where *v* is variance and *m* is mean of the ore grade distribution.

As particle area decreases it is more likely that there is a wider variation in the ore grade of child particles meaning the variance and *CH* rises. Therefore, the higher the *CH* value, the high the degree of liberation of valuable material. *CH* was plotted against scaled particle area, to compare the speed and shape of the changing mineral liberation profile for all synthetic ore textures tested.

3.1.1 Constitutional Heterogeneity of Synthetic Textures

The comparison of *CH* between checkerboard, stripes and composite textures is illustrated by Figure 3.1. The slight noise found in the *CH* curves for all textures is most likely attributed to the pockets of small quantities of particles at certain scaled particle areas. Each particle area bin was

assigned equivalent particles meaning some bins cover a larger range for the same number of particles. This leads to larger gaps between *CH* data points which is the most likely the reason for slight noise in the curves for each texture seen at scaled areas of 0.4, 0.8 and at high scaled areas beyond 3.

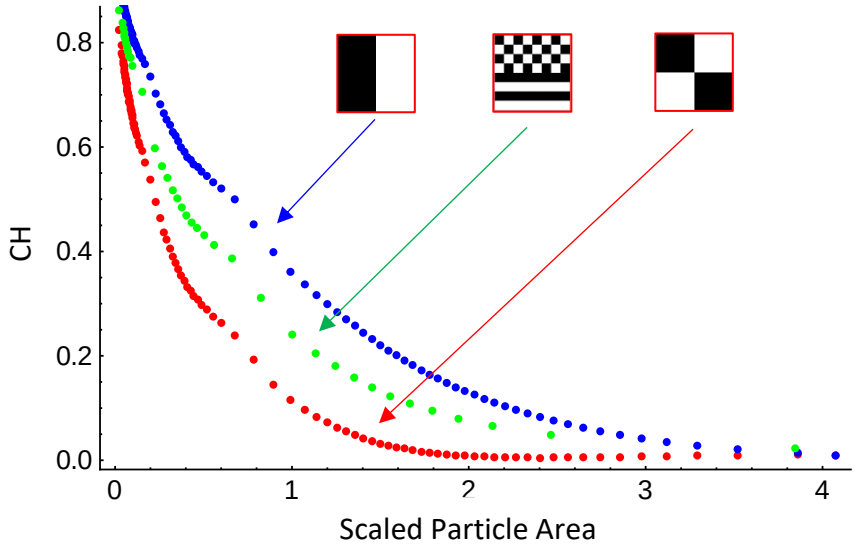

Figure 3.1: *CH* over a range of normalized particle areas for Checkerboard, Stripes and Composite textures.

At a large, scaled particle area around 3.0, the *CH* for the stripes texture (CH_{stripe}) starts to increase at a higher rate while the composite *CH* (CH_{comp}) rises gradually. The checkerboard texture *CH* (CH_{check}) does not start to increase until a scaled particle area of 2, with the largest increase in *CH* occuring at a scaled particle area of 1 and below. The colour of pixels in the stripes texture is alternating, but homogeneous in either the x or y axis (horizontal or vertical stripes). Therefore, it is more likely that particles at any particle size are liberated in the stripes texture when compared with the checkerboard texture which is alternating colours in both directions in 2D space. This agrees with conclusions drawn for the processability characteristic of the checkerboard and stripes texture in Chapter 2.

While the checkerboard texture liberates slowly at large particle areas, at a scaled particle area of 1 CH_{check} starts to climb rapidly. At a scaled particle area of 1 the average particle area is equivalent to the primitive cell area, in the case of the checkerboard texture, the area of a checkerboard square.

Below this point, the area is small enough that the heterogenous nature of the checkerboard texture is less of an influence as more particles are liberated. The composite texture is a 50/50 split of stripes and checkerboard; therefore, as expected, CH_{comp} lies exactly in the center between checkerboard and stripes. This makes intuitive sense, because, for the same ore grade of 50%, any combination of checkerboard and stripe patterns texture should have a *CH* in between the two limiting cases of checkerboard and stripes.

To further analyze the relationship between the checkerboard and stripes texture, the *CH* of both textures illustrated removing completely white or black particles (0s and 1s). Figure 3.2 illustrates the *CH* over a range of scaled particle areas removing completely white and black particles.

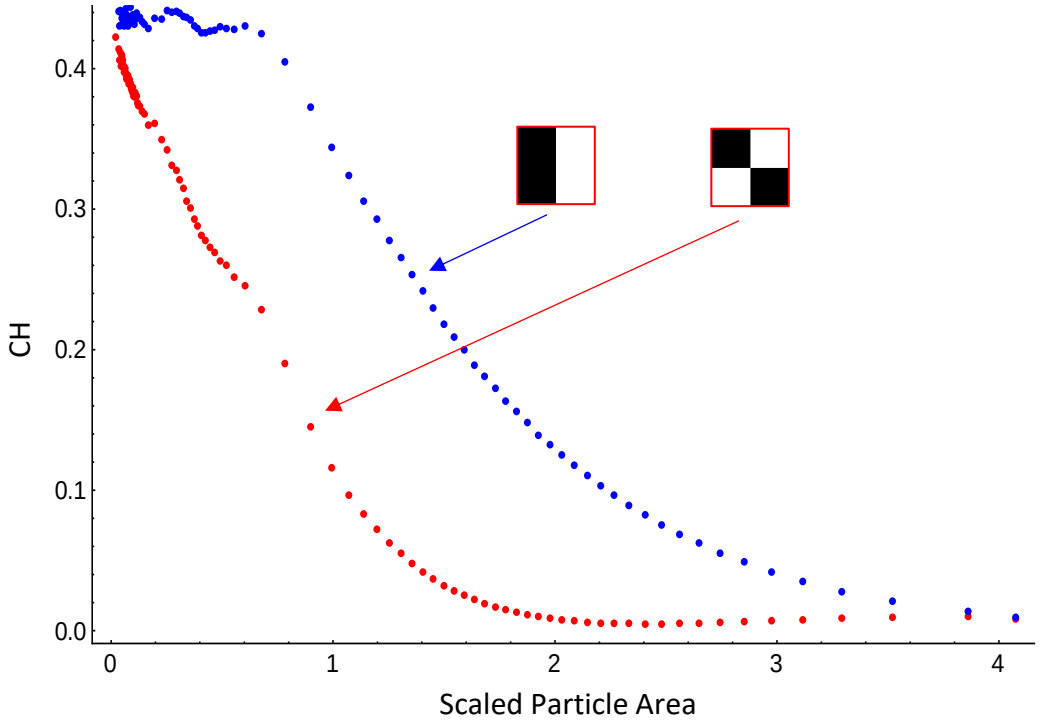

Figure 3.2: *CH* over a range of normalized particle areas excluding completely white or black particles for the checkerboard and stripes textures.

The *CH* for the stripes and checkerboard textures excluding completely white or black particles, $CH_{stripe,n}$ and $CH_{check,n}$ is smaller at all scaled particle areas than CH_{stripe} and CH_{check} respectfully. For $CH_{stripe,n}$ and $CH_{check,n}$, there is a given rate of completely white or black particles being removed from the distribution as particle area decreases. Therefore, particles which contribute to an increase in the variance of the ore grade distribution are being constantly removed, in turn lowering the *CH*. At scaled particle areas below 1, $CH_{stripe,n}$ plateaus. This means that the rate of

particles becoming almost liberated is equivalent to the rate of completely liberated particles being removed from the distribution. Therefore, at a scaled particle area of 1, one can surmise that all particles yet to liberate are depleted, and now only partially liberated particles are now continuing to liberate.

For generated textures with a 60/40 black, white pixel split, *CH* over the range of scale particle areas is lower than 50/50 black/white due to the impact of the increase in overall texture percentage black on *CH*. A similar comparison is found between the constitutional heterogeneity of the two 60/40 textures: staircase *CH* (CH_{stair}) and staircase + checkerboard *CH* (CH_{sc}) and the *CH* of the stripes and checkerboard textures. As seen in Figure 3.3, CH_s increases at a higher rate and at larger scaled particle areas around 4 while CH_{sc} starts to gradually rise once scaled particle area drops below 2.5.

A large portion of the staircase + checkerboard texture is the checkerboard textural feature. The checkerboard texture feature increases in *CH* at a lower rate when compared to homogenous textural features such as stripes. However, due to the contributions of the diagonal homogeneous mineral grain at the center of the staircase +checkerboard texture base pattern, CH_{sc} starts to increase at larger particle areas than the CH_{check}.

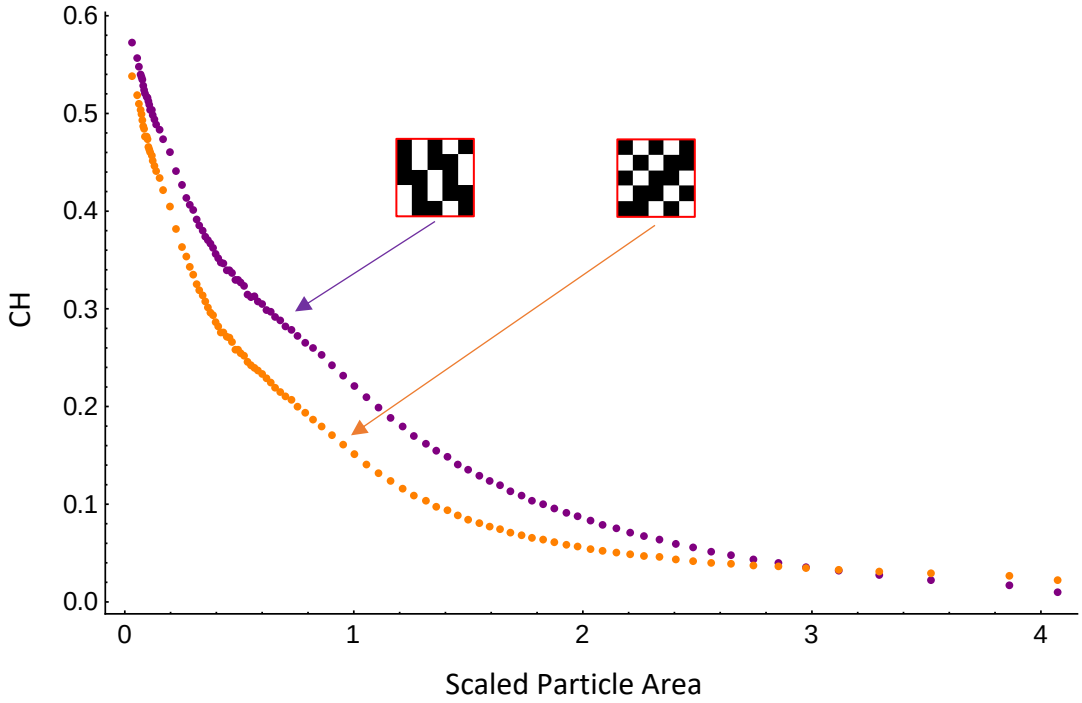

Figure 3.3: *CH* over a range of normalize particle areas for the staircase and staircase + checkerboard textures.

3.1.2 Effect of Ore Grade on Constitutional Heterogeneity

The effect of ore grade on *CH* was examined by comparing the stripes texture at different percentage black in Figure 3.4. To examine the effect of ore grade on *CH*, two stripe textures at 25% and 50% ore grade were analyzed. The textures examined are given by Figure 2.3. As scaled area decrease for both stripe textures, the *CH* exponentially increases. This makes intuitive sense as a greater constitutional heterogeneity means a wider distribution of ore grades which occurs as particle size decreases. If the size reduction process is looked at in reverse, going from small to larger particles, *CH* will exponentially decrease as the average percentage black of particles becomes closer to the overall texture percentage black. Therefore, both *CH* curves were fitted to an exponential decay function given by the equation 3.2. The increase in *CH* as particle area decreases is analogous to an exponential decay function. Furthermore, the exponential decay function equation fit was assessed by examining the R^2 for both textures. The R^2 of 0.98 and 0.93 was determined to be adequate for the exponential decay equation fits of the 25% ore grade and 50% ore grade stripes textures respectfully.

$$CH = Ae^{-kx} \quad [3.2]$$

Where *A* is the pre-exponential factor, *k* is the exponential factor, and *x* is normalized particle area.

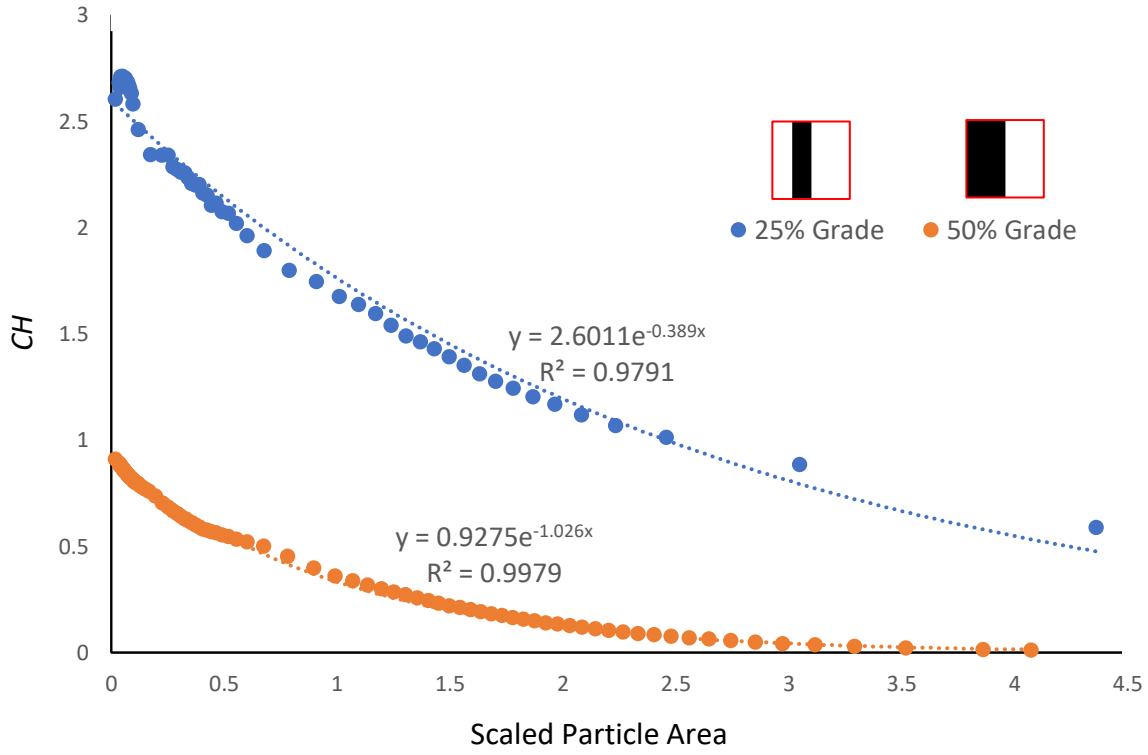

Figure 3.4: Influence of ore grade on *CH* for the vertical stripes texture.

As seen in Figure 3.4, the effect of overall texture ore grade has a major effect on *CH*. *CH* is proportional to 1/mean ore grade^2, therefore as the overall texture ore grade increases, *CH* decrease exponentially. The change in pre-exponential factor *A* and exponential factor *k* when ore grade is doubled is given by Table 3.2. The pre-exponential factor *A* decreases by a factor of 2.6 while *k* increases by a factor of 3.6 when percentage black is doubled for the stripes texture. If the pre-exponential factor increases, *CH* increases while if the exponential factor increases, *CH* will decrease. Therefore, for an increase in A and a decrease in k, as seen in Table 3-2, *CH* should increase significantly. This makes logical sense as a lower overall texture percentage black will increase the denominator of equation 3.1, therefore increasing *CH*.

Table 3-2: Exponential decay constants for the fitted CH vs scaled particle area plot.

Texture Ore Grade	A	k
25%	2.60	0.389
50%	0.928	1.026

3.2 Parametrizing Mineral Liberation Profiles

As mentioned in Section 2.1.4, most liberating mineral profiles have three similar characteristics: At large particle sizes most particles are unliberated which form a single normal peak centered around the overall grade of the orebody. At medium particle sizes, the original peak tends to widen as particles are either being liberated, or gangue is being liberated. At small particles, a binomial distribution will form as almost all particles are either 100% liberated or 100% gangue. What differs when comparing the ore grade by size distribution of different textures is the speed and shape of the changing mineral liberation profile as particle size decreases during the size reduction process.

In order to link textural features to processability characteristics, a predictive model was developed to model the ore grade by size distribution for simple texture types: checkerboard and stripes as illustrated in Figure 2.3, Chapter 2. As seen in Figures 2.2, 2.4, even simple binary synthetic textures like checkerboard and stripes have complex ore grade distributions which vary greatly as particle size decreases. Therefore, in order to ensure adequate modelling as well as reasonable computational time for model parameter acquisition, only the ore grade by size distribution of the checkerboard and stripes textures were modelled.

A mixed beta distribution model was chosen due to the flexibility of the beta distribution, while also having enough parameters to accurate describe the distribution it is fitting. Beta distributions do not contain 1s or 0s therefore, completely white, and black particles were removed from the particle population for modelling purposes. As seen in Figure 3.5, completely white or black particles only start to appear when scaled area is at or below 1 for both texture types. Note only completely black particles were shown as completely white particles follow the same trend.

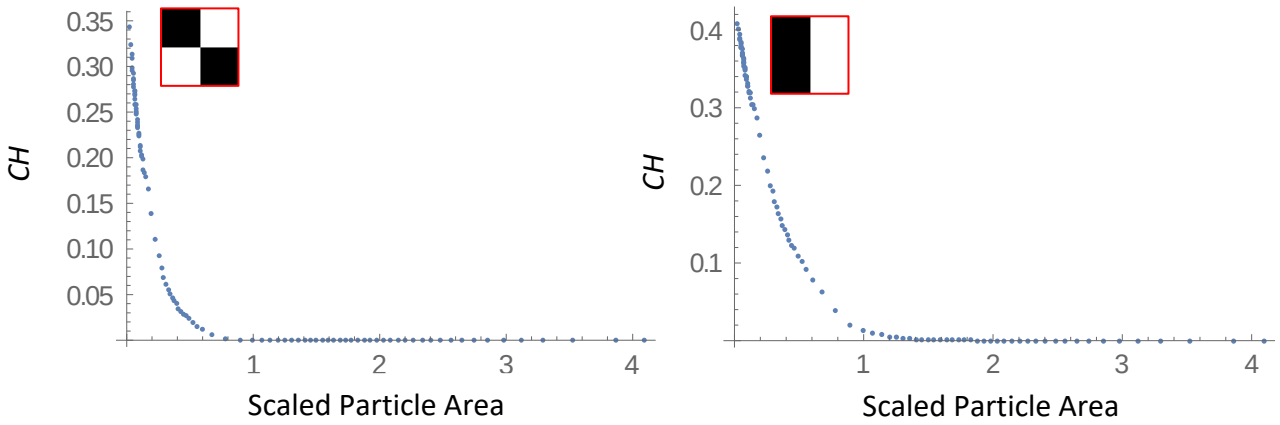

Figure 3.5: Completely black particles over a range of scaled particle areas, checkerboard, and stripes textures.

At a scaled area of 1, the average particle area is equivalent to the area of the primitive cell. In the case of the checkerboard texture, the primitive cell area is the area of a single checkerboard square. For the checkerboard texture, a scaled particle area of 1 is the absolute upper limit for appearance of completely white or completely black particles. However, the likelihood of a particle being 100% white, or 100% black exponentially increases at a scaled area of 0.5 and below. In the stripes texture, the area of the primitive cell is the area of the square with length equal to the width of one stripe. As discussed in Section 2.2.1, particles from stripes texture are more likely to liberate faster and at larger scaled particle areas. Therefore, due to the homogenous but alternating nature of the striping texture, completely white and completely black particles are more likely to start appearing at scaled areas slightly above 1, while the majority still appear below 1. While completely white or black particles will have an effect on the shape of the ore grade distribution, these particles were taken out of the distribution in order to leverage the flexibility and applicability of the beta distribution for modeling of mineral liberation data.

There are five parameters to be fitted, the two sets of shape parameters for the relative contributions of two beta distributions: β_1 β_2 α_1 α_2 as well as the mixture distribution weight w. One of the drawbacks of using a mixture distribution is the addition of more parameters to be fitted which adds to the complexity and reduces the stability of the distribution. Table 3-3 illustrates how the number of fitting parameters increases as the number of distributions increases in a mixture distribution. A balance was found between adequate modeling fitting as well as reducing the number of fitting parameters.

Table 3-3: Number of Parameters in Mixture Distributions

# Of Distributions in the Mixture Model	# Of Parameters before Simplification
2	5
3	8
4	11
5	14

A two-beta mixture model can be simplified by re-arranging α and β in terms of known parameters. The ratio of white to black pixels is known for each synthetic ore texture therefore the mean texture percentage black is also known. If the overall texture percentage black is known only the mean percentage black of one beta distribution is required to determine the other mean as illustrated in equation 3.3.

$$m = w * m_1 + (1 - w) * m_2 \quad [3.3]$$

Furthermore, if the ore grade distribution is symmetrical (50/50 white/black), the weighting of the mixture distribution can be set to 0.5 or 50%. Each "side" of the distribution has equal but opposite contribution to the overall distribution, therefore the weighting for each "side" should be equal. Two simplification methods were used compare and find the best possible fit. These simplifications are summarized in Table 3-4.

Both simplification methods were tested for each texture to obtain the best possible fit.. Both methods reduce the number of fitting parameters, greatly increasing the computational speed of the model fitting procedure. Simplification method 1 leverages equation 3.3 to reduce the number of fitting parameters from five to four. Simplification method 2 further rearranges the beta shape parameters in terms of the mean and variance of the distribution for a total of four fitting parameters.

Table 3-4: Mixture Beta Distribution Simplification Method Summary

Simplification method 1	**Simplification method 2**
1.) Rearrange α in terms of β_i, m_i, and m	1.) Rearrange α and β in terms of v and m
2.) Parameters β_1, β_2, m_i, w	2.) Parameters v_1, v_2, m_i, w

3.) Potential to further simplify depending on the situation by setting m_i or w	3.) Potential to further simplify depending on the situation by setting m_i or w

Simplification method 1 was determined to be most effective when used for the checkerboard texture. The fitted model parameters over the range of scaled particle areas are given by Figure 3.6. Note α_1, α_2 are not shown as they are equivalent to β_1, β_2. Snapshots of the model fit at multiple scaled particle areas is given by Figure 3.7.

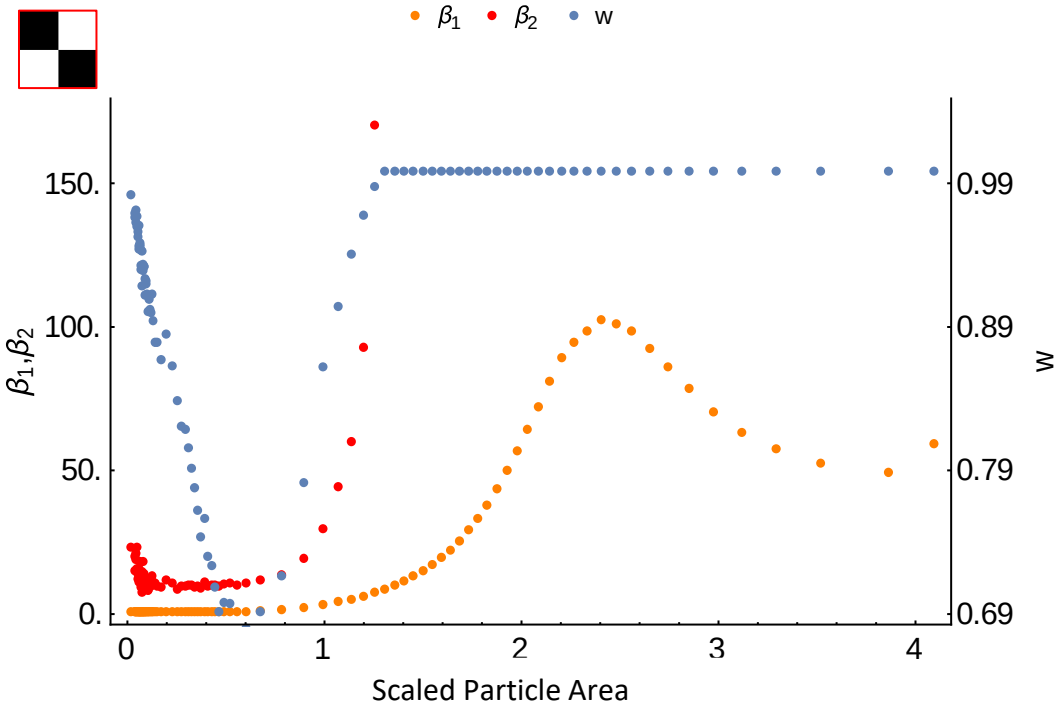

Figure 3.6: Two beta mixture distribution parameters over a range of scaled particle areas for the checkerboard texture

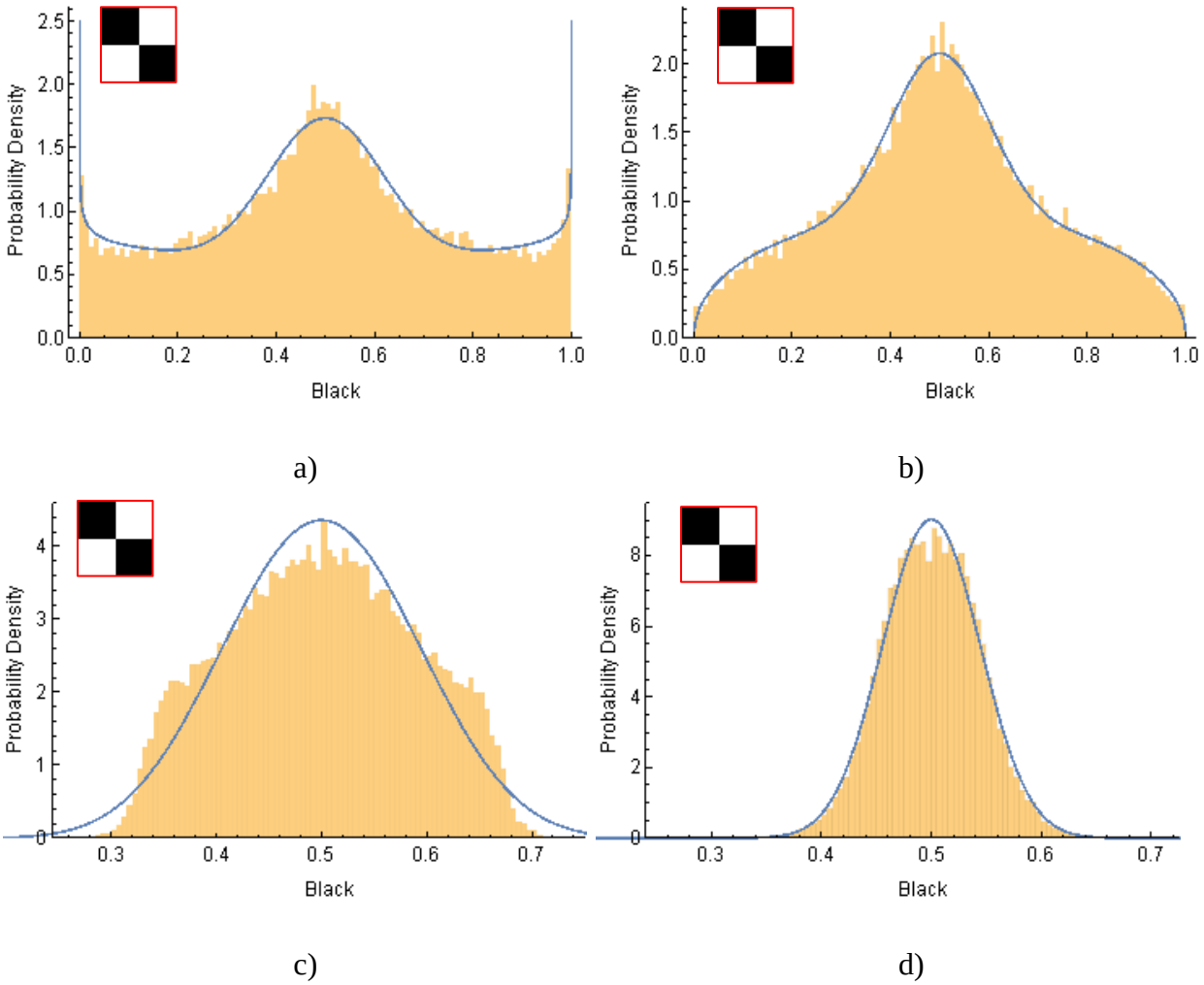

Figure 3.7: Two beta mixture distribution model fit, checkerboard a) 0.5, b) 0.75, c) 1.5, d) 2.0 scaled particle areas.

At large scaled particle areas from 4 to 1, w was set to 1 meaning there is only one beta distribution contribution to the overall mixture distribution. At these larger scaled areas, most particles are likely to be particles yet to be liberated creating a peak centered around the overall texture percentage black of 50%. Therefore, a single beta distribution was deemed sufficient for modelling scaled particle areas from 4 to 1 which required fewer fitting parameters. As seen in Figure 3.7b), a single beta distribution does not completely capture the symmetrical shoulders of particles increasing in percentage white or percentage black. A three-beta mixture distribution model may be required to adequately model the three identifiable peaks in Figure 3.7b). A wide range of scale particle areas only requires one or two beta distributions to describe the ore grade distribution. Furthermore, as beta distribution contributions are added to the overall mixture distribution,

computational time for determining fitting parameters exponentially increases. Therefore, a two-beta mixture distribution was determined to be sufficient to model the percentage black distribution across the complete range of particle sizes.

Illustrated in Figure 3.6, as scaled area decreases from 4 to 2.5, β_1 increases to a maximum at 2.5 leading to the narrowing of the peak of particles centered around the overall texture percentage black of 50%. This does not make intuitive sense, because as particle area decreases, particles are more likely to start liberating, which should broaden this peak. The peak narrowing seen from 4 to 2.5 scaled area is therefore most likely a function of the fitting procedure. There are two likely explanations for this effect, both being a function of the data and the model. The Voronoi mask program uses a bounding box for Voronoi tessellation creation, therefore, particles at the border may be cut off. These leads to a bias in the ore grade of border particles which creates larger variation in ore grades at high particle areas. Secondly, most particles generated have a scaled particle area below 1. Therefore, there is a larger gap in scaled area between bins of equal size at very large scaled areas. Both considerations lead to variations in the ore grade of very large particles which likely contributes to peak widening at those particle areas. As scaled particle area decreases further from 2.5 to 1, β_1 decreases exponentially while remaining above 1. β_1 decreases as liberating particles move towards the extremities, widening the ore grade distribution

From scaled particle areas 1 to 0, w decreases to a minimum of 0.69 at a scaled area of 0.6 and then increases back to 1 as scaled area goes to 0. Referring to Figure 3.7b), at a scaled area of 0.75, there is still a large peak of particles yet to be liberated while the liberating shoulders reach the extremities. Therefore, at these scaled areas, two beta peaks were used to model the ore grade distribution, one narrow peak representing particles yet to be liberated and one broad peak representing particles liberating. Beta distribution 1 ($Beta_1$) was the broad peak contribution while beta distribution 2 ($Beta_2$) was the narrow peak contribution. As w decreases to a minimum at a scaled area of 0.69, the $Beta_2$ contribution increases. This is most likely a function of the fitting procedure because as scaled area decreases from 1 to 0.6, the narrow peak seen in Figure 3.7b) becomes more distinct as particles liberate around it.

At a scaled area of 0.6, β_1 goes below 1, changing the $Beta_1$ model contribution from a broad peak to a U-shape curve. After this flip as scaled area decreases from 0.6 to 0, the contribution of $Beta_1$ increases as more particles liberate towards the extremities. Parameters β_1 and β_2 remain fairly

constant meaning the rising contribution of $Beta_1$ to the overall mixture distribution is the primary effect in the changing model fit as scaled area decreases. At very low scaled areas below 0.1, β_2 increase as scaled area decreases. This is likely a function of the model procedure. The contribution of $Beta_2$ starts to become so small that large changes in β_2 do not have a major impact on the overall model fit.

Simplification method 2 was determined to be the most effective method at modelling the ore grade by size distribution of the stripes texture. Referring back to Figure 2.4 in Chapter 2, as the size reduction process proceeds in the stripes texture, two equal but opposite peaks move towards the either completely liberated black particles or completely gangue white particles. Therefore, w was set as 0.5 in an attempt to mirror the mineral liberation profile behavior with the fitting algorithm. Two equal but opposite beta distributions, were used with related means as seen in equation 3.4.

$$m_1 = 1 - m_2 \qquad [3.4]$$

The change in m_1 as scaled particle area decreases for $Beta_1$ is given by Figure 3.8. Note that m_2 is directly related to m_2 using equation 3.4. The fitted model parameters,v_1, v_2, and w, are given by Figure 3.9, over the complete range of scaled particle areas. Snapshots of the model fitting procedure for the stripes ore grade by size distribution is given by Figure 3.10.

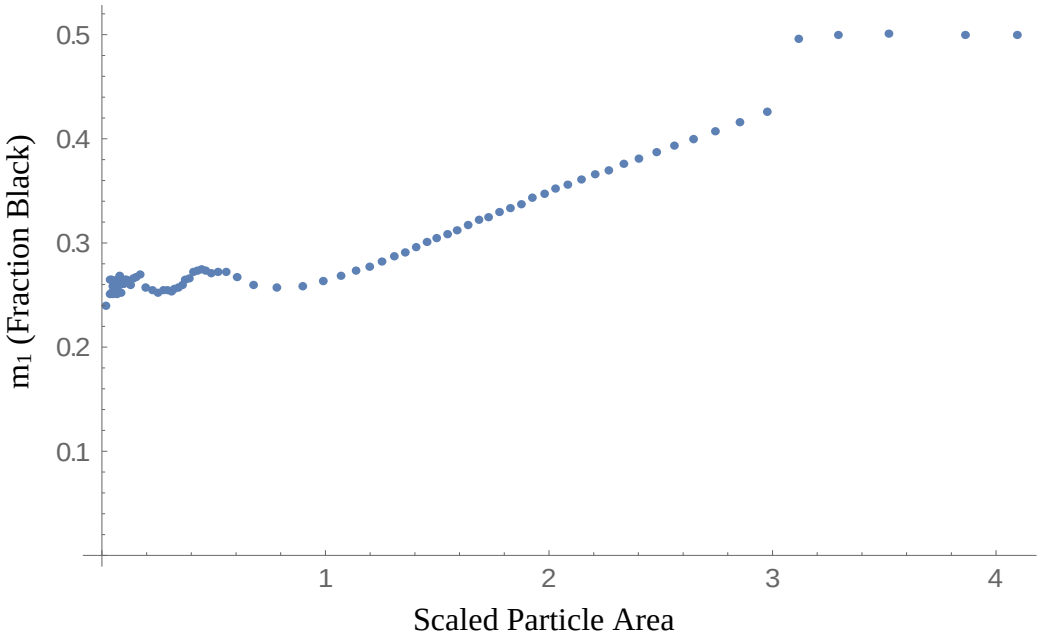

Figure 3.8: Beta distribution 1 mean over the complete range of scaled particle areas for the stripes texture.

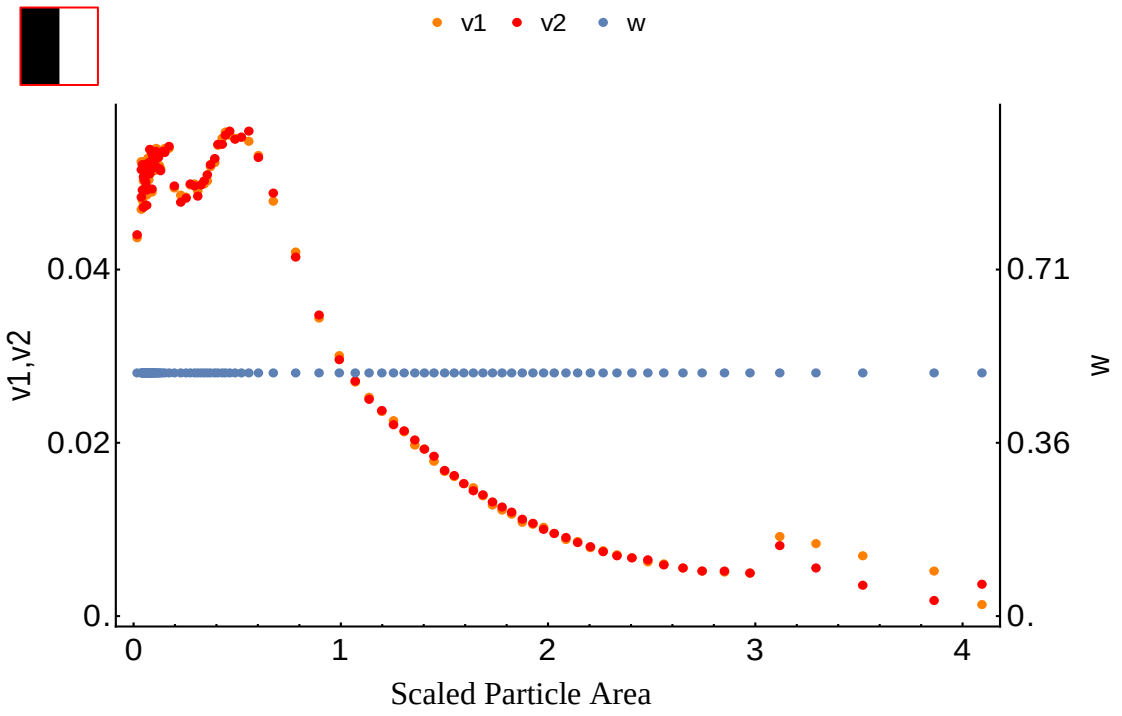

Figure 3.9: Two beta mixture distribution parameters over the complete range of scaled particle areas for the stripe texture.

At any point along the range of scaled areas, the mean of the mixture distribution is 50% black due to the equal contributions of the changing m_1 and m_2 as scaled area changes. At large scaled areas above 3, almost all particles form a peak centered around the overall texture percentage black of 50%. Below a scaled area of 3, two liberating peaks moving towards completely white and completely black start to appear. This is likely the reason for the sudden drop in m_1 as the fitting procedure varied m_1 and m_2 to model the liberating peaks.

As scaled particle area decreases from 3 to 1, m_1 decreases linearly from 0.5 to 0.25 while m_2 linearly increases from 0.5 to 0.72. $Beta_1$ and $Beta_2$ each represents a liberating peak of particles. $Beta_1$ represents the population of particles which are increasing in percentage white, because m_1 (percentage black) decreases as particle size decreases. Therefore, $Beta_2$ represents the population of liberating particles increasing in percentage black. As seen in Figure 3.10b) &c), $Beta_1$ and $Beta_2$ have the mean of the respective peak of the liberating particle populations moving towards completely white or black.

At low scaled particle areas below 1, m_1 remains fairly constant at 25% black, with m_2 being 75% black. The skewed left contribution of $Beta_1$ and the skewed right contribution of $Beta_2$ form the expected U-shape curve as most particles are either completely white or completely black.

Referring to Figure 3.9, as particle area decreases from 4 to 1, v_1 and v_2 increase exponentially similarly to how *CH* increases as particle area decreases. Aa scaled area decreases, particles are more likely to start liberating, increases the distribution of percentage black which increases the variance of the overall distribution. At scaled particle areas above 3, the stripes liberation profile has not yet split into two peaks leading in the slight offset produced by the fitting algorithm.

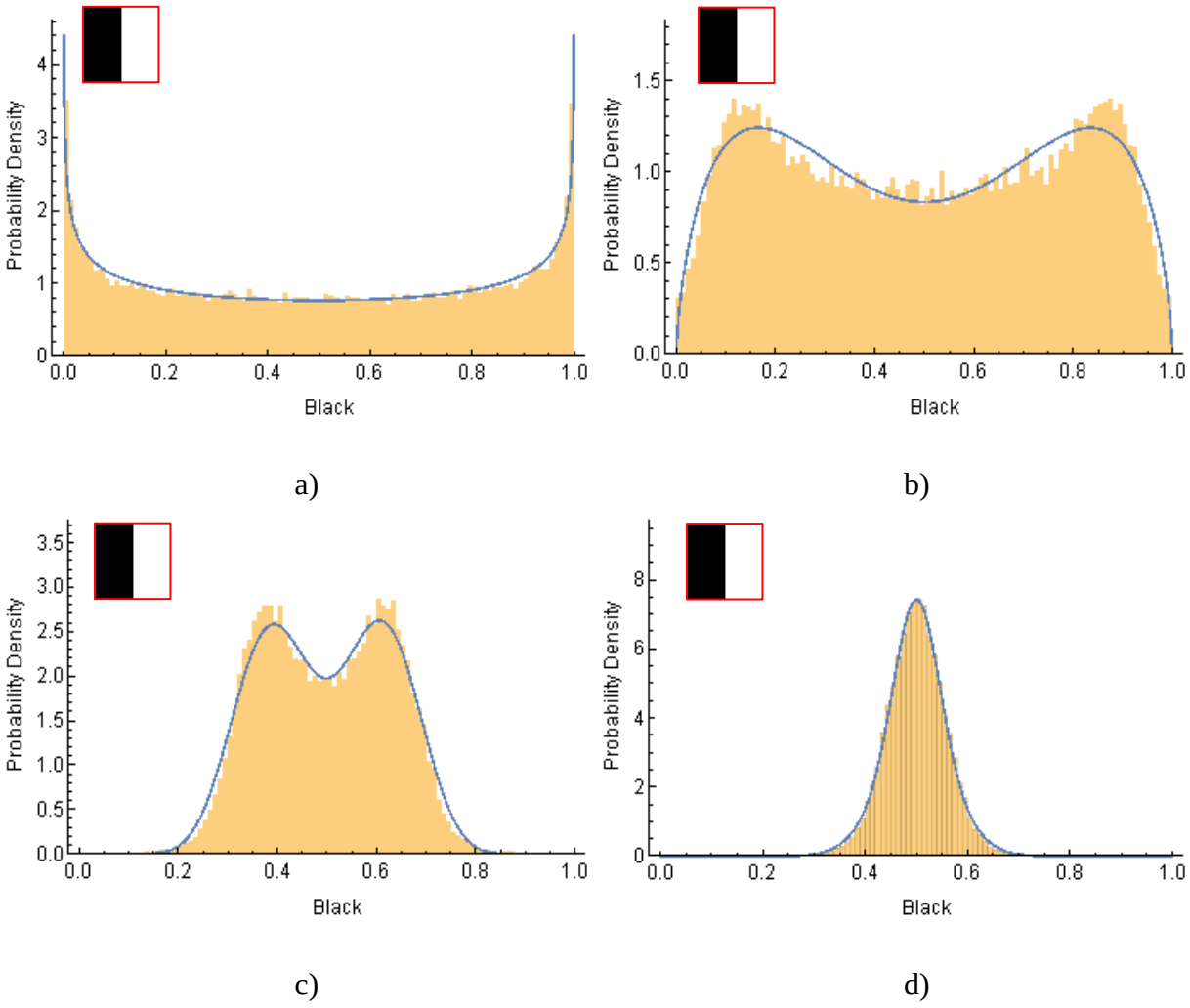

Figure 3.10: Two beta mixture distribution model fit, stripes texture, a) 0.5, b) 1.0, c) 2.5, d) 3.75 scaled particle area.

At low scaled areas below 1, the fitting algorithm oscillates between 0.04 and 0.05 for v_1 and v_2. This effect is not physical and is a function of the fitting algorithm. At very low scaled areas, almost all particles are likely to be either completely white or completely black forming a binomial distribution with two spike peaks, one at 0 and one at 1. As seen in Figure 3.2, when 1s and 0s are taken out of the distribution, CH and variance plateaus below scaled areas of 1. Below a scaled area of 1 the two liberating peaks reach the extremities meaning there is not a population of particle yet to be liberated. Therefore, in the range of scaled areas of 0 to 1, the fitting algorithm finds satisfactory results within the maximum iterations between a variance of 0.04 and 0.05. Overall, the two-beta distribution model found a satisfactory fit for the ore grade distribution across the complete range of particle sizes as illustrated by Figure 3.10.

Due to the complex nature of simulated ore grade by size distributions even for simple textures, only mineral liberation data from the checkerboard and stripes textures were parametrized. Overall, two fitting procedures were used successfully model to percentage black by size distribution of two simple 2D binary synthetic ore textures: checkerboard and stripes. A two-beta mixture distribution model was employed for adequate model flexibility while also attaining acceptable computational times for the fitting procedure.

The percentage black by size distribution for simulated particles from the checkerboard texture were parametrized using a combination of a single beta distribution and a two-beta mixture distribution. For very small and very large particle sizes, it was determined that a single beta distribution could describe the percentage black distribution for the checkerboard texture. At medium particle sizes, the two-beta mixture distribution model was employed. Non-physical effects noticed in the fitted parameters were discussed and explained.

Simulated particles from the stripes texture were parametrized by using a two-beta mixture distribution. The weighted contribution of each beta distribution was set to 50% due to the symmetrical nature of the percentage black distribution data. The two-beta mixture distribution model found very accurate results with a few non-physical fitting algorithm effects which were discussed. Overall a link was made between the distinct texture types: checkerboard and stripes and the distribution of ore grades (percentage black) at different particle sizes. Therefore, the size reduction process of textures with similar textural features can be estimated to give a better idea at what the optimal particle size is for sufficient liberation and reduced energy consumption.

CHAPTER 4
CONCLUSIONS AND FUTURE WORK

4.1 Conclusions

Mineral and metal extraction and processing is important for the production of green and environmentally sustainable technologies such as solar panels, wind turbines, hydrogen fuel cells, and more. Ore textural characteristics can be used to categorize orebodies in order to predict the grade by size distribution and tune size reduction processes appropriately for sufficient mineral liberation without overconsumption of energy. The Voronoi tessellation masking technique was used to simulate ore texture breakage for the generation of realistic product particles for analysis. The ore grade by size distribution of multiple synthetic ore textures was analyzed to mathematically compare how different ore textures break during size reduction.

The complexity of the ore grade by size distribution for even simple textures such as checkerboards and stripes, was very high. A one beta distribution model was determined to be insufficient in modelling the ore grade distribution of populations of particles for the complete range of particle sizes as size reduction proceeds. A beta-beta mixture model was developed to parameterize the processability characteristics of simple texture types: checkerboard and stripes, which have distinct textural features (grain size, shape, orientation). Comparison of fitted parameters mathematically illustrates the difference in speed of shape of the changing mineral liberation profile as particle size decreases depending on 2D texture type. Clear differences in processability were made between texture types with particles in the checkerboard texture liberating slower and at smaller particles sizes then particles from the stripes texture.

Textural features were linked to processability characteristics by finding the distinct effect texture has on the fitted model parameters which modify the speed of mineral liberation and the shape of the overall ore grade by size distribution. Therefore, a mathematical link has been made between textural features and the grade by size distribution of valuable material. In the future, if processability characteristics are known of representative textures on a mine site, then size

reductions processes can be tuned appropriately to achieve sufficient valuable mineral liberation while also reducing energy consumption.

4.2 Future Work and Recommendations

Scaled particle sizes were used to be able to generate a wide range of particle sizes using multiple sizes of like textures. In order to retain pixel data and insured textures remained periodic, it was required that the primitive cell of generated synthetic textures had to be a factor of the overall image dimensions. Therefore, for a given image of X-by-X dimensions, the length of the primitive cell must be a factor of X to retain the periodicity of generated textures. If the primitive cell were not a factor of the texture dimensions, textural features would be cut off making the texture non-periodic (not an infinitely repeating pattern). Common factors for various image dimensions are given in Appendix A.2. The drawback of these common factors is there are fairly big gaps between factor values which in the end creates pockets of scaled particles at given sizes. This led to the scaled particle size distribution of experiments performed to have a large number of small particles and a much smaller distribution of larger sizes. Highly factorable numbers such as 1260, 2520, and others can be used as texture image dimensions to use factors which are closer together. Comparatively to an image dimension of 1000x1000, the available factors for highly factorable numbers are closer together which will create a wider distribution of scaled particles. Furthermore, larger particles can be directly generated by modifying the size of Voronoi masks although this will lead to an increase in computational time for ore breakage simulations. Therefore, in future work, highly factorable image dimensions can be used to generate a more uniform Voronoi cell size distribution.

The ore grade by size distribution is difficult to parametrize even for simple texture such as checkerboard and stripes. A balance was struck between the number of contributions to the mixture distribution and the number of fitting parameters. As particles decrease in size, there is immense variability in the ore grade distribution. More complex mixture distributions with more than two contributions were considered for mineral liberation modelling, but not used due to the growing number of required fitting parameters. As more fitting parameters are added to the model, the overall distribution will lack stability and the fitting algorithm computational time will rise. Although, in order to accurately describe processability characteristics for even simple textures such as checkerboards, models in the future may require the use of more than two contributions to

the mixture distribution or the use of another distribution which can accurately model major changes in ore grade distribution as size reduction processes proceed.

There is inherent stereological bias associated with the inference of 3D structure form 2D data. This worked estimates the volumetric grade of orebodies using 2D ore textures. Therefore, in order to obtain more accurate results, a stereological correction factor should be used to correct for biases in the z-axis.

Furthermore, the Voronoi masking technique used a square bounding box to restrict Voronoi generating seeds in a specific area. This introduces biases at the border as border cells are incomplete Voronoi cells. Periodic Voronoi tessellations can be used without a square bounding box to remove border cell bias. Periodic Voronoi tessellations are Voronoi patterns which can be infinitely repeated in all orientations. If periodic Voronoi tessellations are superimposed onto an infinitely repeating periodic ore texture (no bounding box), the bias from artificial borders can be removed.

Finally, in order to rapidly created a large of realistic child particles using the Voronoi masking technique, random breakage was assumed. In reality, ore breakage is non-random, influenced by many different particle characteristics such as mechanical properties, grain boundary properties and others. Non-random breakage models require specific rules judging how breakage simulations will proceed. Non-random breakage models are more complex but will provide a more accurate and realistic simulation of ore texture breakage. A ruleset guiding the generation of Voronoi cells can be made for the simulation of non-random breakage. For example, Voronoi seed generation can be skewed to generate a large number of seeds in soft material and a low number of seeds in hard material leading to less energy required during size reduction to liberate the softer material.

4.3 Link to Real World Application

In this work, the link between simple textures and processability characteristics of those texture was modeled using a two beta mixture distribution model. Therefore, the ore grade distribution of textures with similar textural features can be predicted across the range of particle sizes. In other words, specific textural features can be classified to be able to predict the ore grade by size distribution. This is a useful tool when considering the efficiency of size reduction operations. Size reduction processes such as crushing, and grinding are high energy consumption processes [6].

Without previous knowledge of the ore grade distribution of crushed/grinded product, redundant size reduction processes may be used to insure adequate liberation. Therefore, the prediction of the ore grade distribution at different sizes can be used to make informed decisions on how small particles should be crushed/grinded for adequate liberation. Secondly, decision making processes can be guided quickly with a predefined database of texture types in which real sample textures can be instantly classified to determine processability characteristics.

By extending this work to real ore textures, a database of textural features can be generated in which the ore grade by size distribution of each textural feature can be predicted across the complete range of particle sizes. This database of predicted ore breakage patterns would be leveraged to make inform decisions quickly on size reduction requirements. For example, a certain textural feature may indicate that a larger average particle size is sufficient for downstream separation and ore sorting processes. This will in turn reduce the energy consumption of size reduction processes such as crushing and grinding. Overall, the goal of this textural database would be to have a quick and readily available tool to predict mineral liberation by leveraging and evaluating texture data collected across a large scale mine site.

REFERENCES

1.) Minerals and the economy. (2021). Retrieved January 15, 2021, from https://www.nrcan.gc.ca/our-natural-resources/minerals-mining/minerals-metals-facts/minerals-and-the-economy/20529#GDP

2.) King, R. P. (2000). "*Technical Notes 10 – Mineral Liberation"*. Retrieved January 15,2021, from http://mineraltech.com/MODSIM/ModsimTraining/Module7/TechnicalNotes-10-Liberation.pdf

3.) King, R. P, and C. L Schneider. (1998). "Mineral Liberation and the Batch Comminution Equation." *Minerals engineering* 11.12: 1143–1160. Print.

4.) King, R.P. (1979). "A Model for the Quantitative Estimation of Mineral Liberation by Grinding." *International journal of mineral processing* 6.3: 207–220. 10.1016/0301-7516(79)90037-1

5.) Canada's GHG Emissions by Sector, End Use and Subsector – Including Electricity-Related Emissions | Natural Resources Canada. (2018). Retrieved January 15, 2021, from https://oee.nrcan.gc.ca/corporate/statistics/neud/dpa/showTable.cfm?type=HB&sector=aaa&juris=ca&rn=3&page=0

6.) Mudd, G. M. (2009). The Environmental sustainability of mining in Australia: key mega-trends and looming constraints. *Resources Policy*, *35*, 98–115. https://doi.org/10.1016/j.resourpol.2009.12.001

7.) Haldar, S. K. (2018). Mineral Exploration Principles and Applications, Waltham, Mass: Elsevier, Print.

8.) Northey, S., Mohr, S., Mudd, G. M., Weng, Z., & Giurco, D. (2014). Modelling future copper ore grade decline based on a detailed assessment of copper resources and mining. *Resources, Conservation and Recycling*, *83*, 190–201. https://doi.org/10.1016/j.resconrec.2013.10.005

9.) Tackling comminution, the largest energy consumer. (2016). Retrieved January 15, 2021, from https://www.nrcan.gc.ca/our-natural-resources/minerals-mining/mining-resources/tackling-comminution-largest-energy-consumer/18296

10.) Canadian Minerals and Metals Plan, (2019). Retrieved January 15, 2021, from https://www.nrcan.gc.ca/sites/www.nrcan.gc.ca/files/CMMP/CMMP_The_Plan-EN.pdf

11.) Zhang, J., & Subasinghe, N. (2013). Prediction of mineral liberation characteristics of comminuted particles of high grade ores. *Minerals Engineering*, *49*, 68–76. https://doi.org/10.1016/j.mineng.2013.05.005

12.) Das, A., & Sarkar, B. (2018). Advanced Gravity Concentration of Fine Particles: A Review, Mineral Processing and Extractive Metallurgy Review, 39:6, 359-394, https://doi.org/10.1080/08827508.2018.1433176

13.) Gupta, A., and D. S. Yan. (2006). Mineral Processing Design and Operation an Introduction . 1st ed. Amsterdam ;: Elsevier, Print.

14.) Stanley, J., Wilkinson, S. T., Moreno Ramírez, D., Maier, R. M., & Chief, K. (2015). *University of Arizona Superfund Research Program Community Engagement Core Tribal Mining Educational Modules Copper Mining and Processing.* Retrieved from http://www.superfund.pharmacy.arizona.edu/learning-modules/tribal-modules

15.) Kitanidis, P. (1997). *Introduction to Geostatistics: Applications in Hydrogeology*. Cambridge: Cambridge University Press. doi:10.1017/CBO9780511626166

16.) King, R. P. (2001). *Modeling and Simulation of Mineral Processing Systems*, Elsevier Science & Technology,. *ProQuest Ebook Central*, https://ebookcentral.proquest.com/lib/ottawa/detail.action?docID=298469.

17.) Mariano, R. A., Evans, C. L., & Manlapig, E. (2016). Definition of random and non-random breakage in mineral liberation - A review. *Minerals Engineering*, Vol. 94, pp. 51–60. https://doi.org/10.1016/j.mineng.2016.05.005

18.) Van Der Wielen, K. P., & Rollinson, G. (2017). *Texture-based analysis of liberation behaviour using Voronoi tessellations*. https://doi.org/10.1016/j.mineng.2015.09.008

19.) Hilden, M. M., & Powell, M. S. (2017). A geometrical texture model for multi-mineral liberation prediction. *Minerals Engineering*, *111*, 25–35. https://doi.org/10.1016/j.mineng.2017.04.020

20.) Gay, S. L. (1999). Numerical verification of a non-preferential-breakage liberation model. In *Int. J. Miner. Process* (Vol. 57).

21.) Barbery, G., & Leroux, D. (1988). Prediction of particle composition distribution after fragmentation of heterogeneous materials. *International Journal of Mineral Processing*, *22*(1–4), 9–24. https://doi.org/10.1016/0301-7516(88)90053-1

22.) Forbes, C., Evans, M., Hastings, N., & Peacock, B. (2010). Statistical Distributions: Fourth Edition. In *Statistical Distributions: Fourth Edition*. https://doi.org/10.1002/9780470627242

23.) Evans, C.L. (2010). Development of a Methodology to Estimate Flotation Separability from Ore Microstructure Ph.D. Dissertation. The University of Queensland.

24.) Mirzaei, Z.S.; Khalesi, M.R. (2019). Development of a Simulator for Random and Non-Random Breakage of Particles and Liberation of Grains Based on Voronoi Tessellation. *Minerals*, *9*, 341. https://doi.org/10.3390/min9060341

25.) Khalesi, M. R., Bazin, C., Hodouin, D., & Bellec, S. (2009). *Simulation of Gold Grain Exposure of Ground Ore Using Voronoi Tessellation*.

26.) Ghazvinian, E., Diederichs, M. S., & Quey, R. (2014). 3D random Voronoi grain-based models for simulation of brittle rock damage and fabric-guided micro-fracturing. *Journal of Rock*

Mechanics and Geotechnical Engineering, *6*(6), 506–521. https://doi.org/10.1016/j.jrmge.2014.09.001

27.) Guimarães, C., & Durão, F. (2006). *Application of a cellular automata based simulation model of size reduction in mineral processing*. https://doi.org/10.1016/j.mineng.2006.11.001

28.) Leißner, T., Hoang, D. H., Rudolph, M., Heinig, T., Bachmann, K., Gutzmer, J., Peuker, U. A. (2016). *A mineral liberation study of grain boundary fracture based on measurements of the surface exposure after milling*. https://doi.org/10.1016/j.minpro.2016.08.014

29.) Wang, Y., & Neethling, S. J. (2006). *Simulating realistic froth surfaces*. https://doi.org/10.1016/j.mineng.2006.03.007

30.) Ueda, T., Oki, T., & Koyanaka, S. (2018). Numerical analysis of the general characteristics of stereological bias in surface liberation assessment of ore particles. *Advanced Powder Technology*, *29*(12), 3327–3335. https://doi.org/10.1016/j.apt.2018.09.010

31.) Ueda, T., Oki, T., & Koyanaka, S. (2018). A general quantification method for addressing stereological bias in mineral liberation assessment in terms of volume fraction and size of mineral phase. *Minerals Engineering*, *119*, 156–165. https://doi.org/10.1016/j.mineng.2018.01.034

32.) Ueda, T., Oki, T., & Koyanaka, S. (2016). Stereological bias for spherical particles with various particle compositions. *Advanced Powder Technology*, *27*(4), 1828–1838. https://doi.org/10.1016/j.apt.2016.06.016

33.) Reyes, F., Lin, Q., Udoudo, O., Dodds, C., Lee, P. D., & Neethling, S. J. (2017). *Calibrated X-ray micro-tomography for mineral ore quantification*. https://doi.org/10.1016/j.mineng.2017.04.015

34.) Bahaaddini, M., & Rahimi, M. (2017). *Distinct element modelling of the mechanical behavior of intact rocks using Voronoi tessellation model*. ***

35.) Austin, L.G., Sutherland, D.N., Gottlieb, P. (1993). An analysis of SAG mill grinding and liberation tests. Miner. Eng. 6, 491–507.

37.) Becker, M., Jardine, M. A., Miller, J. A., & Harris, M. (2016). X-ray Computed Tomography: A geometallurgical tool for 3D textural analysis of drill core? *3nd AusIMM International Geometallurgy Conference*, (june), 15–16.

38.) Carrasco, C., Keeney, L., & Napier-Munn, T. J. (2016). Methodology to develop a coarse liberation model based on preferential grade by size responses. *Minerals Engineering*, *86*, 149–155. https://doi.org/10.1016/j.mineng.2015.12.013

39.) Djordjevic, N. (2013). Image based modeling of rock fragmentation. *Minerals Engineering*, *46–47*, 68–75. https://doi.org/10.1016/j.mineng.2013.03.002

40.) Evans, C. L., Wightman, E. M., Manlapig, E. V, & Coulter, B. L. (2011). Application of process mineralogy as a tool in sustainable processing. *Minerals Engineering*, *24*(12), 1242–1248. https://doi.org/10.1016/j.mineng.2011.03.017

41.) Gay, S. L. (2004). Simple texture-based liberation modelling of ores. *Minerals Engineering*, *17*(11–12), 1209–1216. https://doi.org/10.1016/j.mineng.2004.06.032

42.) Gaudin, A.M. (1939) Principles of Mineral Dressing. Mc Graw-Hill, New York.

43.) Guimarães, C, and F Durão. (2003). "2D Simulation Model of Mineral Particles Yielded by Discriminatory Size Reduction." *Minerals engineering* 16.12: 1339–1348 10.1016/j.mineng.2003.08.006

44.) Kaneko, H. (1988). Fractal feature and texture analysis. *Systems and Computers in Japan*, *19*(8), 28–37. https://doi.org/10.1002/scj.4690190803

45.) Lastra, R. (2007). Seven practical application cases of liberation analysis. *International Journal of Mineral Processing*, *84*(1–4), 337–347. https://doi.org/10.1016/j.minpro.2006.07.017

46.) Lätti, D., & Adair, B. J. I. (2001). An assessment of stereological adjustment procedures. *Minerals Engineering*, *14*(12), 1579–1587. https://doi.org/10.1016/S0892-6875(01)00176-5

47.) Little, L., Mainza, A. N., Becker, M., & Wiese, J. G. (2016). Using mineralogical and particle shape analysis to investigate enhanced mineral liberation through phase boundary fracture. *Powder Technology*, *301*, 794–804. https://doi.org/10.1016/j.powtec.2016.06.052

48.) Musa, F., & Morrison, R. (2009). A more sustainable approach to assessing comminution efficiency. *Minerals Engineering*, *22*(7–8), 593–601. https://doi.org/10.1016/j.mineng.2009.04.004

49.) Mwanga, A., Parian, M., Lamberg, P., & Rosenkranz, J. (2017). Comminution modeling using mineralogical properties of iron ores. *Minerals Engineering*, *111*, 182–197. https://doi.org/10.1016/j.mineng.2017.06.017

50.) Parian, M., Mwanga, A., Lamberg, P., & Rosenkranz, J. (2018). Ore texture breakage characterization and fragmentation into multiphase particles. *Powder Technology*, *327*, 57–69. https://doi.org/10.1016/j.powtec.2017.12.043

51.) Pérez-Barnuevo, L., Lévesque, S., & Bazin, C. (2018). Automated recognition of drill core textures: A geometallurgical tool for mineral processing prediction. *Minerals Engineering*, *118*, 87–96. https://doi.org/10.1016/j.mineng.2017.12.015

52.) Pérez-Barnuevo, L., Lévesque, S., & Bazin, C. (2018). *Drill core texture as geometallurgical indicator for the Mont-Wright iron ore deposit (Quebec, Canada)*. https://doi.org/10.1016/j.mineng.2018.03.020

53.) Sandmann, D., & Gutzmer, J. (2013). Use of Mineral Liberation Analysis (MLA) in the Characterization of Lithium-Bearing Micas. *Journal of Minerals and Materials Characterization and Engineering*, *01*(06), 285–292. https://doi.org/10.4236/jmmce.2013.16043

54.) Sousa, R., Simons, B., Bru, K., de Sousa, A. B., Rollinson, G., Andersen, J., Machado Leite, M. (2018). Use of mineral liberation quantitative data to assess separation efficiency in mineral processing – Some case studies. *Minerals Engineering*, *127*, 134–142. https://doi.org/10.1016/j.mineng.2018.08.004

55.) Ueda, T., Oki, T., & Koyanaka, S. (2017). Comparison of Seven Texture Analysis Indices for Their Applicability to Stereological Correction of Mineral Liberation Assessment in Binary Particle Systems. *Minerals*, *7*(11), 222. https://doi.org/10.3390/min7110222

56.) Zhang, J., & Subasinghe, N. (2012). Extracting ore texture information using image analysis. *Mineral Processing and Extractive Metallurgy*, *121*(3), 123–130. https://doi.org/10.1179/1743285512y.0000000011

57.) Gy, P. (2004). Sampling of discrete materials - A new introduction to the theory of sampling: I. Qualitative approach. *Chemometrics and Intelligent Laboratory Systems*, *74*(1), 7–24. https://doi.org/10.1016/j.chemolab.2004.05.012

58.) Gy, P. (2004). Sampling of discrete materials: II. Quantitative approach - Sampling of zero-dimensional objects. *Chemometrics and Intelligent Laboratory Systems*, *74*(1), 25–38. https://doi.org/10.1016/j.chemolab.2004.05.015

59.) Gy, P. (2004). Sampling of discrete materials: III. Quantitative approach - Sampling of one-dimensional objects. *Chemometrics and Intelligent Laboratory Systems*, *74*(1), 39–47. https://doi.org/10.1016/j.chemolab.2004.05.011

APPENDICES

Appendix A-1: All 2D Synthetic Ore Textures Tested

Table A-1-1: 50/50 black/white 2D binary synthetic ore textures at five texture sizes.

Checkerboard		Horizontal Stripes		Vertical Stripes	
Texture Size	# of Primitive cells	Texture Size	# of Primitive cells	Texture Size	# of Primitive cells
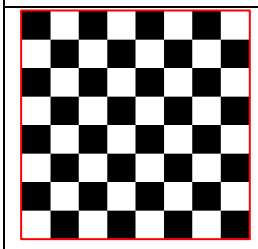	64	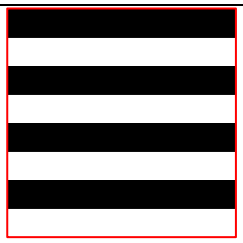	64	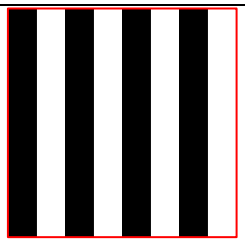	64
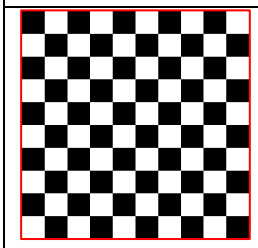	100	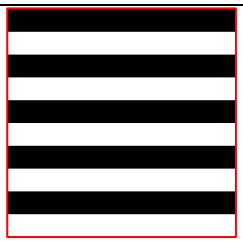	100	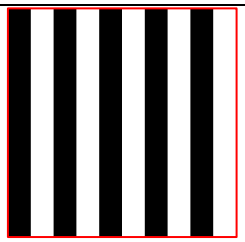	100
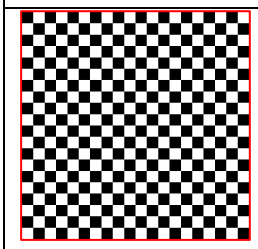	400		400	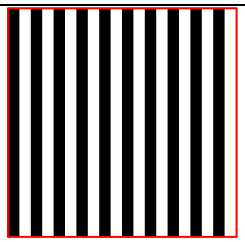	400
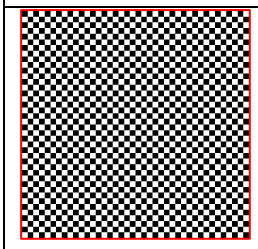	1600	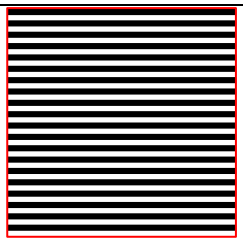	1600	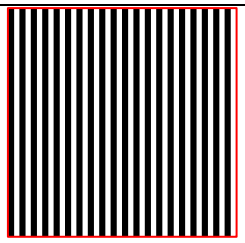	1600
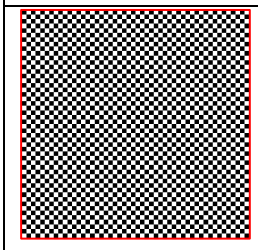	2500	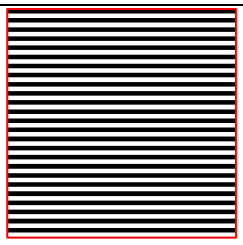	2500	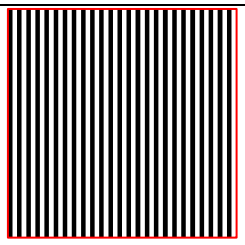	2500

Table A-1-2: Uneven black/white ratio 2D binary synthetic textures at five textures sizes/

Staircase		Staircase + Checkerboard		25% Black Vertical Stripes	
Texture Size	# of Primitive cells	Texture Size	# of Primitive cells	Texture Size	# of Primitive cells
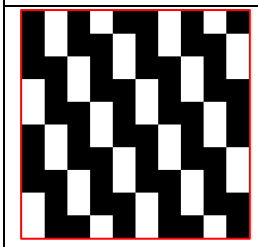	100	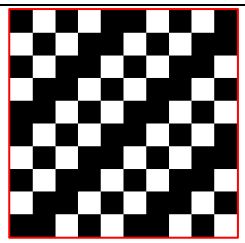	100	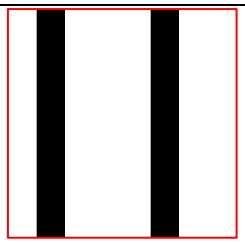	64
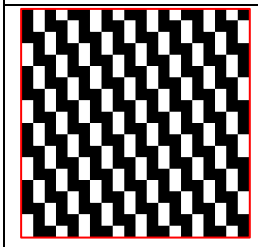	400	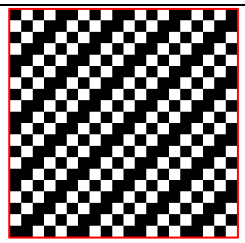	400	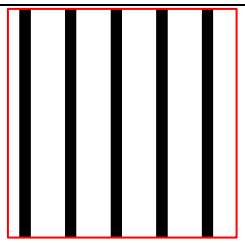	400
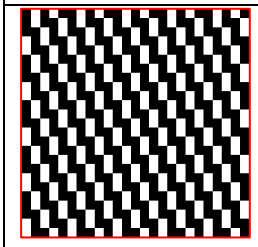	500	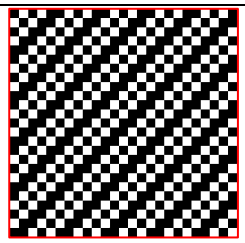	500	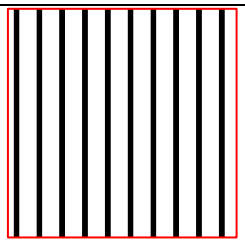	1600
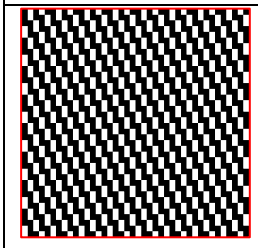	1600	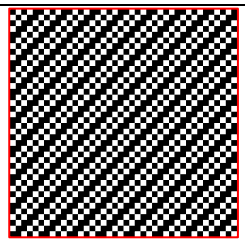	1600	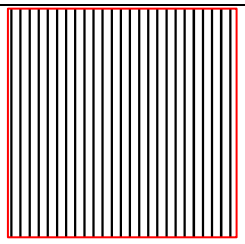	10000
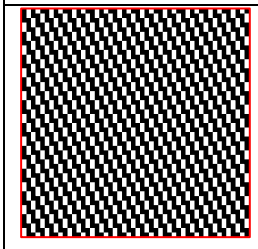	2500	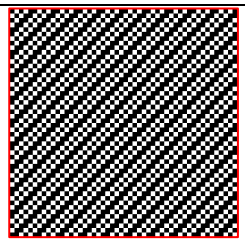	2500	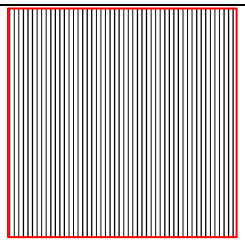	40000

Table A-1-3: 50/50 Checkerboard/stripes composite 2D binary synthetic texture at four textures sizes.

50/50 Checkerboard/Stripes Composite	
Texture Size	# of Primitive cells
	64
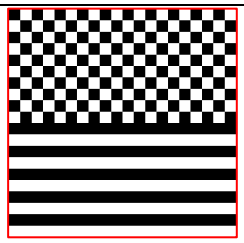	400
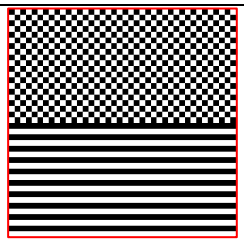	1600
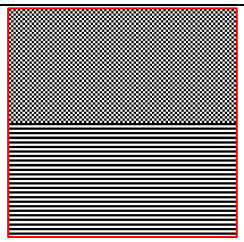	10000

Appendix A-2: Highly Factorable Numbers and the Particle Size Distribution

In order for a texture to remain periodic while changing texture size, the base pattern area and the primitive cell area need to be factors of the total texture area. Therefore, when considering image dimensions of periodic textures, it is important to consider the factors of the X-by-X dimensions. If many factors are close together, then a wide distribution of scaled particle sizes can be generated without dips in quantity of particles at certain particle sizes.

Table A-2-1: Highly factorable numbers and their factors.

Number	Factors	# of Total Factors
840	1,2,3,4,5,6,7,8,10,12,14,15,20,21,24,28,30,35,40,42,56,60,70, 84,105,120,140,168,210,280,420,840	32
1000*	**1,2,4,5,8,10,20,25,40,50,100,125,200,250,500,1000**	**16**
1260	1,2,3,4,5,6,7,9,10,12,14,15,18,20,21,28,30,35,36,42,45,60,63, 70,84,90,105,126,140,180,210,252,315,420,630,1260	36
2520	1,2,3,4,5,6,7,8,9,10,12,14,15,18,20,21,24,28,30,35,36,40,42,45, 56,60,63,70,72,84,90,105,120,126,140,168,180,210,252,280, 315,360,420,504,630,840,1260,2520	48

*1000x1000 image dimensions used for this work

Appendix A-3: Predictive Modelling of Complex Ore Textures

As mentioned in the body of this work, the ore grade by size distribution of even simple textures such as checkerboard and stripes are difficult to model over the compete range of particle sizes. A two-beta distribution model was applied to more complex textures and fitted parameters are given by Figures A-3.1, A-3.2 below. For more complex textures such as staircase and staircase + checkerboard, fitted model parameters were complex and difficult to interpret.

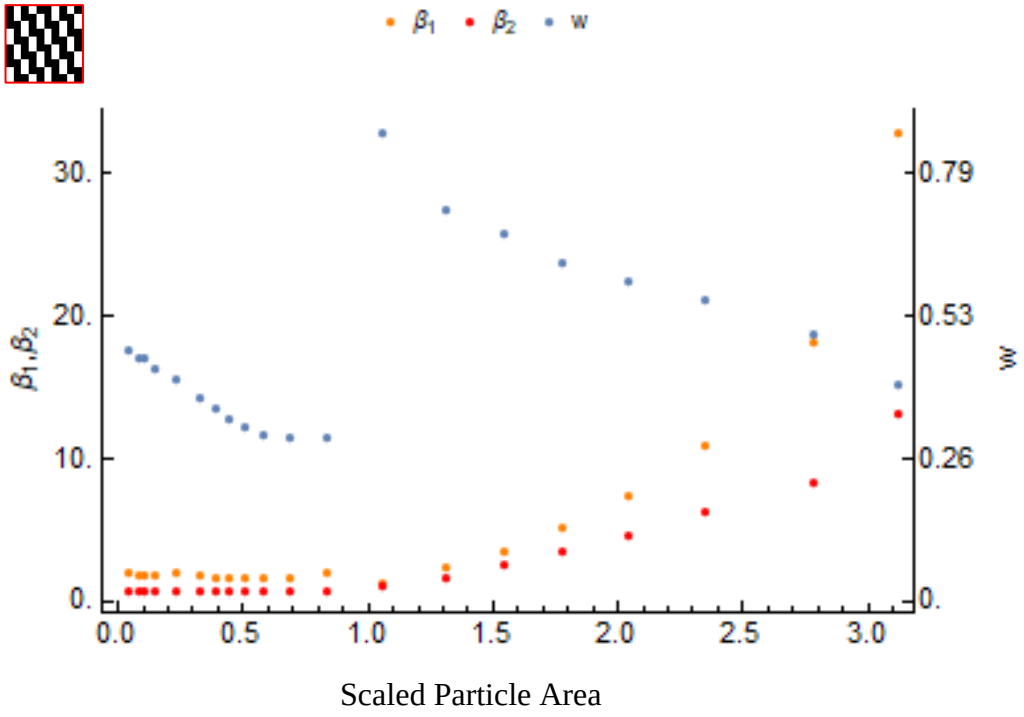

Figure A-3.1: Two beta mixture distribution fitted parameters across the complete range of scaled particle areas, staircase texture

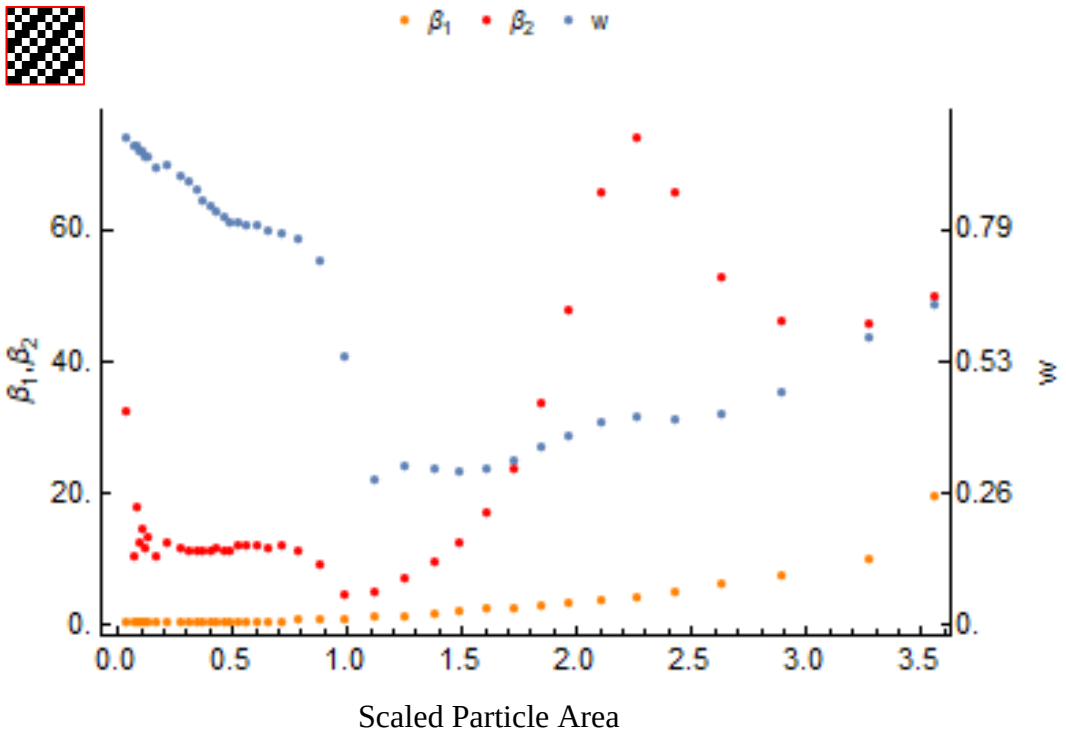

Figure A-3.2: Two beta mixture distribution model fitted parameters across the complete range of scaled particle areas, staircase + checkerboard texture